ADDIS ABABA UNIVERSITY
FACULTY OF TECHNOLOGY
SCHOOL OF GRADUATE STUDIES
DEPARTMENT OF MECHANICAL ENGINEERING

STRESS ANALYSIS OF A COMPOSITE MATERIAL CYLINDRICAL SHELL HAVING SURFACE CRACK

A THESIS SUBMITTED TO THE SCHOOL OF GRADUATE STUDIES OF ADDIS ABABA UNIVERSITY IN PARTIAL FULFILLMENT FOR THE DEGREE OF MASTERS OF SCIENCE IN MECHANICAL ENGINEERING (MECHANICAL DESIGN)

BY
BELACHEW NEGASH

ADVISOR
ALEM BAZEZEW (Dr.)

JULY, 2009

ADDIS ABABA UNIVERSITY

SCHOOL OF GRADUATE STUDIES

DEPARTMENT OF MECHANICAL ENGINEERING

Title:

Stress Analysis of a Composite Material Cylindrical Shell Having Surface Crack

By
Belachew Negash

Approved by Board of Examiners:

Dr. Nurelegne Tefera (Chairman)	July 15/2009 Date
Dr. Alem Bazezew (Advisor)	July 15/09 Date
Dr. Abiy Aweke (External Examiner)	15/07/09 Date
Prof. Idalberto Mendoza (Internal Examiner)	15/07/09 Date

Acknowledgement

First of all, I would like to take this opportunity to express my sincere gratitude to Dr. Alem Bazezew, my supervisor, for having patience to help me to work on this research and for his constant guidance and encouragement throughout the course of the research. He is also greatly acknowledged for delivering his suggestions in streaming the project in the intended direction.

Thanks to my sister, Aster Negash, her affection I never forget in life. She was by my side making life easy and also to Hana Eshetie for her everyday love and affection.

Abrham Bayeh, Taddesse Diga and all my friends around me are also greatly acknowledged for their intimacy and cooperation in the whole period of my study.

My love also goes to my whole family and my father, Negash Amare, at the moral expense of which I am here to accomplish this study.

Finally, I would like to express my deepest appreciation to the staffs of the departments of Mechanical Engineering of BDU and AAU for facilitating my study and arranging everything for me to accomplish this achievement.

Table of Contents

List of Figures

Abstract

Composite materials are combinations of two or more materials giving a third material with highly desirable properties. A composite material cylindrical shell is one of the components used in weight sensitive areas as composite materials are nowadays commonly used in the aviation industry and marine applications. In many practical applications, using composites is more efficient. For example, in highly competitive airline markets, one is continuously looking for ways to lower overall mass of the aircraft without decreasing the stiffness and strength of its components like cylindrical shells or pressure vessels. This is possible by replacing conventional metal alloys with composite materials. However, surface irregularities and micro cracks can be imparted to such materials for various reasons and it is very important to analyze these materials carefully to hinder the damage that could result as a result of failure

In this work the stress and strain distributions around the surface cracked cylindrical shell structure have been presented by studying the properties of composites, anisotropic elasticity relations, stress intensity factors, fracture toughness and stress field equations of surface crack problems in composite material, and finally finite element method simulation is applied to investigate the stress and strain distribution around the surface crack in a composite material cylindrical shell structure.

Mathematical modeling and finite element simulation of the surface cracked cylindrical shell was performed and the problem was finally solved using ANSYS finite element method package. In the mean time, results were obtained in the post processing stage of ANSYS. The main results obtained were the variation of the critical stress and strain distributions around the surface crack which could be cold shielded damaged zone that makes composite materials having unpredicted damage zone sizes. Finally, the critical stress and strain distribution patterns, the crack propagation schemes or styles were compared with literatures from composite material shell structures and conventional isotopic materials to draw conclusions regarding the advantages of composites compared to conventional material in crack advancement

Key words*: Composite materials, anisotropic stress-strain relationship, laminate, surface crack, shielding effect, crack simulation, classical shell theory.*

CHAPTER ONE
THE PROBLEM STATEMENT

1.1 Introduction and Background of the problem

Fracture is a problem that society has faced for as long as there have been man-made structures. The problem may actually be worse today than in the previous centuries, because more can go wrong in our complex technological society [1]

Fortunately, advances in the field of fracture mechanics have helped to offset some of the potential dangers posed by increasing technological complexity. Our understanding of how materials fail and our ability to prevent such failures has increased considerably since World War II. Much remains to be learned, however, and existing knowledge of fracture mechanics is not always applied when appropriate specially for modern technological materials like composites.

The combination of two or more materials can lead to a third material with highly desirable properties known as composite materials. The constituents of a composite material are usually combined on a macroscopic scale through physical rather than chemical means. Composite materials usually consist of a matrix and a reinforcing constituent. The matrix is often soft and ductile compared to the reinforcement. Various types of reinforcement are possible, including continuous fibers, chopped fibers, whiskers, flakes, and particulates [2].

In many practical applications, using composites is more efficient. For example, in highly competitive airline markets, one is continuously looking for ways to lower overall mass of the aircraft without decreasing the stiffness and strength of its components like cylindrical shells or pressure vessel. This is possible by replacing conventional metal alloys with composite materials. Even if the composite material costs may be higher, the reduction in the number of parts in an assembly and the savings in the fuel costs make them more profitable [3].

A shell is an initially curved plate defined by a middle surface, about which a constant or variable thickness is symmetrically situated. A typical ratio of a shell thickness to its radius is of the order 1:20 [4]. Shells are generally subjected to in-plane loading and to the forces and couples normal to the surfaces, which are called here lateral loading [4]. This nature of loading implies that the common mode of failure of shell structures is either in

buckling or fracture (burst) of its walls. However, surface irregularities and micro cracks can be imparted to materials for various reasons. This could be while a joint is made, during manufacturing, assembly, etc. Hence, it is very important to analyze how the stress varies in the vicinity of crack in composite structures.

A shell is, in essence, a structure that can be derived from a plate by initially forming the middle surface as a singly (or doubly) curved surface. The way in which the shell supports external loads is quite different from that of a flat plate. The stress resultants acting on the middle surface of the shell have both tangential and normal components, which carry a major part of the load, a fact that explains the economy of shells as load-carrying structures and their well-deserved popularity [5]. The derivation of detailed governing equations for a curved shell problem presents many difficulties and, in fact, leads to many alternative formulations, each depending on the approximations introduced.

In the finite element treatment of shell problems, difficulties referred to above are eliminated, at the expense of introducing a further approximation. This approximation is of a physical, rather than mathematical nature. In this, it is assumed that the behavior of a continuously curved surface can be adequately represented by the behavior of a surface built up of small flat elements. Intuitively, as the size of the subdivision decreases it would seem that convergence must occur and indeed experience indicates such a convergence [5].

Moreover, the nonlinearity imparted by material properties and geometric variations are also the contributing factors to the structural analysis of composite shells. The limitation in the analytical relation development for composite materials in general is also another important factor that compels us to use the finite element method of stress analysis in the vicinity of a cracked composite structure.

Due to their high strength-to-weight and high stiffness-to-weight ratios, fiber-reinforced composite laminated shell structures have been widely used in the aerospace, marine, automobile and other engineering industries. Thus, it is very important to study the behavior of composite material cylindrical shell structure for the distribution of stresses and strains with an introduction of a surface crack.

1.2 Objectives of the problem

The objective of this thesis is to analyze the effect of crack on the stresses and their distribution around the crack in a composite material cylindrical shell by using finite element method (FEM). This will be done through modeling and simulating the cracked composite material cylindrical shell and applying the loads which actually exist in shells, like tangential and axial loads, with the following conditions to have a justified conclusion.

- A pre-defined dimension of the shell with tangential surface crack oriented on the interior and exterior surfaces of the cylindrical shell structure will be taken and the stress and strain distributions around the surface crack will be analyzed and discussed for Mode I loading condition subjected to far field axial stress.
- A pre-defined dimension of the shell with axial surface crack oriented on the interior and exterior surfaces of the cylindrical shell structure will be taken and the stress and strain distributions around the surface crack will be analyzed and discussed for Mode I loading condition subjected to far field tangential stress.

1.3 Scope and limitation

The aim of this thesis is to analyze surface cracked composite material cylindrical shell structure for the stress and strain distributions around the crack using finite element method package ANSYS software due its availability. This will be done for the above specific objectives. The relevant equations governing the state of stress in a shell material will be derived using mechanics of materials and related with theoretical fracture mechanics for the analysis to be done showing an orthotropic material property on the software.

The scope of this thesis is limited to studying the properties of composites, anisotropic elasticity relations, fracture mechanics approaches for composites, mathematical modeling of the surface cracked composite material cylindrical shell structure under in-plane loading for stress intensity and fracture toughness, and finally applying finite element method to investigate the stress and strain distributions around the surface crack oriented on the composite material cylindrical shell structure.

CHAPTER TWO
LITERATURE SURVEY

2.1 Literature Review

As composite materials were introduced into the world, the initial impetus for using them was their high strength-to-weight and stiffness-to-weight ratios, along with very significant improvement in fatigue life and damage tolerance compared to most metallic materials. Furthermore, when composite materials are used to tailor a structure, they provide excellent opportunities for design flexibility and potential optimization of design criteria by controlling their directional natures to achieve certain performance goals or eliminate undesirable instabilities. Composite shell structures are one of those structures, finding applications in a variety of systems; including aircraft and submarine structures, space structures, automobiles, sport equipment, medical prosthetic devices and electronic circuit boards.

Exceptionally high stiffness and strength to weight ratios are the driving forces behind the success story of fibre reinforced composite structures in advanced lightweight constructions. For aerospace applications the triumphant progress is evident, culminating in the late announcement of a “First Composite Jetliner” [15]. But also high-speed ships, terrestrial vehicles and machines where high velocity or acceleration is requested utilize the advantage of this material more and more often. A set-up from layers with unidirectional reinforcement oriented in different directions, termed ‘multidirectional laminate’, has developed as a standard design. Homogenization of fiber and matrix behavior results in effective layer properties. In the assessment a homogeneous orthotropic layer is assumed as the smallest entity of the structure.

The structure with the cutouts of various shapes is adopted by the structural requirements or geometrical condition. Stress concentration of cylindrical shell with a cutout is important in many industrial structures such as aircrafts, vessels, submarines, nuclear reactors, etc. [7]. According to Lee *et al*.[7], the strain distribution around the un-stiffened and stiffened circular cutout of the isotropic stainless steel (ANSI type 304) and the GFRP laminated composite cylindrical shells subjected to axial compression have been studied and the obtained experimental results have been compared with numerical analysis. In their experiment, the strain was measured around the circular cutout by strain measuring system under the axial uniform compression loading. The numerical analysis was

performed by the commercial finite element code ANSYS and the strain concentration factor (SCF) was defined to investigate the strain concentration around the circular cutout. The SCF of the stainless steel cylindrical shell with a stiffened cutout was decreased 39% in experiment and 50% in numerical analysis. The SCF of GFRP laminated composite cylindrical shell was decreased 22% in experiment and 31% in numerical analysis.

Many composite components in aerospace structures are made of flat or curved panels with co-cured or adhesively bonded frames and stiffeners. Over the last decade a consistent stepwise approach has been developed which uses experiments to detect the failure mechanism, computational stress analysis to determine the location of first matrix cracking and computational fracture mechanics to investigate the potential for delamination growth [13]. According to Ronald Krueger [13] description, testing of thin skin stiffened panels designed for aircraft fuselage applications has shown that bond failure at the tip of the frame flange is an important and very likely failure mode. Debonding also occurs when a thin-gage composite fuselage panel is allowed to buckle in service. A methodology based on fracture mechanics has proven useful for characterizing the onset and growth of delamination in composites and has been used with limited success to investigate delamination onset and debonding in simple laboratory coupon type specimens. Future acceptance of a fracture mechanics methodology by industry and certification authorities however, requires the successful demonstration of the methodology on structural level.

A computer method to model crack growth in composite material shell finite elements undergoing large displacements and damage has been developed by Charoenphan *et al*. [19]. In the paper, they implemented a domain integral energy method for modeling crack growth in composite material shell structures using the finite element method. Volume integral expressions to evaluate the dynamic energy release rate in a through-thickness three-dimensional crack were derived. Using the domain integral, the energy release rate computation was implemented in the DYNA3D explicit non-linear dynamic finite element analysis program wherein crack propagation was modeled by releasing the constraints between initially constrained node pairs. The implementation enabled the program to either determine the energy resistance response for the material or predict the rate of crack propagation in shell structures. The numerical implementation was verified by simulating Mode I and Mode III slow crack growth problems in semi-infinite transversely isotropic

media, for which analytic solutions were available. Oscillations of energy following the release of nodal constraints as the crack propagates in discrete increments were suppressed using light mass proportional damping and a moving averaging scheme.

The behavior of an axis-symmetrical circumferential crack occurring in dissimilar materials represents such a non planar problem and has been investigated by Liu *et al.* [21]. In their study an axis-symmetrical fiber-matrix cylindrical model with a circumferential crack in the matrix of finite diameter was formulated within elastostatic scope. The problem was considered by means of integral transforms and a singular integral equation with a dominant generalized Cauchy kernel was obtained. Following the numerical solution technique developed by Erdogan, Gupta and Cook, the singular integral equation was reduced to a system of linear equations. By solving the linear equations, stress intensity factors associated with the crack length and the material properties were calculated and discussed. The solutions presented in their study were found to be general, including the solutions as special cases of their formulation for a homogeneous solid cylindrical bar and a thick-walled shell with an outer circumferential crack.

Jan Stegmann [23] has developed finite element based optimization techniques for laminated composite shell structures. The platform of implementation was the finite element based analysis and design tool MUST (MUltidisciplinary Synthesis Tool) and a number of features have been added and updated. This includes an updated implementation of finite elements for shell analysis, tools for investigation of nonlinear effects in multilayered topology optimization and a novel framework called discrete material optimization (DMO) for solving the material layout and orientation problem.

A necessary tool for optimization was robust finite elements and consequently, the finite element library in MUST was extended with a new three-node element and an updated four-node element. These were designated MITC3 and MITC4, respectively, since they used mixed interpolation of tensorial components to avoid problems with shear locking. The SHELLn family of standard isoparametric shell finite elements in MUST has also been updated for improved performance. All elements have laminate and geometrically nonlinear capabilities and tests showed that the performance and computational efficiency were very good.

In his work [23], geometrically nonlinear effects were investigated to determine if these should be taken into account when designing for maximum stiffness of laminated composite structures using structural optimization. Facilities for nonlinear topology optimization of multilayered shell structures was implemented using a Newton-Raphson scheme for the analysis, the adjoint variable method for sensitivity analysis and the MMA optimizer for solving the optimization problem. The SIMP method was used for layer-wise stiffness scaling to allow material to be added or removed in specific layers.

Existing methods for solving for optimal material orientation and maximum stiffness inherently suffer from problems with local optima, which inspired the development of discrete material optimization (DMO), which was a novel approach for simultaneous solution for material distribution and orientation. The DMO method uses an element level parameterization in a weighted sum formulation that allowed the optimizer to choose a single material from a set of pre-defined materials by pushing the weights to 0 and 1. As in his work [23], the success of the method was therefore dependent on the optimizer's ability to push the weights to 0 and 1 and several weighting schemes were implemented. Numerical examples of his work indicated that the method was indeed able to solve the combined material distribution and orientation problem. Furthermore, an industry related design problem of a wind turbine blade main spar was solved and the obtained results were very encouraging. The DMO method thus showed promising potential for application to problems of industrial relevance and no problems with local optima could be identified in the tested examples.

Anisotropy is an important characteristic of composite materials that must be taken into account both in elastic and inelastic analysis, including damage. Continuum damage mechanics (CDM) had important developments since the initial works of Kachanov and Rabotnov, and constitutes now a practical tool to account for macrocospic damage in materials and structures [15]. Roberto and Guillermo [15], has presented an application of the anisotropic damage theory based in Murakami work. In his formulation, the fourth order damage tensor (that related Cauchy and effective stress tensors) was determined on the basis of the tensor (three-dimensional area density of damage) that, in turn, can be determined through experimental data. The analytical formulation has been set in incremental form and implemented into a finite element program (for plates and shells structure in composite material) taken in to account of geometrically non-linear effects. In

order to verify and validate the numerical model, comparisons with analytical and experimental results for simple situations has been presented.

Composite laminates are now widely used in both civil and military aircraft structures leading to weight saving. However, study of the behavior of such materials has shown that they are more damage-sensitive than metallic materials, specially to delaminations due to edge effects or low velocity impacts [17]. In his paper, Yves Ousset [17], described a numerical method to simulate delamination growth in layered composite plates within the framework of fracture mechanics. It was based on the search for the stationary points of the total energy of the plate (the sum of the mechanical energy and the fracture energy associated with the delamination growth). The resulting non-linear problem was solved by Newton's method. The expressions for the first and second derivatives of energy with respect to a crack front displacement were derived analytically and numerical examples were presented for DCB (double cantilever beam) specimens loaded in Mode I.

The characteristic properties of shell element with similar shapes are used to generate a so-called super element for the analysis of the crack problems for cylindrical pressure vessels. The formulation is processed by matrix condensation without the involvement of special treatment. This method can deal with various singularity problems and it also presents excellent results to crack problems for cylindrical shell. Specially, the knowledge of the kind of singular order is not necessary in super element generation; it is very economical in terms of computer memory and programming. This method also exhibits versatility to solve the problem of kinked crack at cylindrical shell [18].

Storakers *et al*. [25] have carried out a theoretical study for compressive loading of a thin circular embedded delamination located bellow a cylindrical surface. The delaminated member is subjected to nominally uniaxial and balanced bi axial loading with the main objective to analyze its influence on surface curvature specially as regards imminent crack growth. A finite element program earlier developed for delaminated plates has been generalized to apply also for shells and used to determine energy release rates and mode intensities along the delaminated front. A parameter study was made of the influence of curvature of the delaminated shell in particular as regards initiation and stability of crack growth.

Zheng-Ming Huang [26] in his paper focused on the ultimate flexural strength of a polymer based composite cylinder subjected to bending. According to the paper the out most filament of the cylinder subjected to the maximum bending stress failed the first. The complexity, however, lied in the fact that the failure of this outmost filament generally did not correspond to the ultimate failure. Additional loads can still be applied to the cylinder and a progressive failure process will result. To deal with such a problem in his paper, the cylinder has been discretized into a number of lamina layers with different widths. The bridging micromechanics model [Huang, Z. M., composites part A, 2001] combined with the classical lamination theory has been applied to understand the progressive failure process generated in the cylinder. Only its constituent fibre and matrix properties under bending are necessary for this understanding and reasonably good accuracy has been achieved. However, the ultimate failure of the cylinder cannot be figured out only based on a stress failure criterion, as one cannot know a priori which ply failure corresponds to the ultimate failure. An additional critical deflection (curvature) condition must be employed also. By using both the stress and the deflection conditions, the estimated ultimate strength of the cylinder agreed well with an experimental measurement

Dynamic analysis of composite cylindrical shells has attracted much attention of researchers. A quick and accurate prediction of dynamic behavior of such cylindrical shells is of very much interest to designers and experimentalists alike. This normally requires a comprehensive development of a mathematical model. Due to the complexity of engineering characteristics of composite shell type structures, analytical solutions cannot be obtained in a straight forward manner. The differential quadrature method (DQM) is an efficient numerical technique which transforms governing equations of dynamic equilibrium to a matrix form by using weighted matrices. The DQM requires a small amount of computer capacity and provides accurate results. The DQM was successfully employed in various structural problems [14]. Haftchenari *et al.* [14] has presented a solution to the free vibration problem of laminated fibrous composite cylindrical shells. The governing equations of dynamic equilibrium were derived based on first order shear deformation theory. These were then solved by using the differential quadrature method by taking two types of boundary conditions (simply supported and clamped free ends) for a cylindrical shell. The results from the DQM solution were compared with some available theoretical as well as experimental results. It was observed that there was a very good

agreement between the results from this method and the corresponding ones found before by various researchers.

Khdier [16] has developed analytical solutions of the dynamic response of the classical, first-order and third-order theories of cross-ply laminated shallow shells for various boundary conditions. The solutions of his work are applicable to laminated shells with two opposite edges simply supported and the remaining ones can have arbitrary combinations of free, clamped and simply supported boundary conditions. A Levy type method in conjunction with generalized modal approach, were used to obtain these solutions. For thick shells, the classical shell theory predicts deflections and stresses significantly different from those of the third-order theory. The third-order theory and the first-order theory results were very close to each other for response and normal stress. However, the third-order theory did not require the use of shear correction factors as he concluded.

Hui-Shen Shen *et al*. [20] have presented post buckling analysis for an anisotropic laminated cylindrical shell of finite length subjected to combined loading of axial compression and torsion. The governing equations are based on classical shell theory with von Karman-Donnell-type of kinematics nonlinearity and including the extension-twist, extension-flexural and flexural-twist couplings. The nonlinear pre-buckling deformations and initial geometric imperfections of the shell were both taken into account. A singular perturbation technique was employed to determine interactive buckling loads and post buckling equilibrium paths. The numerical illustrations concern the post buckling response of perfect and imperfect, anisotropic laminated cylindrical shells for different values of load-proportional parameters. The results showed that the post buckling characteristics depend significantly upon the load-proportional parameter. The results revealed that in combined loading cases the post buckling equilibrium path was unstable and the shell structure was imperfection-sensitive.

Before 1992, substantial efforts have been devoted to developing techniques and standards for measuring fracture toughness and subcritical crack growth. These methods use specimens containing two-dimensional (2-D), through the thickness flaws because of the relative ease of fabrication and the availability of accepted analytical and numerical solutions. However, many defects observed in practice, and often responsible for failures or questions regarding structural integrity, are three-dimensional (3-D) surface flaws. The efficiency of data generated from standard specimens containing 2-D defects in predicting

crack growth behavior of 3-D flaws, including crack initiation, subcritical crack growth, and unstable fracture, is a major concern [30].

Raju and Newman [8], in their paper presented stress intensity factor influence coefficients for a wide range of semi-elliptical surface cracks on the inside or outside of an isotropic cylinder. The crack surfaces were subjected to four stress distributions: uniform, linear, quadratic, and cubic. These four solutions can be superimposed to obtain stress intensity factor solutions for other stress distributions, such as those caused by internal pressure and by thermal shock. The results for internal pressure were given for the ratio of crack depth to crack length ranged from 0.2 to 1; the ratio of crack depth to wall thickness ranged from 0.2 to 0.8; and the ratio of wall thickness to vessel radius was 0.1 or 0.25. The stress intensity factors were calculated by a three dimensional finite element method. The finite element models employ singularity elements along the crack front and linear strain element somewhere. The stress intensity factors were evaluated from a nodal-force method. The presented results were also compared to other analyses of surface cracks in cylinders. Similarly Nishioka and Atluri [9], Ezzat and erdogan [10], and Newman and Raju [11] had focused on the stress intensity factor solutions for internal and external surface crack problems.

More recently Jiregna Hirko [6] in his work has targeted at the carrying out of the stress variation analysis of composite material cylindrical shell. The analysis was performed by studying the properties of composites, their areas of application, anisotropic elasticity relations, fracture mechanics approach for composites, and finally finite element method application has been applied to investigate the stress distribution at the crack tip in the composite material shell. Moreover, mathematical modeling and finite element simulation of the cracked shell was performed and the problem was at the end solved using ANSYS finite element analysis package. Consequently, results were obtained in the post processing stage of ANSYS. The main results obtained were the mode of stress and strain variation, the profile of the cracked surface, and the localized critical stress and strain regions at the crack front which could be cold shielded damaged zone. Ultimately, the stress and strain variation, the crack propagation schemes were compared to isotropic material shell and he has drawn conclusion on the advantages of composites compared to conventional materials with regard to crack advancement.

2.2 Motivation

The survey of literature highlighted that most of the analytical solutions are for infinite length plate and for shells of uniform cutouts (circular or elliptical) and for each shape of hole a new solution has to be derived all together. It is very difficult to find analytical solutions for complicated shapes like surface cracks on composite material shell structures. So the only alternative in such cases as it is concluded from the review is finite element method which can give good results for a variety of cracks, holes and ranges of loadings. Even the application of the concept of fracture mechanics approach to anisotropic material structures is very limited in view of the complexity of the deformation process.

Many of the works done by the various researchers in the past to recent reveals that there are some finite element and few analytical solutions available for shells with holes and rarely available for surface cracks on composite material shells. Most of these solutions deals with regular shapes of holes, for example, circular, elliptical, triangular etc. As the strength of composite material is influenced by a number of factors, these includes the anisotropic and non-homogeneous nature of the materials, the mechanical incompatibility of the constituent phases, the effect of interfacial bonding, the elastic and plastic behavior of the matrices and the reinforcing materials, the volume fraction of the component materials, the direction of the applied loads, so it will be expected to have cracks in or on the surface of these structures. Also the manufacturing processes or assembly can further induce flaws or cracks in these structures. Hence, the researcher is motivated to analyze the effect of surface crack (oriented both on internal and external of the shell surface) on the stresses and strains distribution around the crack induced in such material shell structure by considering modern design concept-fracture mechanics.

CHAPTER THREE
BACKGROUND OF THE STUDY

3.1 COMPOSITE MATERIALS

3.1.1 Introduction to Composite Materials

The history of the development of modern composite materials can be dated back to the early 1940s. It was in 1940 when fibreglass was first employed to reinforce plastics. The first successful application was found in its use in nose radar domes, known as radomes, to protect aircraft antennas. Glass-polyester radomes were used to replace the plywood and canvas-urea domes. This type of fibrous composite demonstrated excellent load-bearing capacity, thermostability, and resistance to weathering. But, above all, it is their 'transparency' to electromagnetic waves that made them most desirable for housing electronic equipment. Radomes made from fibreglass-reinforced plastics have since been widely deployed on ships and ground installations, as well as aircraft. The first fibreglass boat was moulded in 1942. In the same year, laminates of fibreglass with polyester resin were produced. Then, in 1946, the United States Government patented the first filament-winding process [27].

Composite materials are those formed by combining two or more materials on a macroscopic scale such that they have better engineering properties than the conventional materials, for example, metals. Some of the properties that can be improved by forming a composite material are stiffness, strength, weight reduction, corrosion resistance, thermal properties, fatigue life, and wear resistance. Most man-made composite materials are made from two materials: a reinforcement material called fibre and a base material, called matrix material [24]. The function of the matrix is to support and protect the fibres and to provide a means of distributing load among and transmitting load between the fibres.

3.1.2 Classification of composites

Composites are classified by the geometry of the reinforcement; particulate, flake and fibres, or by the type of matrix; polymer, metal, ceramics and carbon.

Particulate composites consist of particles immersed in materials such as alloys and ceramics. They are usually isotopic since the particles are added randomly. Particulate composites have the advantages such as improved strength, increased operating temperature and oxidation resistance etc. Typical examples include use of aluminum

particles in rubber, silicon carbide particles in aluminum, and gravel, sand and cement to make concrete.

Flake composites consist of flat reinforcements of materials. Typical flake materials are glass, mica, aluminum and silver. Flake composite provide advantages such as high out-of plane flexural modulus, higher strength, and low cost. However, flakes can not be oriented easily and only a limited number of materials are available for use.

Fibre composite consist of materials reinforced by short (discontinuous) or long (continuous) fibre. Fibres are generally anisotropic and examples include carbon and aramids. The fundamental units of continuous fibre matrix composite are unidirectional or woven fibre laminas.

Polymer matrix composites

The most common advanced composites are polymer matrix composites (PMC). These polymers consist of a polymer (example epoxy, polyester, urethane) reinforced by thin diameter fibres (graphite, aramids, boron, carbon). For example, graphite epoxy composites are approximately five times stronger than steel on a weight-for-weight basis. The reasons why they are the most common composites include their low cost, high strength, and simple manufacturing principles. The main drawbacks of PMCs include low operating temperatures, high coefficient of thermal and moisture expansion, and low elastic properties in certain directions.

Metal matrix composites

Metal matrix composites (MMCs) as the name implies, have a metal matrix. Examples of matrices in such composites include aluminum, magnesium and titanium. Typical fibres include carbon and silicon carbide. Metals are mainly reinforced to increase or decrease their properties to suit the needs of the design. For example, the elastic stiffness and strength of metals can be increased while large coefficients of thermal expansion and thermal and electrical conductivities of metals can be reduced by the addition of fibres such as silicon carbide.

Ceramic Matrix Composites (CMC)

Ceramic Matrix Composites have a ceramic matrix such as alumina, calcium, aluminum silicate reinforced by fibres such as carbon and silicon carbide. Advantages of CMCs include high strength, hardness, high service temperature, chemical inertness, and low

density. However, ceramics by themselves have low fracture toughness. Under tensile or impact loading, they fail catastrophically. Reinforced ceramics with fibres, such as silicon carbide or carbon, increases their fracture toughness because it causes gradual failure of the composite. This combination of a fibre ceramic matrix composite make more attractive for application where both high mechanical properties and extreme service temperatures are desired.

Carbon-Carbon composites

Carbon-carbon composites use carbon fibers in a carbon matrix. Carbon-carbon composites are used in very high temperature environments of up to 6000^0F (3315^0c), and are 20 times stronger and 30% lighter than graphite fibers. Carbon by itself is brittle and flaw sensitive like ceramics. Reinforcement of a carbon matrix allows the composite to fail gradually and also gives advantages such as ability to withstand high temperatures, low creep at high temperatures, low density, good tensile and comprehensive strengths, high fatigue resistance, high thermal conductivity, and high coefficient of friction. Drawbacks include high cost, low sheer strength, and susceptibility to oxidations at high temperatures.

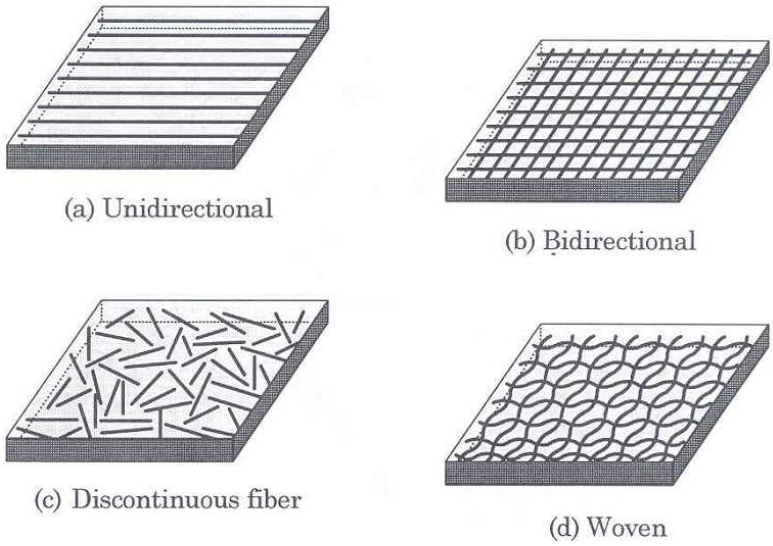

Figure 3.1 Various types of fibre-reinforced composite lamina [24].

A lamina or ply is a typical sheet of composite material. It represents a fundamental building block. A fibre-reinforced lamina consists of many fibres embedded in a matrix material, which can be a metal like aluminum, or a nonmetal like a thermoset or thermoplastic polymer. Often, coupling (chemical) agents and fillers are added to improve the bonding between fibres and matrix material and increase toughness. The fibres can be

continuous or discontinuous, woven, unidirectional, bidirectional, or randomly distributed (figure 3.1).

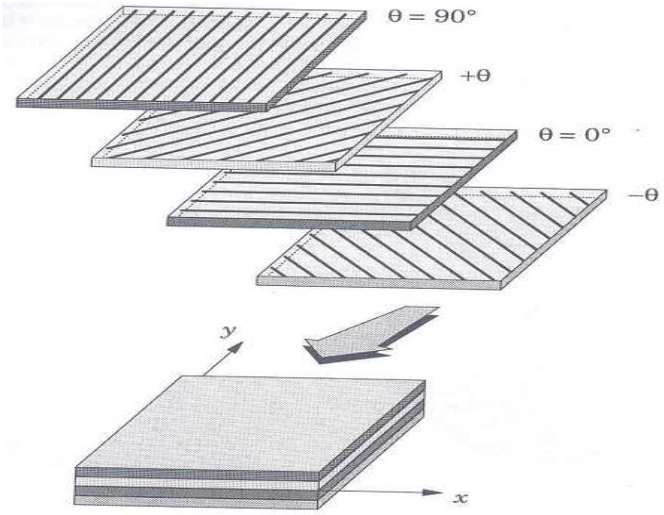

Figure 3.2 A laminate made up of lamina with different fibre orientation [24].

A laminate is a collection of lamina stacked to achieve the desired stiffness and thickness. For example, unidirectional fibre-reinforced lamina can be stacked so that the fibres in each lamina are oriented in the same or different direction (figure 3.2). The sequence of various orientations of a fibre-reinforced composite layer in a laminate is termed the lamination scheme or stacking sequence. The layers are usually bonded together with the same matrix material as that in a lamina. A unidirectional lamina (i.e., all lamina have the same fibre orientation) will be very strong a long the fibre direction and weak in the transverse direction.

3.1.3. Mechanical Behavior of Composite Materials

Today, composite materials are coming into prominence. Fibre-reinforced composite materials are uniquely useful because they can be constructed in such a manner that they have higher strength-to-density ratios or stiffness-to-density ratios of any materials at moderate temperatures and the fibres can be oriented to provide minimum structural weight for a given structural geometry and given system of loads.

Composite materials have many characteristics that are different from conventional engineering materials. Some characteristics are merely modifications of conventional behavior; others are totally new and require new analytical and experimental procedures. Most common engineering materials are homogeneous and isotropic.

A homogeneous body has, uniform properties throughout, i.e., the properties are not a function of position in the body. An isotropic body has material properties that are the same in every direction at a point in the body, i.e., the properties are not a function of orientation at a point in the body. In contrast, composite materials are often both inhomogeneous and non isotropic (orthotropic or, more generally, anisotropic). An inhomogeneous body has non-uniform properties over the body, i.e., the properties are a function of position in the body [3].

An orthotropic body has material, properties that are different in three mutually perpendicular directions at a point in the body and, further, have three mutually perpendicular planes of material symmetry. Thus, the properties are a function of orientation at a point in the body. An anisotropic body has material properties that are different in all directions at a point in the body. There are no planes of material property symmetry. Again, the properties are a function of orientation at a point in the body.

Because of the inherent heterogeneous nature of composite materials, they are conveniently studied from two points of view: micromechanics and macro mechanics. Micromechanics - is the study of composite material behavior wherein the interaction of the constituent materials is examined on a microscopic scale. This is particularly concerned with the composition of the composites in their early fabrication process. Macro mechanics - is the study of composite material behavior wherein the material is presumed homogeneous and the effects of the constituent materials are detected, only as averaged apparent properties of the composite.

Basic Assumptions

The basic assumptions made in material science approach model of fibre reinforced composites are [3]:

- The bond between fibres and matrix is perfect
- The fibres are continuous and parallally aligned in each. They are packed regularly; i.e. the space between fibres is uniform.
- Fibre and matrix materials are linear elastic, they follow approximately Hooke’s law and each elastic model is constant.
- The composite is free of voids.

How is a composite structure analyzed mechanically?

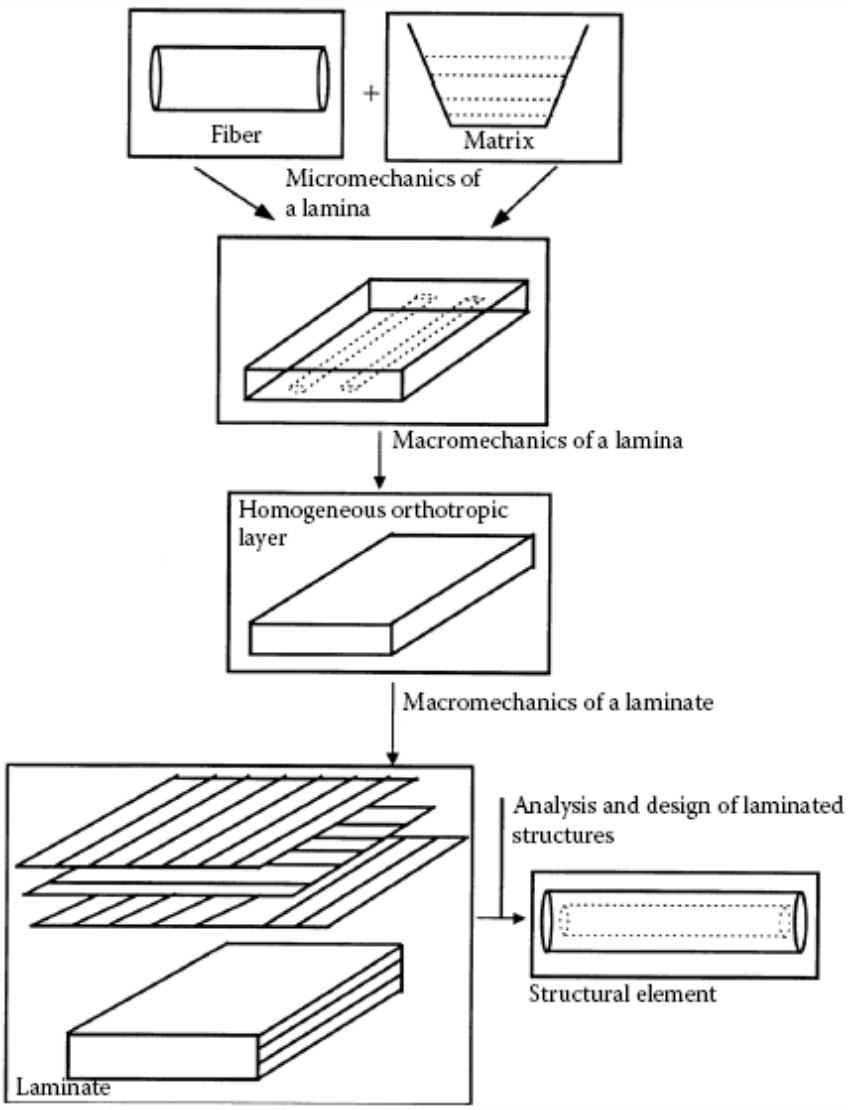

Figure 3.3 Schematic analysis of laminated composites [3]

A composite material consists of two or more materials or constituents and hence the analysis and design of such materials are different from the conventional materials such as steel. The approach followed to analyze the mechanical behavior of a composite structure is as given in figure 3.3.

First, find the average properties of a composite ply from the individual properties of the constituents' properties including stiffness, strength, and thermal and moisture expansion coefficients. Note that the average properties are derived by considering the ply to be homogeneous. At this level, one can optimize for the stiffness and strength requirements of a lamina. This is called micromechanics of a lamina.

Second, develop the stress-strain relationship for a unidirectional or bidirectional lamina. Loads may be applied along the principal directions of the symmetry of a lamina or off-axis. Also one can develop relationships for stiffness, thermal and moisture expansion coefficients and strengths of angle plies. Failure theories of a lamina are based on the stress in the lamina and strength properties of a lamina. This is called Macro mechanics of a lamina [3].

A structure made of composite materials is generally a laminate structure made of various laminas stacked on top of each other. Knowing the macro mechanics of a lamina, it is possible to develop the mechanics of a laminate. Stiffness, strength and thermal and moisture expansion coefficients can be found for the whole laminate. Laminate failure is based on stresses and application of failure theories to each ply. This knowledge of analysis of composites can then eventually form the basis for the mechanical design of structures made of composites.

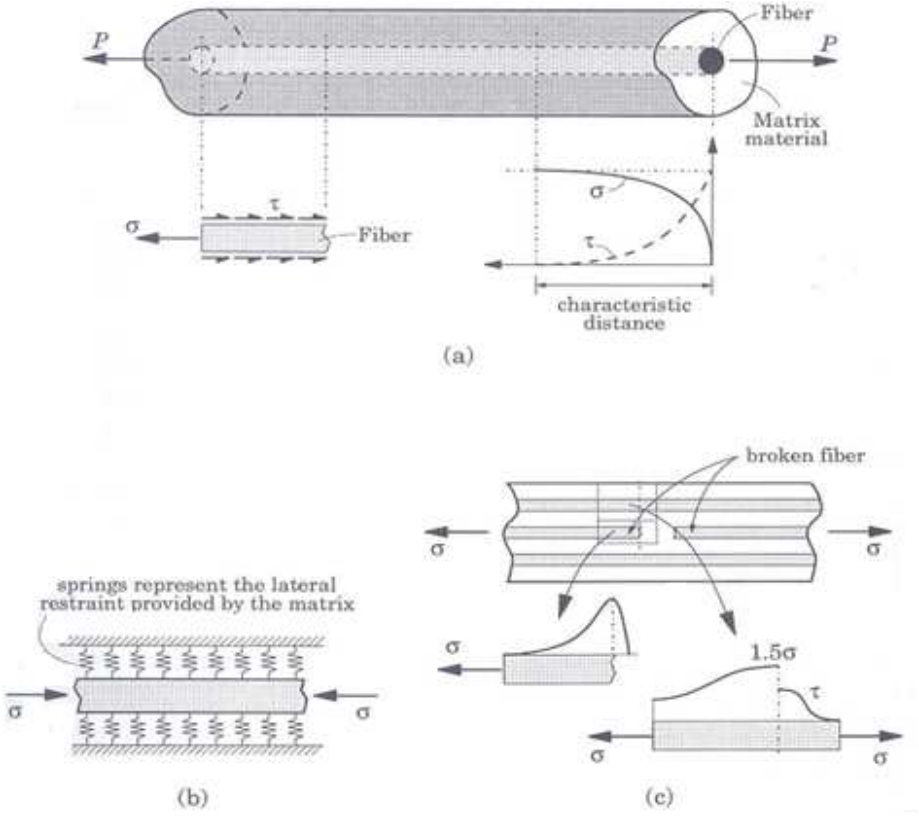

Figure 3.4 Load transfer and stress distribution in a single fibre embedded in a matrix material and subjected to an axial load [24].

The basic mechanism of load transfer between the matrix and a fibre can be explained by considering a bar of single fibre in a matrix material (figure 3.4). The load transfer

between the matrix material and fibre takes place through shear stress. When the applied load is tensile, shear stress τ develops on the outer surface of the fibre, and its magnitude decreases from a high value at the end of the fibre to zero at a distance from the end. The tensile stress σ in the fibre cross-section has the opposite trend, starting from zero value at the end of the fibre to the maximum at a distance from the end. The two stresses together balance the applied load, P. The distance from the free end to the point at which the normal stress attains its maximum and shear stress becomes zero is known as the characteristics distance. The pure tensile state continues along the rest of the fibre.

When a compressive load is applied, the stresses in the region of characteristic length are reversed in sign; in the compressive region, i.e., rest of the fibre length, the fibre tends to buckle, much like a wire subjected to compressive load. At this stage, the matrix provides a lateral support to reduce the tendency of the fibre to buckle (figure 3.4b). When a fibre is broken, the load carried by the fibre is transferred through shear stress to the neighboring two fibres (figure 3.4c), elevating the fibre axial stress level to a value of 1.5σ.

Definition of stress

Stress is the intensity of force per unit area (figure 3.5). It is given by

$$\sigma = \lim_{dA \to 0} \frac{P}{dA} \qquad (a)$$

Where, $\vec{P} = P_x i + P_y j + P_z k$ in its rectangular components

Definition of strain

Let $u = u(x, y, z)$ is the displacement along the x-axis at a point (x, y, z)

$v = v(x, y, z)$ is the displacement along the y-axis at a point (x, y, z)

$w = w(x, y, z)$ is the displacement along the z-axis at a point (x, y, z)

And the corresponding strain components of the above mentioned displacements are respectively ϵ_x, ϵ_y and ϵ_z. Then we have the following relationship between the strain components and the corresponding displacements:

$$\epsilon_x = \frac{\partial u}{\partial x}, \epsilon_y = \frac{\partial v}{\partial y}, and\ \epsilon_x = \frac{\partial w}{\partial z} \qquad (b)$$

$$\gamma_{xy} = \frac{\partial u}{\partial y} + \frac{\partial v}{\partial x}, \qquad \gamma_{xz} = \frac{\partial w}{\partial x} + \frac{\partial u}{\partial z}, and\ \gamma_{yz} = \frac{\partial w}{\partial y} + \frac{\partial v}{\partial z} \qquad (c)$$

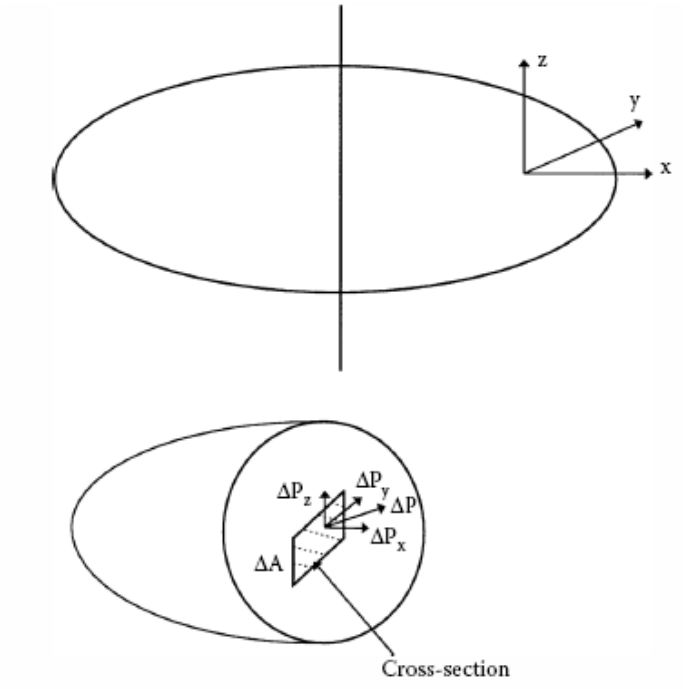

Figure 3.5 Forces on an infinitesimal area on the y-z plane [3]

3.2 ANISOTROPIC ELASTICITY

3.2.1 Derivation of the Orthotropic Elasticity Tensor

The general elasticity equation can be written as

$$\sigma_{ij} = C_{ijkl}\epsilon_{kl} \qquad (i,j,k,l = x,y,z) \tag{3.1}$$

where σ_{ij} is the second-order stress tensor, ϵ_{kl} is the second-order strain tensor, C_{ijkl} is the fourth order elasticity tensor, and $x, y,$ and z directions form a right-handed orthogonal co-ordinate system. The stress and strain tensors are each symmetric, i.e. $\sigma_{ij} = \sigma_{ji}$, and $\epsilon_{kl} = \epsilon_{lk}$

The general equation (3.1) may be written as

$$\begin{Bmatrix} \sigma_{xx} \\ \sigma_{yy} \\ \sigma_{zz} \\ \tau_{xy} \\ \tau_{xz} \\ \tau_{yz} \end{Bmatrix} = \begin{bmatrix} C_{11} & C_{12} & C_{13} & C_{14} & C_{15} & C_{16} \\ C_{21} & C_{22} & C_{23} & C_{24} & C_{25} & C_{26} \\ C_{31} & C_{32} & C_{33} & C_{34} & C_{35} & C_{36} \\ C_{41} & C_{42} & C_{43} & C_{44} & C_{45} & C_{46} \\ C_{51} & C_{52} & C_{53} & C_{54} & C_{55} & C_{56} \\ C_{61} & C_{62} & C_{63} & C_{64} & C_{65} & C_{66} \end{bmatrix} \begin{Bmatrix} \epsilon_{xx} \\ \epsilon_{yy} \\ \epsilon_{zz} \\ \gamma_{xy} \\ \gamma_{xz} \\ \gamma_{yz} \end{Bmatrix} \tag{3.2}$$

It is seen that the symmetry of the stress and strain tensor reduces the number of components of the elasticity tensor in three-dimensional space from 81 to 36 components.

If the strain energy density function, W, exists, where

$$W = \frac{1}{2}\sigma_{ij}\epsilon_{ij}$$

Such that

$$\frac{\partial w}{\partial \epsilon_{ij}} = \ C_{ijkl}\epsilon_{kl} = \sigma_{ij} \tag{3.3}$$

Then the independent components of elasticity tensor are reduced to 21, since eqn. (3.3) requires that $C_{ijkl} = C_{klij}$, or in the short hand notation, $C_{ij} = C_{ji}$. Eqn. (3.3) can be written as:

$$\begin{Bmatrix} \sigma_{xx} \\ \sigma_{yy} \\ \sigma_{zz} \\ \tau_{xy} \\ \tau_{xz} \\ \tau_{yz} \end{Bmatrix} = \begin{bmatrix} C_{11} & C_{12} & C_{13} & C_{14} & C_{15} & C_{16} \\ & C_{22} & C_{23} & C_{24} & C_{25} & C_{26} \\ & & C_{33} & C_{34} & C_{35} & C_{36} \\ & & & C_{44} & C_{45} & C_{46} \\ & 0 & & & C_{55} & C_{56} \\ & & & & & C_{66} \end{bmatrix} \begin{Bmatrix} \epsilon_{xx} \\ \epsilon_{yy} \\ \epsilon_{zz} \\ \gamma_{xy} \\ \gamma_{xz} \\ \gamma_{yz} \end{Bmatrix} \tag{3.4}$$

For materials having one plane of symmetry (monoclinic) the elasticity tensor has the following array, which involves 13 independent components.

$$\begin{Bmatrix} \sigma_{xx} \\ \sigma_{yy} \\ \sigma_{zz} \\ \tau_{xy} \\ \tau_{xz} \\ \tau_{yz} \end{Bmatrix} = \begin{bmatrix} C_{11} & C_{12} & C_{13} & 0 & 0 & C_{16} \\ & C_{22} & C_{23} & 0 & 0 & C_{26} \\ & & C_{33} & 0 & 0 & C_{36} \\ & & & C_{44} & C_{45} & 0 \\ & 0 & & & C_{55} & 0 \\ & & & & & C_{66} \end{bmatrix} \begin{Bmatrix} \epsilon_{xx} \\ \epsilon_{yy} \\ \epsilon_{zz} \\ \gamma_{xy} \\ \gamma_{xz} \\ \gamma_{yz} \end{Bmatrix} \tag{3.5}$$

Materials which have three mutually orthogonal planes of elasticity symmetry are called orthotropic (a short term for orthogonally anisotropic). For these orthotropic materials the elasticity tensor is written as follows where it is seen that for an orthotropic, three dimensional elastic body there are nine independent components. Hence nine independent elastic properties must be determined.

$$\begin{Bmatrix} \sigma_{xx} \\ \sigma_{yy} \\ \sigma_{zz} \\ \tau_{xy} \\ \tau_{xz} \\ \tau_{yz} \end{Bmatrix} = \begin{bmatrix} C_{11} & C_{12} & C_{13} & 0 & 0 & 0 \\ & C_{22} & C_{23} & 0 & 0 & 0 \\ & & C_{33} & 0 & 0 & 0 \\ & & & C_{44} & 0 & 0 \\ & 0 & & & C_{55} & 0 \\ & & & & & C_{66} \end{bmatrix} \begin{Bmatrix} \epsilon_{xx} \\ \epsilon_{yy} \\ \epsilon_{zz} \\ \gamma_{xy} \\ \gamma_{xz} \\ \gamma_{yz} \end{Bmatrix} \tag{3.6}$$

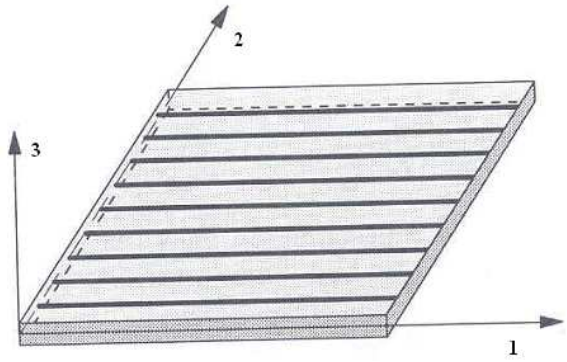

Figure 3.6 A unidirectional lamina with the material (local) coordinate system (1, 2, 3)

Unidirectional fibre composites can be regarded as orthotropic materials which possess three mutually orthogonal planes of symmetry. The directions perpendicular to these planes are called the material principal directions.

In general, we can summarize the number of independent elastic constants for various types of materials:

- Anisotropic: 21
- Monoclinic: 13
- Orthotropic: 9
- Transversely isotropic: 5
- Isotropic: 2

3.2.2 Reduction of the Constitutive Equation

For a three-dimensional body eqn. (3.2) can be written in compliance form and equivocally expressed in 1-2-3 orthogonal Cartesian coordinate system as

$$\begin{Bmatrix} \epsilon_1 \\ \epsilon_2 \\ \epsilon_3 \\ \gamma_{23} \\ \gamma_{31} \\ \gamma_{12} \end{Bmatrix} = \begin{bmatrix} S_{11} & S_{12} & S_{13} & S_{14} & S_{15} & S_{16} \\ S_{21} & S_{22} & S_{23} & S_{24} & S_{25} & S_{26} \\ S_{31} & S_{32} & S_{33} & S_{34} & S_{35} & S_{36} \\ S_{41} & S_{42} & S_{43} & S_{44} & S_{45} & S_{46} \\ S_{51} & S_{52} & S_{53} & S_{54} & S_{55} & S_{56} \\ S_{61} & S_{62} & S_{63} & S_{64} & S_{65} & S_{66} \end{bmatrix} \begin{Bmatrix} \sigma_1 \\ \sigma_2 \\ \sigma_3 \\ \tau_{23} \\ \tau_{31} \\ \tau_{12} \end{Bmatrix} \tag{3.7}$$

A unidirectional lamina falls under the orthotropic material category. If the lamina is thin and does not carry any out-of-plane loads, one can assume plane stress conditions for the lamina. Therefore, taking eqn. (3.7) and inverse of eqn. (3.6) and assuming, $\sigma_3, \tau_{23},$ and $\tau_{31} = 0$, then

$\epsilon_3 = S_{13}\sigma_1 + S_{23}\sigma_2, \gamma_{23} = \gamma_{31} = 0$

The normal strain ϵ_3 is not an independent strain because it is a function of the other two normal strains ϵ_1 and ϵ_2. Therefore, the normal strain, ϵ_3 can be omitted from the stress-strain relationship eqn. (3.7) or its inverse. Also, the shearing strains, $\gamma_{23}\ and\ \gamma_{31}$, can be omitted because they are zero. Inverting Equation (3.6) for an orthotropic plane stress problem, it can then be written as

$$\begin{Bmatrix}\epsilon_1\\ \epsilon_2\\ \gamma_{12}\end{Bmatrix}=\begin{bmatrix}S_{11} & S_{12} & 0\\ S_{21} & S_{22} & 0\\ 0 & 0 & S_{66}\end{bmatrix}\begin{Bmatrix}\sigma_1\\ \sigma_2\\ \tau_{12}\end{Bmatrix} \tag{3.8}$$

where, S_{ij} are the elements of the compliance matrix. Note the four independent compliance elements in the matrix.

Inverting eqn. (3.8) gives

$$\begin{Bmatrix}\sigma_1\\ \sigma_2\\ \tau_{12}\end{Bmatrix}=\begin{bmatrix}Q_{11} & Q_{12} & 0\\ Q_{21} & Q_{22} & 0\\ 0 & 0 & Q_{66}\end{bmatrix}\begin{Bmatrix}\epsilon_1\\ \epsilon_2\\ \gamma_{12}\end{Bmatrix} \tag{3.9}$$

Where, Q_{ij} are the reduced stiffness coefficients which are related to the compliance coefficients as

$$Q_{11}=\frac{S_{11}}{S_{11}S_{22}-{S_{12}}^2}=\frac{E_{11}}{1-\nu_{12}\nu_{21}} \tag{3.10}$$

$$Q_{12}=Q_{21}=\frac{S_{12}}{S_{11}S_{22}-{S_{12}}^2}=-\frac{\nu_{21}E_{11}}{1-\nu_{12}\nu_{21}}=\frac{\nu_{12}E_{22}}{1-\nu_{12}\nu_{21}} \tag{3.11}$$

$$Q_{22}=\frac{S_{22}}{S_{11}S_{22}-{S_{12}}^2}=\frac{E_{22}}{1-\nu_{12}\nu_{21}} \tag{3.12}$$

$$Q_{66}=\frac{1}{S_{66}}=G_{12} \tag{3.13}$$

where,

E_{11} = longitudinal young's modulus (in direction 1)

E_{22} = transverse young's modulus (in direction 2)

ν_{12} = Major poison's ratio, where the general poison's ratio, ν_{ij} is defined as the ratio of the negative of the normal strain in direction 'j' to the normal strain in direction 'i', when the only normal load is applied in direction 'i'

G_{12} = in-plane shear modulus (in plane 1–2)

3.2.3 Hook's Law for a Two-Dimensional Angle Lamina

Generally, a laminate does not consist only of unidirectional lamina because of their low stiffness and strength properties in the transverse direction. Therefore, in most laminates,

some lamina is placed at an angle. It is thus necessary to develop the stress-strain relationship for an angle lamina.

The coordinate system used for showing an angle lamina is as given in figure 3.7. The axes in the 1-2 coordinate systems are called the local axes or the material axes. The direction 1 is parallel to the fibers and the direction 2 is perpendicular to the fibers. The axes in the x-y coordinate system are called the global axes or the off-axes.

The angle between the two axes is denoted by an angle θ. The global and local stresses in an angle lamina are related to each other through the angle of the lamina, θ.

$$\begin{Bmatrix}\sigma_1\\ \sigma_2\\ \tau_{12}\end{Bmatrix}=[T]\begin{Bmatrix}\sigma_x\\ \sigma_y\\ \tau_{xy}\end{Bmatrix} \tag{3.14}$$

where $[T]$is called the transformation matrix and is defined as

$$[T]=\begin{bmatrix} m^2 & n^2 & 2mn\\ n^2 & m^2 & -2mn\\ -mn & mn & (m^2-n^2)\end{bmatrix} \tag{3.15}$$

$$m=cos\,\theta\,, n\ =\ sin\,\theta$$

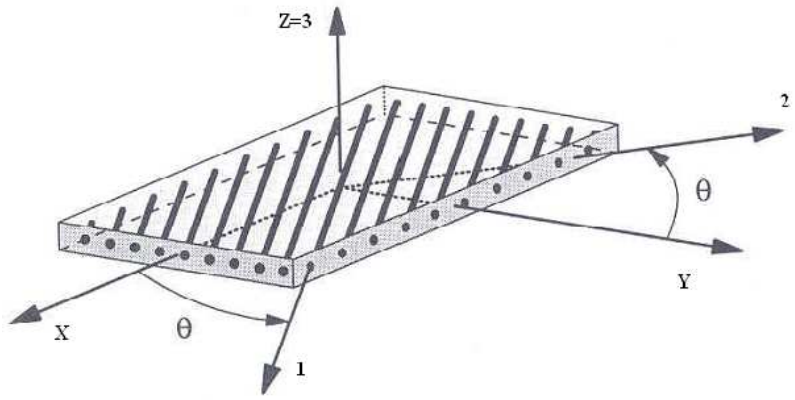

Figure 3.7 Local and global axes of an angle lamina [24]

Multiplying both sides of eqn. (3.14) by $[T]^{-1}$, and remembering that $[T][T]^{-1}=[I]$, then

$$\begin{Bmatrix}\sigma_x\\ \sigma_y\\ \tau_{xy}\end{Bmatrix}=[T]^{-1}\begin{Bmatrix}\sigma_1\\ \sigma_2\\ \tau_{12}\end{Bmatrix} \tag{3.16}$$

Substituting eqn. (3.9) into eqn. (3.16) results in

$$\begin{Bmatrix}\sigma_x\\ \sigma_y\\ \tau_{xy}\end{Bmatrix}=\ [T]^{-1}[Q]\begin{Bmatrix}\epsilon_1\\ \epsilon_2\\ \gamma_{12}\end{Bmatrix} \tag{3.17}$$

The global and local strains are also related through the transformation matrix

$$\begin{Bmatrix} \epsilon_1 \\ \epsilon_2 \\ \gamma_{12} \end{Bmatrix} = [T] \begin{Bmatrix} \epsilon_x \\ \epsilon_y \\ \gamma_{xy} \end{Bmatrix} \tag{3.18}$$

Finally substituting eqn. (3.18) into (3.17) results in the constitutive equations for a generally orthotropic lamina, that is to say a lamina composed of an orthotropic material in which the geometric and material axes are not aligned ($\theta \neq 0, 90^o, 180^o, 270^o$)

$$\begin{Bmatrix} \sigma_x \\ \sigma_y \\ \tau_{xy} \end{Bmatrix} = [T]^{-1}[Q][T] \begin{Bmatrix} \epsilon_x \\ \epsilon_y \\ \gamma_{xy} \end{Bmatrix} = [\bar{Q}] \begin{Bmatrix} \epsilon_x \\ \epsilon_y \\ \gamma_{xy} \end{Bmatrix} \tag{3.19}$$

where $[\bar{Q}]$is the generally orthotropic lamina stiffness matrix, whose components are given by

$$[\bar{Q}] = \begin{bmatrix} \bar{Q}_{11} & \bar{Q}_{12} & \bar{Q}_{16} \\ \bar{Q}_{12} & \bar{Q}_{22} & \bar{Q}_{26} \\ \bar{Q}_{16} & \bar{Q}_{26} & \bar{Q}_{66} \end{bmatrix} \tag{3.20}$$

3.2.4 Stress-Strain Relationship in a Laminate

A lamina (also called a ply or layer) is a single flat layer of unidirectional fibers or woven fibers arranged in a matrix. It is the building block of a laminate. A laminate is a stack of plies of composites. Each layer can be laid at various orientations and can be made up of different material systems. The stiffness, strengths, and hygrothermal properties of a laminate will depend on:

- Elastic moduli
- The staking position
- Thickness
- Angle of orientation
- Coefficients of thermal expansion
- Coefficients of moisture expansion of each individual lamina

3.2.4.1 Laminate Code

Each layer in a laminate is identified by:

- Its location in a laminate
- Its material
- Its angle of orientation with respect to reference axes

Each lamina is represented by the angle of ply and separated from other plies by slash sign. The first ply is the bottom of the laminate.

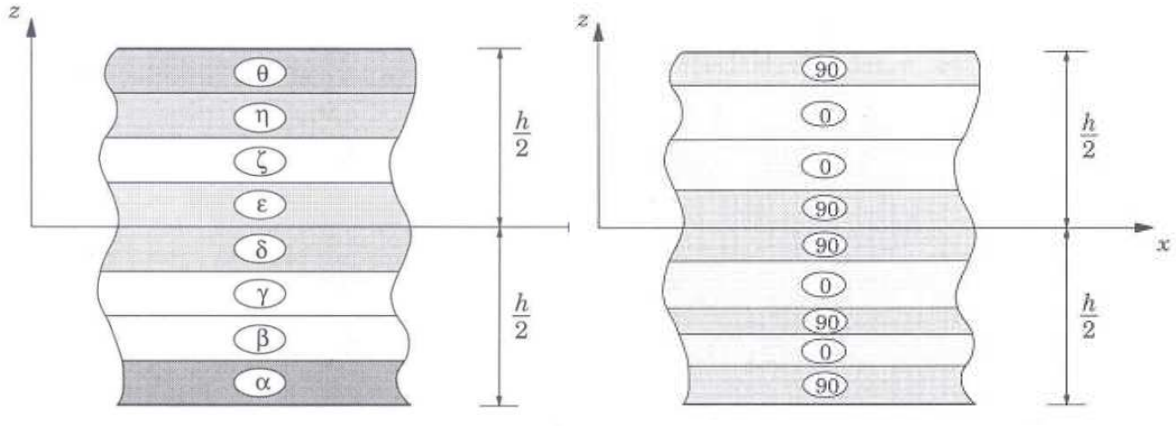

(a) (b)

Figure 3.8 Laminate Stacking Sequence, (a) a laminate with general stacking sequence, (b) a cross ply laminate with a **0** and $\mathbf{90^0}$ layers [24]

The lamination scheme of a laminate will be denoted by $[\alpha/\beta/\gamma/\,\delta/\varepsilon/\ldots]$, where α the orientation of the first ply, β is the orientation of the second ply, and so on (figure 3.8(a)). The plies are counted in the positive z direction. [90/0/90/0/90/90…] denotes the code for the above (figure 3.8(b)) laminate. It consists of nine plies, each of which has different angle to the reference x-axis. A slash separates each lamina. The above code also implies that each ply is made of the same material and is of the same thickness.

3.2.4.2 Strain-Displacement Relationship

The following assumptions are made in the classical lamination theory to develop the relationships:

- Each lamina is orthotropic.
- Each lamina is homogeneous.
- A line straight and perpendicular to the middle surface remains straight and perpendicular to the middle surface during deformation($\gamma_{xz} = \gamma_{yz} = 0$).
- The laminate is thin and is loaded only in its plane($\sigma_z = \tau_{xz} = \tau_{yz} = 0$).
- Displacements are continuous and small throughout the laminate
- Each lamina is elastic.
- No slip occurs between the lamina interfaces.

At any point other than the mid-plane, the two displacements in the x-y plane will depend on the axial location of the point and the slope of the laminate mid-plane with the x and y-directions. For example, as shown in figure 3.9

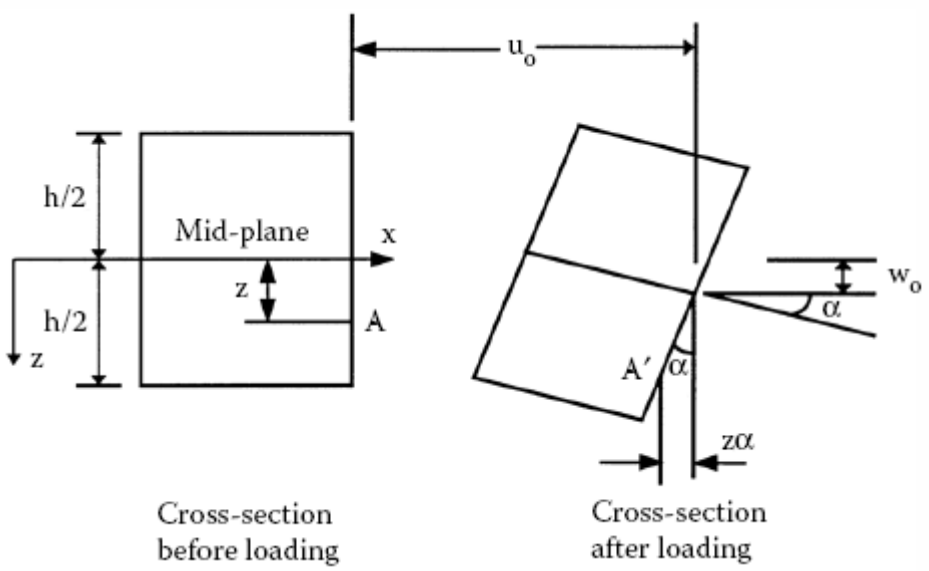

Figure 3.9 Relationship between mid-plane displacements and curvatures [3]

$u = u_o - z\alpha$, where, z-is the location from the mid-plane

$$\alpha = \frac{\partial w_o}{\partial x}$$

$$\frac{\partial u}{\partial x} = \frac{\partial u_o}{\partial x} - z\frac{\partial^2 w_o}{\partial x^2}$$

$$\epsilon_x = \frac{\partial u}{\partial x} = \frac{\partial u_o}{\partial x} - z\frac{\partial^2 w_o}{\partial x^2} \tag{3.21}$$

$$\epsilon_y = \frac{\partial v}{\partial y} = \frac{\partial v_o}{\partial y} - z\frac{\partial^2 w_o}{\partial y^2} \tag{3.22}$$

$$\gamma_{xy} = \frac{\partial u}{\partial y} + \frac{\partial v}{\partial x} = \frac{\partial u_o}{\partial y} + \frac{\partial v_o}{\partial x} - 2z\frac{\partial^2 w_o}{\partial x \partial y} \tag{3.23}$$

From (3.21), (3.22) and (3.23) the strain displacement equation in matrix form becomes:

$$\begin{Bmatrix} \epsilon_x \\ \epsilon_y \\ \gamma_{xy} \end{Bmatrix} = \begin{Bmatrix} \frac{\partial u_o}{\partial x} \\ \frac{\partial v_o}{\partial y} \\ \frac{\partial u}{\partial y} + \frac{\partial v}{\partial x} \end{Bmatrix} + z \begin{Bmatrix} -\frac{\partial^2 w_o}{\partial x^2} \\ -\frac{\partial^2 w_o}{\partial y^2} \\ -2\frac{\partial^2 w_o}{\partial x \partial y} \end{Bmatrix} \tag{3.24}$$

mid-plane strain *mid-plane curvature*

Laminate strain can be written as:

$$\begin{Bmatrix} \epsilon_x \\ \epsilon_y \\ \gamma_{xy} \end{Bmatrix} = \begin{Bmatrix} \epsilon_x^0 \\ \epsilon_y^0 \\ \gamma_{xy}^o \end{Bmatrix} + z \begin{Bmatrix} \kappa_x \\ \kappa_y \\ \kappa_{xy} \end{Bmatrix} \tag{3.25}$$

Equation (3.25) shows linear relation between strains in the laminate to the curvatures of the laminate. Where, z= the distance from the mid-plane of the point in the laminate (figure 3.9).

3.2.4.3 Laminates of Composite Materials

Having formulated the constitutive relations for a lamina composed of a generally orthotropic material, eqns. (3.19), and (3.20), the next step is to derive the constitutive relations accruing from bonding several laminas together, each with any general orientation of material axes and composed of any material system.

Substituting eqn. (3.25) in to (3.19) we obtain

$$\begin{Bmatrix} \sigma_x \\ \sigma_y \\ \tau_{xy} \end{Bmatrix} = \begin{bmatrix} \overline{Q}_{11} & \overline{Q}_{12} & \overline{Q}_{16} \\ \overline{Q}_{12} & \overline{Q}_{22} & \overline{Q}_{26} \\ \overline{Q}_{16} & \overline{Q}_{26} & \overline{Q}_{66} \end{bmatrix} \begin{Bmatrix} \epsilon_x^0 \\ \epsilon_y^0 \\ \gamma_{xy}^o \end{Bmatrix} + z \begin{bmatrix} \overline{Q}_{11} & \overline{Q}_{12} & \overline{Q}_{16} \\ \overline{Q}_{12} & \overline{Q}_{22} & \overline{Q}_{26} \\ \overline{Q}_{16} & \overline{Q}_{26} & \overline{Q}_{66} \end{bmatrix} \begin{Bmatrix} \kappa_x \\ \kappa_y \\ \kappa_{xy} \end{Bmatrix} \tag{3.26}$$

Where for $m = cos\,\theta, n = sin\,\theta$

$\overline{Q}_{11} = Q_{11}m^4 + 2(Q_{12} + 2Q_{66})m^2n^2 + Q_{22}n^4$

$\overline{Q}_{22} = Q_{11}n^4 + 2(Q_{12} + 2Q_{66})m^2n^2 + Q_{22}m^4$

$\overline{Q}_{12} = (Q_{11} + Q_{22} - 2Q_{12} - 2Q_{66})\, m^2n^2 + Q_{66}(m^4 + n^4)$

$\overline{Q}_{16} = (Q_{11} - Q_{12} - 2Q_{66})\, nm^3 + (Q_{12} - Q_{22} + 2Q_{66})\, n^3m$

$\overline{Q}_{26} = (Q_{11} - Q_{12} - 2Q_{66})\, n^3m + (Q_{12} - Q_{22} + 2Q_{66})\, nm^3$

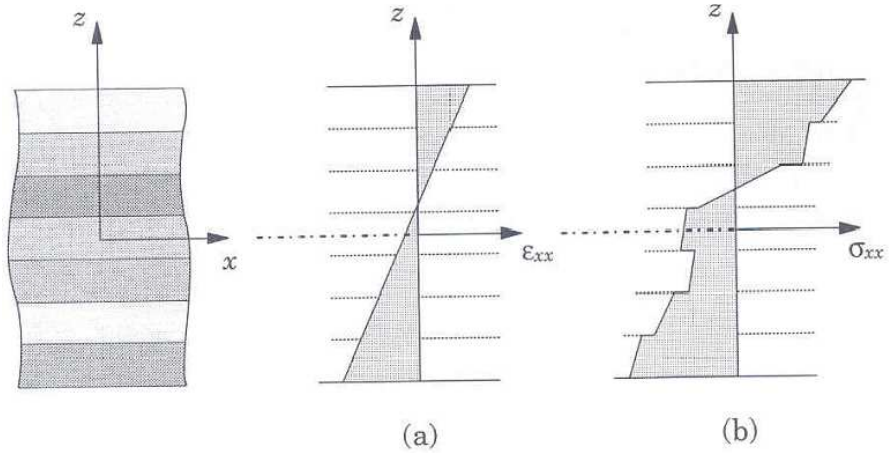

Figure 3.10 Variation of strains and stresses through the layer and laminate thickness.

(a) Variation of a typical in plane strain. (b) Variation of corresponding stress [24]

Thus, if the middle surfaces displacements and the lateral displacement are obtained, eqn. (3.26) is used to compute the stresses at any location in any of the lamina. The stresses variation of eqn. (3.26) is shown in figure 3.10.

3.2.4.4 Loads related to mid plane strain and curvatures

The mid-plane strains and shell curvatures in eqn. (3.25) are the unknowns for finding the lamina strains and stresses. However, eqn. (3.26) gives the stresses in each lamina in terms of these unknowns. The stresses in each lamina can be integrated through the laminate thickness to give resultant forces and moments (or applied forces and moments) as shown in figure 3.11. The forces and moments applied to a laminate will be known, so the mid-plane strains and shell curvatures can then be found. This relationship between the applied loads and the mid-plane strains and curvatures is developed in this section.

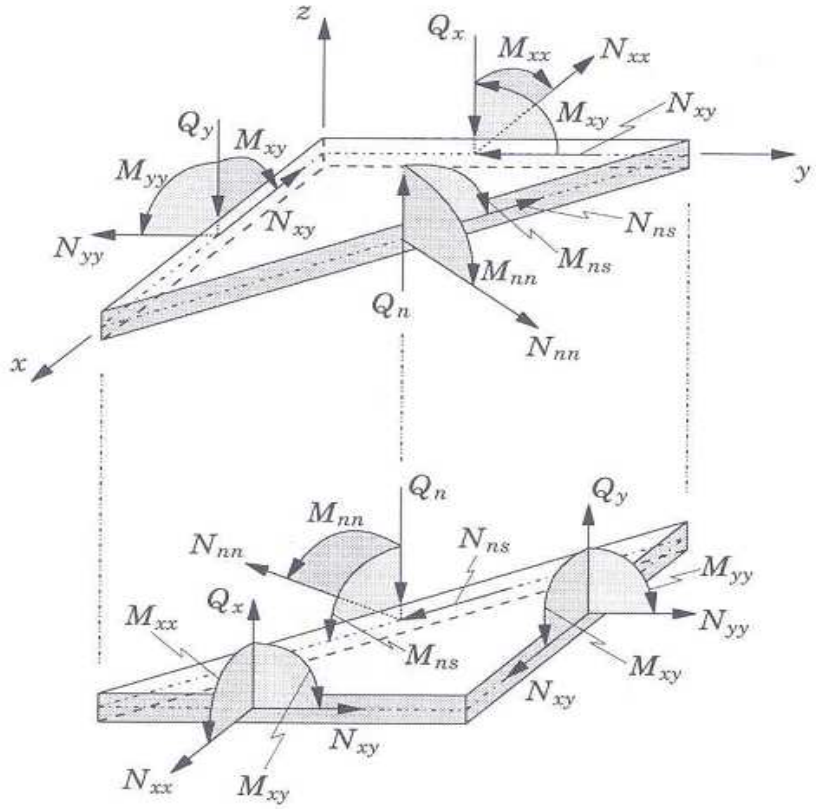

Figure 3.11 Resultant forces and moments on a laminate [24]

Consider a laminate made of 'n' plies shown in figure 3.12, each ply has a thickness of t_k. then the total thickness of the laminate 'h' is:

$$h = \sum_{k=1}^{n} t_k \tag{3.27}$$

Then, the location of the mid-plane is $h/2$ from the top or the bottom surface of the laminate. The z-axis is taken positive upward from the mid-plane. The k^{th} layer is located between the points $z = z_k$ and $z = z_{k+1}$ in the thickness direction. The top surface and bottom surfaces are represented each by $z = h/2$ and $-h/2$ respectively.

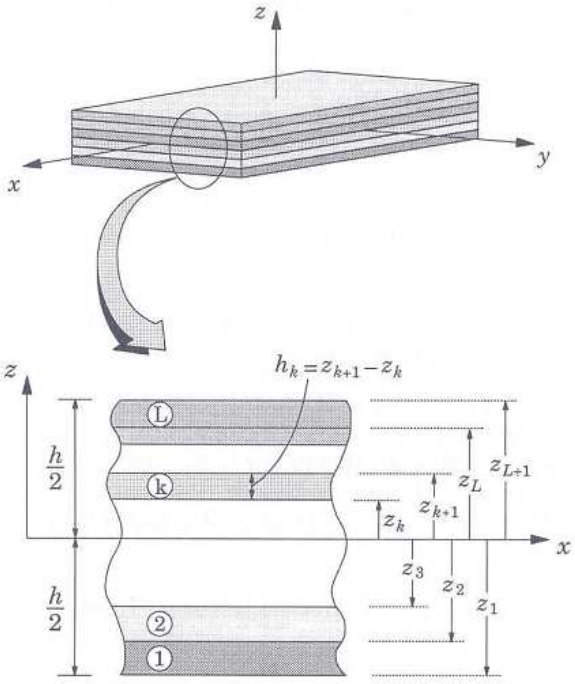

Figure 3.12 Coordinate system and layer numbering used for a typical laminate plate [24]

Integrating the global stresses in each lamina give the resultant forces per unit length in x-y plane through the laminate thickness.

$$N_x = \int_{-\frac{h}{2}}^{\frac{h}{2}} \sigma_x dz \tag{3.28}$$

$$N_y = \int_{-\frac{h}{2}}^{\frac{h}{2}} \sigma_y dz \tag{3.29}$$

$$N_{xy} = \int_{-\frac{h}{2}}^{\frac{h}{2}} \tau_{xy} dz \tag{3.30}$$

where, N_x, N_y - normal forces per unit length.

N_{xy}- shear force per unit length

$h/2$ - half thickness of the laminate

Similarly, the resultant moment will be (x-y plane)

$$M_x = \int_{-\frac{h}{2}}^{\frac{h}{2}} \sigma_x z d \tag{3.31}$$

$$M_y = \int_{-\frac{h}{2}}^{\frac{h}{2}} \sigma_y z dz \tag{3.32}$$

$$M_{xy} = \int_{-\frac{h}{2}}^{\frac{h}{2}} \tau_{xy} z dz \tag{3.33}$$

where M_x, M_y - bending moments per unit length.

M_{xy}, - twisting moment per unit length

From eqns. (3.28) through (3.33) for a laminate can be written in a matrix form

$$\begin{bmatrix} N_x \\ N_y \\ N_{xy} \end{bmatrix} = \int_{-\frac{h}{2}}^{\frac{h}{2}} \begin{bmatrix} \sigma_x \\ \sigma_y \\ \sigma_{xy} \end{bmatrix} dz \tag{3.34}$$

$$\begin{bmatrix} M_x \\ M_y \\ M_{xy} \end{bmatrix} = \int_{-\frac{h}{2}}^{\frac{h}{2}} \begin{bmatrix} \sigma_x \\ \sigma_y \\ \sigma_{xy} \end{bmatrix} z dz \tag{3.35}$$

However, for a laminated plate the stresses that are integrated across the thickness of the plate or shell are the sum of the stresses across each lamina, or, the in-plane stress resultants can be written as using eqn. (3.26) [24].

$$\begin{bmatrix} N_x \\ N_y \\ N_{xy} \end{bmatrix} = \sum_{k=1}^{n} \int_{h_{k-1}}^{h_k} \begin{bmatrix} \sigma_x \\ \sigma_y \\ \sigma_{xy} \end{bmatrix} dz$$

$$= \sum_{k=1}^{n} \int_{h_{k-1}}^{h_k} \left[\begin{bmatrix} \overline{\mathrm{Q}}_{11} & \overline{\mathrm{Q}}_{12} & \overline{\mathrm{Q}}_{16} \\ \overline{\mathrm{Q}}_{12} & \overline{\mathrm{Q}}_{22} & \overline{\mathrm{Q}}_{26} \\ \overline{\mathrm{Q}}_{16} & \overline{\mathrm{Q}}_{26} & \overline{\mathrm{Q}}_{66} \end{bmatrix} \begin{Bmatrix} \epsilon_{\mathrm{x}}^0 \\ \epsilon_{\mathrm{y}}^0 \\ \gamma_{\mathrm{xy}}^{\mathrm{o}} \end{Bmatrix} \right] dz + \sum_{k=1}^{n} \int_{h_{k-1}}^{h_k} \left[\begin{bmatrix} \overline{\mathrm{Q}}_{11} & \overline{\mathrm{Q}}_{12} & \overline{\mathrm{Q}}_{16} \\ \overline{\mathrm{Q}}_{12} & \overline{\mathrm{Q}}_{22} & \overline{\mathrm{Q}}_{26} \\ \overline{\mathrm{Q}}_{16} & \overline{\mathrm{Q}}_{26} & \overline{\mathrm{Q}}_{66} \end{bmatrix} \begin{Bmatrix} \kappa_{\mathrm{x}} \\ \kappa_{\mathrm{y}} \\ \kappa_{\mathrm{xy}} \end{Bmatrix} \right] z dz \tag{3.36}$$

Similarly

$$\begin{bmatrix} M_x \\ M_y \\ M_{xy} \end{bmatrix} = \sum_{k=1}^{n} \int_{h_{k-1}}^{h_k} \begin{bmatrix} \sigma_x \\ \sigma_y \\ \sigma_{xy} \end{bmatrix} z dz = \sum_{k=1}^{n} \int_{h_{k-1}}^{h_k} \left[\begin{bmatrix} \overline{\mathrm{Q}}_{11} & \overline{\mathrm{Q}}_{12} & \overline{\mathrm{Q}}_{16} \\ \overline{\mathrm{Q}}_{12} & \overline{\mathrm{Q}}_{22} & \overline{\mathrm{Q}}_{26} \\ \overline{\mathrm{Q}}_{16} & \overline{\mathrm{Q}}_{26} & \overline{\mathrm{Q}}_{66} \end{bmatrix} \begin{Bmatrix} \epsilon_{\mathrm{x}}^0 \\ \epsilon_{\mathrm{y}}^0 \\ \gamma_{\mathrm{xy}}^{\mathrm{o}} \end{Bmatrix} \right] z \, dz +$$

$$\sum_{k=1}^{n} \int_{h_{k-1}}^{h_k} \left[\begin{bmatrix} \overline{\mathrm{Q}}_{11} & \overline{\mathrm{Q}}_{12} & \overline{\mathrm{Q}}_{16} \\ \overline{\mathrm{Q}}_{12} & \overline{\mathrm{Q}}_{22} & \overline{\mathrm{Q}}_{26} \\ \overline{\mathrm{Q}}_{16} & \overline{\mathrm{Q}}_{26} & \overline{\mathrm{Q}}_{66} \end{bmatrix} \begin{Bmatrix} \kappa_{\mathrm{x}} \\ \kappa_{\mathrm{y}} \\ \kappa_{\mathrm{xy}} \end{Bmatrix} \right] z^2 dz \tag{3.37}$$

However, since mid-plane strain $[\epsilon^o]$ and mid-plane curvature $[\kappa]$ are not functions of z and within each lamina $[\bar{Q}]_k$ is not a function of z, eqns. (3.36), and (3.37) can be written as

$$\begin{bmatrix} N_x \\ N_y \\ N_{xy} \end{bmatrix} = \left\{ \sum_{k=1}^{n} [\bar{Q}]_k \int_{h_{k-1}}^{h_k} dz \right\} [\epsilon^o] + \left\{ \sum_{k=1}^{n} [\bar{Q}]_k \int_{h_{k-1}}^{h_k} dz \right\} [\kappa] \tag{3.38}$$

$$\begin{bmatrix} M_x \\ M_y \\ M_{xy} \end{bmatrix} = \left\{ \sum_{k=1}^{n} [\bar{Q}]_k \int_{h_{k-1}}^{h_k} z dz \right\} [\epsilon^o] + \left\{ \sum_{k=1}^{n} [\bar{Q}]_k \int_{h_{k-1}}^{h_k} z^2 dz \right\} [\kappa] \tag{3.39}$$

Or finally

$$\begin{bmatrix} N_x \\ N_y \\ N_{xy} \end{bmatrix} = \begin{bmatrix} A_{11} & A_{12} & A_{16} \\ A_{12} & A_{22} & A_{26} \\ A_{16} & A_{26} & A_{66} \end{bmatrix} \begin{Bmatrix} \epsilon_x^0 \\ \epsilon_y^0 \\ \gamma_{xy}^o \end{Bmatrix} + \begin{bmatrix} B_{11} & B_{12} & B_{16} \\ B_{12} & B_{22} & B_{26} \\ B_{16} & B_{26} & B_{66} \end{bmatrix} \begin{Bmatrix} \kappa_x \\ \kappa_y \\ \kappa_{xy} \end{Bmatrix} \tag{3.40}$$

$$\begin{bmatrix} M_x \\ M_y \\ M_{xy} \end{bmatrix} = \begin{bmatrix} B_{11} & B_{12} & B_{16} \\ B_{12} & B_{22} & B_{26} \\ B_{16} & B_{26} & B_{66} \end{bmatrix} \begin{Bmatrix} \epsilon_x^0 \\ \epsilon_y^0 \\ \gamma_{xy}^o \end{Bmatrix} + \begin{bmatrix} D_{11} & D_{12} & D_{16} \\ D_{12} & D_{22} & D_{26} \\ D_{16} & D_{26} & D_{66} \end{bmatrix} \begin{Bmatrix} \kappa_x \\ \kappa_y \\ \kappa_{xy} \end{Bmatrix} \tag{3.41}$$

Where

$$A_{ij} = \sum_{k=1}^{n} \left[\left(\bar{Q}_{ij} \right) \right]_k (h_k - h_{k-1}) \qquad i,j = 1,2,6 \tag{3.42}$$

$$B_{ij} = \frac{1}{2} \sum_{k=1}^{n} \left[\left(\bar{Q}_{ij} \right) \right]_k (h_k^2 - h_{k-1}^2) \qquad i,j = 1,2,6 \tag{3.43}$$

$$D_{ij} = \frac{1}{3} \sum_{k=1}^{n} \left[\left(\bar{Q}_{ij} \right) \right]_k (h_k^3 - h_{k-1}^3) \qquad i,j = 1,2,6 \tag{3.44}$$

The [A], [B], and [D] matrices are called the extensional, coupling, and bending stiffness matrices, respectively. Combining eqns. (3.40) and (3.41) gives six simultaneous equations and six unknowns.

$$\begin{bmatrix} N_x \\ N_y \\ N_{xy} \\ M_x \\ M_y \\ M_{xy} \end{bmatrix} = \begin{bmatrix} A_{11} & A_{12} & A_{16} & B_{11} & B_{12} & B_{16} \\ A_{12} & A_{22} & A_{26} & B_{12} & B_{22} & B_{26} \\ A_{16} & A_{26} & A_{66} & B_{16} & B_{26} & B_{66} \\ B_{11} & B_{12} & B_{16} & D_{11} & D_{12} & D_{16} \\ B_{12} & B_{22} & B_{26} & D_{12} & D_{22} & D_{26} \\ B_{16} & B_{26} & B_{66} & D_{16} & D_{26} & D_{66} \end{bmatrix} \begin{pmatrix} \epsilon_x^0 \\ \epsilon_y^0 \\ \gamma_{xy}^o \\ \kappa_x \\ \kappa_y \\ \kappa_{xy} \end{pmatrix} \tag{3.45}$$

The extensional stiffness matrix [A] relates the resultant in-plane forces to the in-plane strains, and the bending stiffness matrix [D] relates the resultant bending moments to the plate curvatures. The coupling stiffness matrix [B] couples the force and moment terms to the mid-plane strains and mid-plane curvatures. Eqn. (3.45) will be used later in the modeling of the shell structure.

3.2.4.5 Special types laminates

There are variety types of special laminates like symmetric laminates, cross-ply laminates, angle-ply laminates, anti-symmetric laminates, and balanced laminates. From now on wards cross-ply laminates will be used.

Cross-Ply Laminates

A laminate is called a cross-ply laminate (also called laminates with specially orthotropic layers) if only 0 and 90° plies were used to make a laminate. An example of a cross-ply laminate is a [0/90/0/90/0] laminate:

For cross-ply laminates, A_{16}= 0, A_{26}= 0, B_{16}= 0, B_{26}= 0, D_{16} = 0, and D_{26} = 0. Thus, eqn. (3.45) can be written as

$$\begin{bmatrix} N_x \\ N_y \\ N_{xy} \\ M_x \\ M_y \\ M_{xy} \end{bmatrix} = \begin{bmatrix} A_{11} & A_{12} & 0 & B_{11} & B_{12} & 0 \\ A_{12} & A_{22} & 0 & B_{12} & B_{22} & 0 \\ 0 & 0 & A_{66} & 0 & 0 & B_{66} \\ B_{11} & B_{12} & 0 & D_{11} & D_{12} & 0 \\ B_{12} & B_{22} & 0 & D_{12} & D_{22} & 0 \\ 0 & 0 & B_{66} & 0 & 0 & D_{66} \end{bmatrix} \begin{pmatrix} \epsilon_x^0 \\ \epsilon_y^0 \\ \gamma_{xy}^o \\ \kappa_x \\ \kappa_y \\ \kappa_{xy} \end{pmatrix} \tag{3.46}$$

In these cases, decoupling occurs between the normal and shear forces, as well as between the bending and twisting moments. If a cross-ply laminate is also symmetric, then in addition to the preceding uncoupling, the coupling matrix $[B_{ij}]$ = 0 and no coupling takes place between the force and moment terms.

3.2.4.6 Failure Condition of Laminates

Like any isotropic materials there are different failure conditions for laminates. Some of these are maximum normal stress theory of failure, von misses theory of failure, normal strain theory of failure and others. These failure conditions are customized to predict failures of composite structures.

The Tsai-Hill failure theory is derived from the von Misses distortional energy yield criterion for isotropic materials but is applied to anisotropic materials with the appropriate modifications. In this theory, failure is assumed to occur whenever the distortional yield energy equals or exceeds a certain value related to the strength of the lamina. In this theory, there is no distinction between the tensile and compressive strengths [22].

The Tsai-Hill failure theory is written mathematically for the lamina as follows:

$$\frac{\sigma_1^2}{(\sigma_1^F)^2} - \frac{\sigma_1\sigma_2}{(\sigma_1^F)^2} + \frac{\sigma_2^2}{(\sigma_2^F)^2} + \frac{\tau_{12}^2}{(\tau_{12}^F)^2} \leq 1 \qquad (3.47)$$

where,

σ_1, σ_2 - is the applied stress in the principal direction 1 and 2 respectively

σ_1^F, σ_2^F - is the ultimate tensile strength in the Principal direction 1 and 2 respectively

τ_{12} - is the applied shear stress in plane 1-2

τ_{12}^F - is the ultimate shear strength in plane 1-2

3.3 SURFACE CRACKS

3.3.1 Introduction to Surface Crack

In recent years the increasing use of composite plates in many engineering structures and specially in the aero-space industry has brought up the need for more intensive stress analysis of anisotropic materials. Up to 1986 no completely analytical solution of the related failure problems has been available due to the inherent difficulties involving the stress analysis and material characterization. In many cases the failure is attributed to the growth of cracks or crack-like flaws which exist in the structure. During the 1970's and 1980's many investigators have studied the stress state in the immediate neighborhood of the crack tip since the local fracture of a structure appears to be governed mainly by this stress field. The singular behavior of the stress state near the crack-tip as characterized by the stress intensity factor depends on the magnitude of the external loads, the configuration of the body including the crack size and shape, and the material properties. Problems of a surface crack in a structural component which may locally be represented by "plate" or "shell" have long attracted the attention of investigators who have been interested in fracture mechanics. In the mentioned decades there has been some renewed interest in the line-spring model, (which was originally developed by Rice) for solving surface crack problems in plates and shells [28].

3.3.2 A Surface Crack Review: Elastic and Elastic-Plastic Behavior

The scope of mechanics and material behavior phenomenon relevant to a discussion of fracture in general, or surface cracks in particular, is too broad to review in this thesis, however, it is possible to survey major developments in both the analysis and the experimental characterization of surface flaws.

In discussing analytical aspects of the surface crack, we are immediately struck by the fact that the geometrical complexity of three dimensions all but precludes closed-form continuum analysis, so that computational or analytical tools become the means for constructing solutions. The array of such tools, as well as their adaptability, power, and precision, has vastly expanded in the 1990's [30].

The major use to which these tools have been put is the quantification of asymptotically dominant crack-front stress and deformation fields. In the context of the surface crack, this includes, for example, the variation of crack front stress intensity factors $K_I(s), K_{II}(s)$, and $K_{III}(s)$ of linear-elastic fracture mechanics (LEFM), and the J integral variation, $J(s)$, in nonlinear elastic fracture mechanics (NLEFM) for quasi-stationary crack fronts. If such single parameter asymptotic characterizations actually dominate the complete near crack front fields (including the zone of operative microfracture processes) in a surface cracked geometry, then crack growth exhibited in the surface crack may be expected to be similar to that obtained in, for example, a through cracked two dimensional (2-D) laboratory specimens of the same material loaded to the same dominant asymptotic field strength. Indeed, such correlations form the practical basis of nearly all fracture mechanics approaches.

At least three important caveats regarding the justification of dominant singularity based cracking correlations between through crack and surface crack configurations should be noted. First, the notion of maintaining single parameter dominance of the crack tip fields driving microstructural fracture processes such as void growth and cleavage is somewhat fuzzily defined. For example, it is difficult to answer precisely the question, when is the plastic zone too large to use LEFM? Careful interpretation of information generated by experimental and analytical studies of the surface crack can, however, provide guidance as to inherent parametric limits of applicability of dominant singularity approaches. Second, the gradients in deformation intensity along the surface crack fronts are often substantially greater than in nominally 2-D through crack geometries. This feature can stabilize the

process of cracking. Finally, it is implicitly assumed in fracture mechanics based correlation of cracking that there are similar distributions of operable fracture process sites along respective crack fronts.

Analytical/Computational tools

Three classes of analytical/computational tools are seen as having major or potentially major impact on the understanding of the mechanics of surface cracks. These are identified as dealing with linear elasticity, with virtual crack extension formulations for J evaluation, and with the development of simplified models. Each class of tool is reviewed.

Linear Elastic Fracture Mechanics

Many conceptual aspects of fracture mechanics are common to linear elastic, as well as nonlinear material behavior, so analytical procedures based on them are likewise independent of material behavior. On the other hand, special properties of solutions in linear elasticity, such as superposition, can be exploited effectively by specially tailored tools. In view of the overwhelming preponderance and relative importance of linear elastic behavior in engineering aspects of surface cracks, several specialized approaches have been developed.

The task of engineering stress analysis in LEFM is to evaluate numerically $K_I(s)$ [and $K_{II}(s)$, $K_{III}(s)$ if present] for a given body containing crack(s) of a given shape and size, subject to various loadings. There are many methods for obtaining such calibrations. While exact elasticity solutions have been obtained for many configurations, the complexity of 3-D surface crack geometries has required the use of numerical methods such as singular integral equations, boundary integral equations, finite differences and the finite element method.

Singular Integral Formulations- A powerful tool for 2-D elastic crack analysis is based on the representation of a crack by a continuous distribution of dislocations. The technique can be notionally appreciated by considering the opening profile of a crack along the axis as approximated by a finite element number of opening (and closing) steps. An important limitation of such techniques, however, has been the difficulty associated with finite boundaries (other than the cracks themselves).

Virtual crack extension and domain integrals

One of the most broadly applicable and widely used computational tools in fracture mechanics analysis is based on virtual perturbations of the crack front. This approach has permitted very accurate evaluations of $J(s)$ to be obtained in 3-D configurations such as surface cracks while using relatively coarse discretizations.

Simplified Models

The geometric and parametric complexities of surface crack problems remain as formidable obstacles for exact continuum solutions, even if they are obtained with the aid of powerful computers executing sophisticated computational algorithms. In engineering practice, there is great need for simplified mechanics models of surface crack behavior which approximately account for major observed features. However, the scope and quantitative effects of the assumptions made in constructing a simplified model may be difficult to determine a priori. There is also an element of style to modeling: one person's model may be another's empirical correlation.

If we bear these points in mind, attention is limited to two classes of simplified models which have had great impact on the understanding of surface crack behavior: the line spring and the plastic hinge idealizations of part-through circumferentially cracked pipes in bending.

Line-spring analysis of surface cracked shells

Part-through cracks in plates and shells are an important class of surface crack configurations encountered in engineering practice. Although detailed 3-D analysis of these problems (using, for example, the VCE method) is possible, such detailed modeling generally requires extensive computational time and (equally important) large amounts of data preparation in the form of mesh generation and input deck creation. Some time ago, Rice and Levy [31] introduced a simplified line-spring model for approximate analysis of such problems, which Parks and coworkers and others have recently applied and extended. In general, K and J results from the solutions compare favorably (say, within ~10% or so) with results of detailed continuum solutions, but typically involve one to two orders of magnitude less computer and data preparation time.

Consider the surface cracked plate of thickness t shown schematically in figure 3.13. The presence of the surface crack introduces an additional compliance into the structure which

is accounted for in the model by introducing a distributed foundation along the cut of length equal to the surface projection, $2c$, of the surface crack. In symmetric structures, the generalized shell resultants which the foundation transmits are a moment M and a membrane force N per unit length. Work-conjugate variables are relative separation, δ, and relative rotation, θ, of the two sides of the model through-crack. The compliance of the distributed foundation at any position s along the cut depends on local crack depth, $a(s)$, at that point. More precisely, the foundation compliance at s is equated to the cracked compliance of a single-edge notched (SEN) specimen of the same material having thickness t and crack depth a equal to $a(s)$, and subject to combined tension and bending.

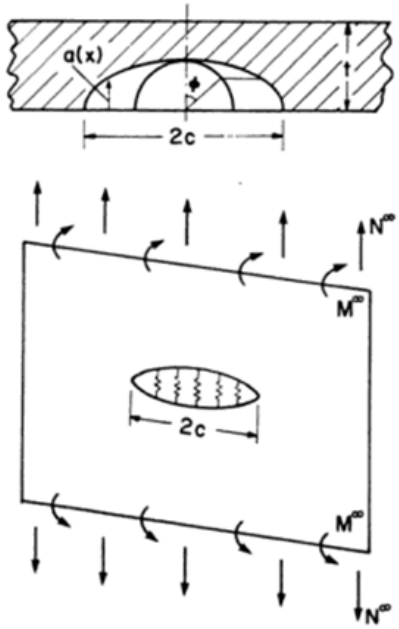

Figure 3.13 Schematic cross section of a surface crack with varying depth of $\boldsymbol{a(x)}$ and projected length $\boldsymbol{2c}$ in a shell of thickness $\boldsymbol{t}$ [30]

Let the force variables (N, M) be denoted by $Q_\alpha, \alpha = 1,2$ and work-conjugate displacement $(\delta, \theta) = q_\alpha$. Total and incremental displacements are additively decomposed into elastic and plastic parts

$$q_\alpha = q_\alpha^e + q_\alpha^p \tag{3.48}$$

and

$$dq_\alpha = dq_\alpha^e + dq_\alpha^p \tag{3.49}$$

The assumed stress intensity factor calibration of the SEN specimen under tension and bending is

$$K_I = \sqrt{\pi\alpha} \times \left[\frac{N}{t}.F_1\left({}^{a}/_{t}\right) + \frac{6M}{t^2}.F_2\left({}^{a}/_{t}\right)\right] \tag{3.50}$$

Approximate formulae for the function F_α can be obtained, for example from Tada *et al*. [32]. For elastic response, the line-spring has been generalized to include mixed mode loading on a surface crack [32]. Within the context of the line-spring, K_{II} loading of a surface cracked shell is due to the transverse shear force V, which is generally relatively small compared to typical membrane forces. Mode K_{III} loading of the line-spring is caused by both the membrane shear force Q and the twisting moment, T, in the shell.

3.3.3 The Surface Crack Problem in an Orthotropic Plate under Bending and Tension

In their study [28] the elasticity problem for an infinite orthotropic flat plate containing a series of through and part-through cracks and subjected to bending and tension loads has been considered. The problem was formulated by using Reissner's plate bending theory and considering three dimensional material orthotropy. The line-spring model developed by Rice and Levy [31] has been used to formulate the surface crack problem in which a total of nine material constants have been used. Here it is presented their formulation to determine the stress intensity factor for surface crack problems in plates and shells subjected to bending and tension.

3.3.3.1 The Governing Equations for an Orthotropic Plate under Bending and Tension

In this section a brief derivation of the fundamental equations for an orthotropic plate under bending and in-plane stretching is given. The problem of bending and the problem of in-plane loading are uncoupled. The material of the plate is assumed to be orthotropic with principal axes or orthotropy parallel to the coordinate axes. Thus the strain-stress relations may be expressed as

$$\begin{Bmatrix} \epsilon_{xx} \\ \epsilon_{yy} \\ \epsilon_{zz} \\ \epsilon_{yz} \\ \epsilon_{xz} \\ \epsilon_{xy} \end{Bmatrix} = \begin{bmatrix} S_{11} & S_{12} & S_{13} & 0 & 0 & 0 \\ S_{21} & S_{22} & S_{23} & 0 & 0 & 0 \\ S_{31} & S_{32} & S_{33} & 0 & 0 & 0 \\ 0 & 0 & 0 & S_{44} & 0 & 0 \\ 0 & 0 & 0 & 0 & S_{55} & 0 \\ 0 & 0 & 0 & 0 & 0 & S_{66} \end{bmatrix} \begin{Bmatrix} \sigma_{xx} \\ \sigma_{yy} \\ \sigma_{zz} \\ \sigma_{yz} \\ \sigma_{xz} \\ \sigma_{xy} \end{Bmatrix} \tag{3.51}$$

where the quantities S_{ij} characterize elastic properties of the plate material.

The plate under bending

The bending problem is based on the Reissner's plate theory [34]. Consider a thin elastic plate bounded by the planes $z = \pm h/2$. The resultant forces are shown in figure 3.14,

where M_{ij}, and V_{ij} ($i, j = x, y$) are respectively the moment and transverse shear resultants.

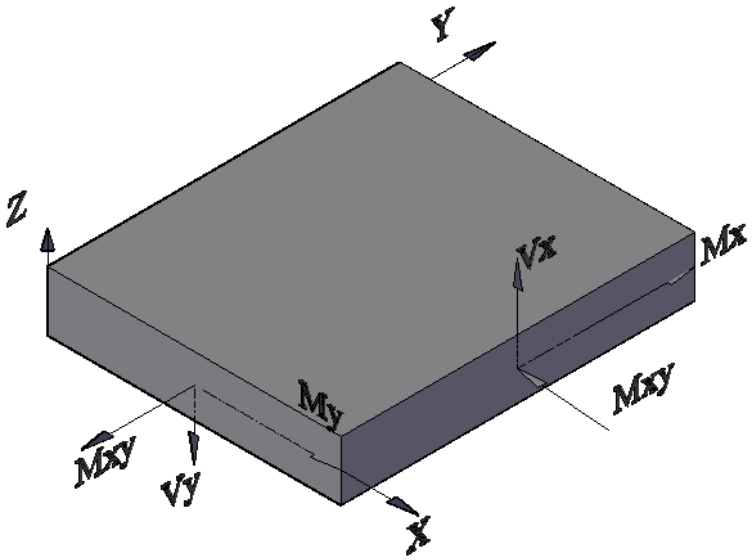

Figure 3.14 Notation for moment and transverse shear resultants

The equilibrium equations may be expressed as

$$\frac{\partial M_x}{\partial x} + \frac{\partial M_{xy}}{\partial y} - V_x = 0 \tag{3.52}$$

$$\frac{\partial M_y}{\partial y} + \frac{\partial M_{xy}}{\partial x} - V_y = 0 \tag{3.53}$$

$$\frac{\partial V_x}{\partial x} + \frac{\partial M_y}{\partial y} + q = 0 \tag{3.54}$$

and, in terms of the moment and shear resultants, the stress components are given by

$$\sigma_{xx} = \frac{M_x z}{h^3/12}, \sigma_{yy} = \frac{M_y z}{h^3/12}, \sigma_{xy} = \frac{M_{xy} z}{h^3/12},$$

$$\sigma_{xz} = \frac{3V_x}{2h}\left[1 - \frac{4z^2}{h^2}\right], \sigma_{yz} = \frac{3V_y}{2h}\left[1 - \frac{4z^2}{h^2}\right], \tag{3.55}$$

$$\sigma_{zz} = \frac{3q}{4}\left[\frac{2z}{h} - \frac{8z^3}{3h^3} + \frac{2}{3}\right]$$

The displacement fields assumed are [29]:

$$u(x, y, z) = u^o(x, y) + z\varphi_x(x, y)$$

$$v(x, y, z) = v^o(x, y) + z\varphi_y(x, y) \tag{3.56}$$

$$w = w^o(x, y)$$

where u, v, and w are the displacement components in the x, y and z directions respectively. u^o, v^o are the displacement components in x and y directions of reference

plane ($z = 0$) and φ_x and φ_y are the rotations of the sections of $x =$ constant and $y =$ constant.

Also, the following relations between some average values w, φ_x and φ_y and the displacements u^o, v^o and w^o are introduced in accordance with the balance of the work done by the resultant forces on the average values and by the corresponding stresses on the actual displacements

$$w = \frac{3}{2h}\int_{-\frac{h}{2}}^{+\frac{h}{2}} \mathrm{w^o}\left[1 - \frac{4z^2}{h^2}\right]dz$$

$$\varphi_x = \frac{6}{h^2}\int_{-\frac{h}{2}}^{+\frac{h}{2}} \mathrm{u^o}\frac{z}{h/2}\,dz \qquad (3.57)$$

$$\varphi_y = \frac{6}{h^2}\int_{-\frac{h}{2}}^{+\frac{h}{2}} \mathrm{v^o}\frac{z}{h/2}\,dz$$

From eqn. (3.51) and the strain-displacement relations it follows that:

$$\begin{Bmatrix}\epsilon_{xx}\\ \epsilon_{yy}\\ \epsilon_{zz}\\ \epsilon_{yz}\\ \epsilon_{xz}\\ \epsilon_{xy}\end{Bmatrix} = \begin{Bmatrix}\frac{\partial u_o}{\partial x}\\ \frac{\partial v_o}{\partial y}\\ \frac{\partial w_o}{\partial z}\\ \frac{\partial w_o}{\partial y}+\frac{\partial v_o}{\partial z}\\ \frac{\partial u_o}{\partial z}+\frac{\partial w_o}{\partial x}\\ \frac{\partial u_o}{\partial y}+\frac{\partial v_o}{\partial x}\end{Bmatrix} = \begin{bmatrix} S_{11} & S_{12} & S_{13} & 0 & 0 & 0\\ S_{21} & S_{22} & S_{23} & 0 & 0 & 0\\ S_{31} & S_{32} & S_{33} & 0 & 0 & 0\\ 0 & 0 & 0 & S_{44} & 0 & 0\\ 0 & 0 & 0 & 0 & S_{55} & 0\\ 0 & 0 & 0 & 0 & 0 & S_{66}\end{bmatrix}\begin{Bmatrix}\sigma_{xx}\\ \sigma_{yy}\\ \sigma_{zz}\\ \sigma_{yz}\\ \sigma_{xz}\\ \sigma_{xy}\end{Bmatrix} \qquad (3.58)$$

If we now solve eqn. (3.58) for σ_{ij} $(i, j = x, y, z)$, substitute into eqn. (3.55), integrate in z and use eqn. (3.57) we obtain:

$$M_x = \frac{h^3}{12}[S_{22}S_{11} - S_{12}S_{12}]^{-1}\left[\left(S_{22}\frac{\partial\varphi_x}{\partial x} - S_{12}\frac{\partial\varphi_y}{\partial y}\right) + (S_{12}S_{23} - S_{22}S_{13})\frac{6q}{5h}\right],$$

$$M_y = \frac{h^3}{12}[S_{22}S_{11} - S_{12}S_{12}]^{-1}\left[\left(S_{11}\frac{\partial\varphi_y}{\partial y} - S_{21}\frac{\partial\varphi_x}{\partial x}\right) + (S_{12}S_{13} - S_{23}S_{11})\frac{6q}{5h}\right], \qquad (3.59)$$

$$M_{xy} = \frac{h^3}{12}(S_{66})^{-1}\left(\frac{\partial\varphi_x}{\partial y} + \frac{\partial\varphi_y}{\partial x}, \varphi_x = -\frac{\partial w}{\partial x} + S_{55}\frac{6V_x}{5h}, \varphi_y = -\frac{\partial w}{\partial y} + S_{44}\frac{6V_y}{5h}\right.$$

Technically eqns. (3.52-3.54) and (3.59) would give the complete formulation of the problem, the eight equations accounting for the eight variables, M_x, M_y, M_{xy}, V_x, V_y, φ_x, φ_y and w. Eliminating first, φ_x and φ_y then $M_x, M_y,$ and M_{xy} and assuming $q = 0$, we obtain the system of equations governing the small deflection of elastic orthotropic plates as follows:

$$V_{x,x} + V_{y,y} = 0,$$
$$V_x + A_1 V_{x,xx} + A_2 V_{x,yy} - A_3 w_{,xxx} - A_4 w_{,yyx} = 0, \tag{3.60}$$
$$V_y + A_5 V_{y,xx} + A_6 V_{y,yy} - A_7 w_{,xxy} - A_8 w_{,yyy} = 0,$$

where the A_i are constants defined in the appendix of [28]. The remaining unknowns can be obtained from

$$\varphi_x = -w_{,x} + \frac{6S_{55}}{5h} V_x, \qquad \varphi_y = -w_{,y} + \frac{6S_{44}}{5h} V_y \tag{3.61}$$

$$M_x = -\frac{h^3}{12\kappa}\left(S_{22} w_{,xx} - S_{12} w_{,yy}\right) + \frac{h^2}{10\kappa}\left(S_{22}S_{55} - S_{12}S_{44}\right) V_{x,x}$$
$$M_y = -\frac{h^3}{12\kappa}\left(S_{11} w_{,yy} - S_{12} w_{,xx}\right) + \frac{h^2}{10\kappa}\left(S_{11}S_{44} - S_{12}S_{55}\right) V_{y,y} \tag{3.62}$$
$$M_{xy} = -\frac{h^3}{12S_{66}} w_{,xy} + \frac{h^2}{10S_{66}}\left(S_{55} V_{x,y} - S_{44} V_{y,x}\right)$$

where $\kappa = S_{11}S_{22} - S_{12}S_{12}$

Note that since the basic system of eqn. (3.60) is sixth order, three conditions must be prescribed on the boundary of the plate.

Following [35], to simplify this bending problem a stress function $F(x, y)$ is introduced as follows:

$$w = F_{,y} + A_1 F_{,xxy} + A_2 F_{,yyy}$$
$$V_x = A_3 F_{,xxxy} + A_4 F_{,xyyy} \tag{3.63}$$
$$V_y = -A_3 F_{,xxxx} - A_4 F_{,xxyy}$$

Then eqn. (3.60) are identically satisfied provided the stress function $F(x, y)$ satisfies the following equation:

$$B_1 \frac{\partial^4 F}{\partial x^4} + B_2 \frac{\partial^4 F}{\partial x^2 \partial y^2} + B_3 \frac{\partial^4 F}{\partial y^4} + B_4 \frac{\partial^6 F}{\partial x^6} + B_5 \frac{\partial^6 F}{\partial x^4 \partial y^2} + B_6 \frac{\partial^6 F}{\partial x^2 \partial y^4} + B_7 \frac{\partial^6 F}{\partial y^6} = 0 \tag{3.64}$$

where the B_i are known constants defined in the appendix of [28]

Eqn. (3.64) is called the fundamental equation. It is essentially a special case of that given in [35]

In-plane stretching problem

Beginning with the usual plane stress assumption

$\sigma_{zz} = \sigma_{zx} = \sigma_{zy} = 0$

We define the Airy stress function $\Phi(x, y)$ as follows:

$$\sigma_{xx} = \frac{\partial^2 \Phi}{\partial y^2}, \sigma_{yy} = \frac{\partial^2 \Phi}{\partial x^2}, \sigma_{xy} = \frac{\partial^2 \Phi}{\partial x \partial y}$$

Along with the stress-strain relation eqn. (3.51), the compatibility condition for an orthotropic plate may be expressed as:

$$\frac{\partial^4 \Phi}{\partial x^4} + 2C_1 \frac{\partial^4 \Phi}{\partial x^2 \partial y^2} + C_2^2 \frac{\partial^4 \Phi}{\partial y^4} \qquad (3.65)$$

where,

$$C_1 = \frac{S_{66}}{2S_{22}} + \frac{S_{12}}{S_{22}}, C_2 = \left(\frac{S_{11}}{S_{22}}\right)^{1/2}$$

The fourth order differential eqn. (3.65) is subject to two conditions on the plate boundary. As we know, the solutions satisfying eqn. (3.65) yield the following characteristic equation

$$m^4 + 2C_1 m^2 + C_2^2 = 0 \qquad (3.65a)$$

The roots of eqn. (3.65) are

$$m_1 = q_1 + iq_2$$

$$m_2 = q_3 + iq_4 \qquad (3.65b)$$

$$m_3 = -m_1, m_4 = -m_2$$

where m_1 and m_2 are both real or complex conjugates. The material is defined as type 1 when both roots are real and as type 2 when they are complex conjugates.

Eqns. (3.64) and (3.65) give the governing equations for an orthotropic plate subjected to bending and in-plane stretching.

3.3.3.2 The line-spring model for surface crack

The most general description of the line-spring model introduced in [31] has been given in [36]. In a plate containing a part-through crack and subjected to membrane and bending

loads, the net ligament (the uncracked portion) around the crack would generally have a constraining effect on the crack surface displacement. By approximately representing the net-ligament stress as a membrane load N and a bending moment M and the crack surface displacement due to N and M as an opening δ and a rotation θ, the three-dimensional crack problem could be reduced to a two-dimensional coupled bending-membrane plate problem. Furthermore, assuming that the relationship between (N, M) and (δ, θ)may be found through the plane strain results obtained from the solution of an edge-notched strip, the pair of functions (δ, θ) and (N, M), then, are determined from the corresponding mixed boundary value problem for a plate having a through crack in which N and M are treated as unknown crack surface loads.

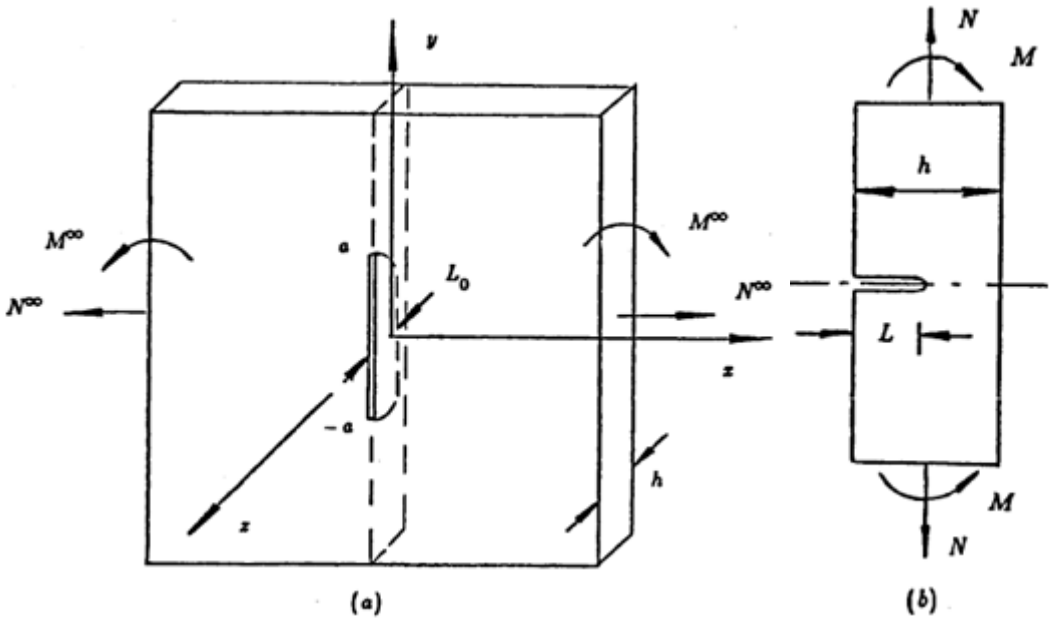

Figure 3.15 Notation for the part-through surface crack [28]

Let the stress intensity factor for the plane strain problem in figure 3.15 be given as

$$K(\delta) = \sqrt{h}[\sigma_t g_t(\delta) + \sigma_b g_b(\delta)] \tag{3.66}$$

$$\delta(y) = L(y)/h \tag{3.67}$$

where functions $g_b(\delta)$ and $g_t(\delta)$ are called the shape functions for tension and bending, respectively and given as:

$$\mathrm{g_t}(\delta) = \sqrt{\pi\delta}\sum_{\mathrm{i=1}}^{\mathrm{n}} \mathrm{AT_i}\,\delta^{2(i-1)}, \mathrm{g_b}(\delta) = \sqrt{\pi\delta}\sum_{\mathrm{i=1}}^{\mathrm{n}} \mathrm{AB_i}\,\delta^{2(i-1)} \tag{3.68}$$

The coefficients $\mathrm{AT_i}$ and $\mathrm{AB_i}$ can be found by applying a suitable curve fitting to the results obtained from [37] which are valid for $0 < L_o/h < 0.8$.

The strain energy release rate G, in an orthotropic medium may be obtained as:

$$G_I = K_I^2 \left(\frac{\mathrm{b}_{11}\mathrm{b}_{22}}{2}\right)^{1/2} \left[\left(\frac{\mathrm{b}_{22}}{\mathrm{b}_{11}}\right)^{1/2} + \frac{2\mathrm{b}_{12} + \mathrm{b}_{66}}{2\mathrm{b}_{11}}\right]^{1/2} = K_I^2 \, 1/\mu_3 \tag{3.69}$$

where

K_I is the stress intensity factor and the elastic constants b_{ij} are given by (see eqn. (3.51))

$$\mathrm{b}_{11} = \frac{S_{33}S_{22} - S_{23}}{S_{22}}, \mathrm{b}_{22} = \frac{S_{11}S_{22} - S_{12}S_{12}}{S_{22}}, \mathrm{b}_{12} = \mathrm{S}_{55}, \qquad \mathrm{b}_{11} = \frac{S_{13}S_{22} - S_{12}S_{23}}{S_{22}}$$

$$\mu_3 = \left(\frac{\mathrm{b}_{11}\mathrm{b}_{22}}{2}\right)^{-1/2} \left[\left(\frac{\mathrm{b}_{22}}{\mathrm{b}_{11}}\right)^{1/2} + \frac{2\mathrm{b}_{12} + \mathrm{b}_{66}}{2\mathrm{b}_{11}}\right]^{-1/2} \tag{3.70}$$

Also, the energy available for fracture can be expressed as:

$$G_I = \frac{\partial}{\partial L}(U - V) = \frac{1}{2}\left(N\frac{\partial \delta}{\partial L} + M\frac{\partial \theta}{\partial L}\right) \tag{3.71}$$

Combining now eqn. (3.69) and (3.71) and using (3.66) we obtain:

$$\frac{1}{\mu_3}(\sigma_t^2 g_t^2 + 2\sigma_t\sigma_b \mathrm{g_b g_t} + \sigma_b^2 g_b^2) = \frac{1}{2}\left[\sigma_t \frac{\partial}{\partial L}(h\delta) + \sigma_b \frac{\partial}{\partial L}\left(\frac{h^2\theta}{6}\right)\right] \tag{3.72}$$

From eqn. (3.72) it can be shown that

$$\frac{h}{6}\theta = 2h\frac{1}{\mu_3}(\alpha_{bb}\sigma_b + \alpha_{bt}\sigma_t), \delta = 2h\frac{1}{\mu_3}(\alpha_{tb}\sigma_b + \alpha_{tt}\sigma_t) \tag{3.73}$$

where α_{ij} are the compliance coefficients and are given by

$$\alpha_{ij} = \frac{1}{h}\int_0^L g_i g_j \, dL, \qquad (i, j = b, t) \tag{3.74}$$

Defining new unknown functions G_1 and G_2 [28] as

$$G_1(y) = \frac{\partial}{\partial y}\varphi_x(0, y) \qquad -\infty < y < +\infty \tag{3.75a}$$

$$G_2(y) = \frac{\partial}{\partial y}u(0^+, y) \tag{3.75b}$$

From eqn. (3.75a) and (3.75b) it may be seen that

$$\theta = 2\varphi_x(0, y) = 2\int_{a_i}^{y} G_1(t)\, dt, \qquad \delta = 2u(0, y) = 2\int_{a_i}^{y} G_2(t)\, dt \tag{3.76}$$

where a_i $(\mathrm{i} = 1, \ldots, \mathrm{n})$ defines the crack along y axis for collinear cracks

Solving eqn. (3.73) for σ_t and σ_b and substituting from (3.76), we obtain

$$M_y = \frac{h^2}{6}\sigma_b = \mu_3\left[\frac{h^2}{36}\gamma_{bb}\int_{a_i}^{y} G_1(t)\,dt + \frac{h}{6}\gamma_{bt}\int_{a_i}^{y} G_2(t)\,dt\right] \tag{3.77a}$$

$$N_y = h\sigma_t = \mu_3\left[\frac{h}{6}\gamma_{tb}\int_{a_i}^{y} G_1(t)\,dt + \gamma_{tt}\int_{a_i}^{y} G_2(t)\,dt\right] \tag{3.77b}$$

$$\gamma_{bb} = \frac{\alpha_{bb}}{\Delta}, \qquad \gamma_{bt} = -\frac{\alpha_{bt}}{\Delta}, \qquad \gamma_{tb} = -\frac{\alpha_{tb}}{\Delta}, \qquad \gamma_{tt} = \frac{\alpha_{tt}}{\Delta}$$

$$\Delta = \alpha_{bb}\alpha_{tt} - {\alpha_{bt}}^2 \tag{3.78}$$

As seen from eqn. (3.77) in the surface crack problem the integral equation for bending and tension are coupled. One should keep in mind that $\alpha_{ij,}$, consequently γ_{ij}, are functions of $L(y)/y$ and that $L(y)$ describes the surface crack profile

As an example let us now consider a plate containing a single surface crack, as shown in figure 3.15. By using this model, the crack may be assumed to be a through crack of length 2a and the constraint caused by the net ligament may be accounted for by applying the membrane and bending resultants $N(y)$ and $M(y)$ on the crack surfaces. One may note that these net ligament stresses tend to prevent the crack face from opening and rotating. The mixed boundary condition and the integral equations given in [28] may be expressed as:

$$M_{xx}(0,y) = G_1(y) + M(y), \qquad -a < y < a \tag{3.79a}$$

$$\varphi_x(0,y) = 0 \qquad |y| > a \tag{3.79b}$$

and

$$N_{xx}(0,y) = G_2(y) + N(y), \qquad -a < y < a \tag{3.80a}$$

$$u(0,y) = 0 \qquad |y| > a \tag{3.80b}$$

$$\mu_1\int_{-a}^{a}\left[\frac{1}{t-y} + k(y,t)\right]G_1(t)\,dt = p_1(y) + M(y), \qquad |y| > a \tag{3.81}$$

$$\mu_2\int_{-a}^{a}\left[\frac{1}{t-y}\right]G_2(t)\,dt = p_2(y) + N(y) \qquad |y| < a \tag{3.82}$$

where μ_1, μ_2 are material constants, $p_1(y)$, $p_2(y)$ and $k(y,t)$ are defined in [28]

$M(y), N(y)$ are defined in eqn. (3.77)

Single Surface Cracks

Referring to figure 3.15, assuming the plate subjected to the uniform bending M^∞ and tension N^∞ and introducing the following change in variables

$$\tau = \frac{t}{a} \qquad -a < (t, y) < a$$
$$\delta = \frac{y}{a} \qquad -1 < (\tau, \delta) < 1 \tag{3.83}$$
$$G_i(t) = g_i(\tau) \qquad (i = 1,2)$$
$$k(y,t) = k_1(\delta, \tau)$$

From eqn. (3.81-3.82) and using (3.77), we obtain:

$$\mu_3 \frac{h^2}{36} \gamma_{bb} a \int_{-1}^{\delta} g_1(\tau)\, d\tau - \mu_1 \int_{-1}^{1} \left[\frac{1}{\tau - \delta} + a k_1(\delta, \tau)\right] g_1(\tau)\, d\tau + \mu_3 \frac{h}{6} \gamma_{bt} a \int_{-1}^{\delta} g_2(\tau)\, d\tau = M^{\infty} \tag{3.84a}$$

$$\mu_3 \frac{h}{6} \gamma_{tb} a \int_{-1}^{\delta} g_1(\tau)\, d\tau - \mu_2 \int_{-1}^{1} \frac{1}{\tau - \delta} g_2(\tau)\, d\tau + \mu_3 \gamma_{tt} a \int_{-1}^{\delta} g_2(\tau)\, d\tau = N^{\infty} \tag{3.84b}$$

Eqn. (3.84) may be solved numerically. The two most commonly known numerical methods for solving such singular integral equations are quadrature method and collocation method [29]

After solving eqn. (3.84) for g_1 and g_2 the stress and moment resultants $M(y)$, $N(y)$ may be obtained from eqn. (3.77), and the stress intensity factor $K(y)$ along the crack front is then determined from eqn. (3.66).

CHAPTER FOUR

MODELING OF THE CYLINDERICAL SHELL STRUCTURE

4.1 Mathematical Modeling

Mathematical modeling is the activity devoted to the study of the simulation of physical phenomena by computational processes. The goal of the mathematical simulation is to predict the behavior of some product within its environment. Mathematical modeling subsumes a number of activities, as illustrated by figure 4.1.

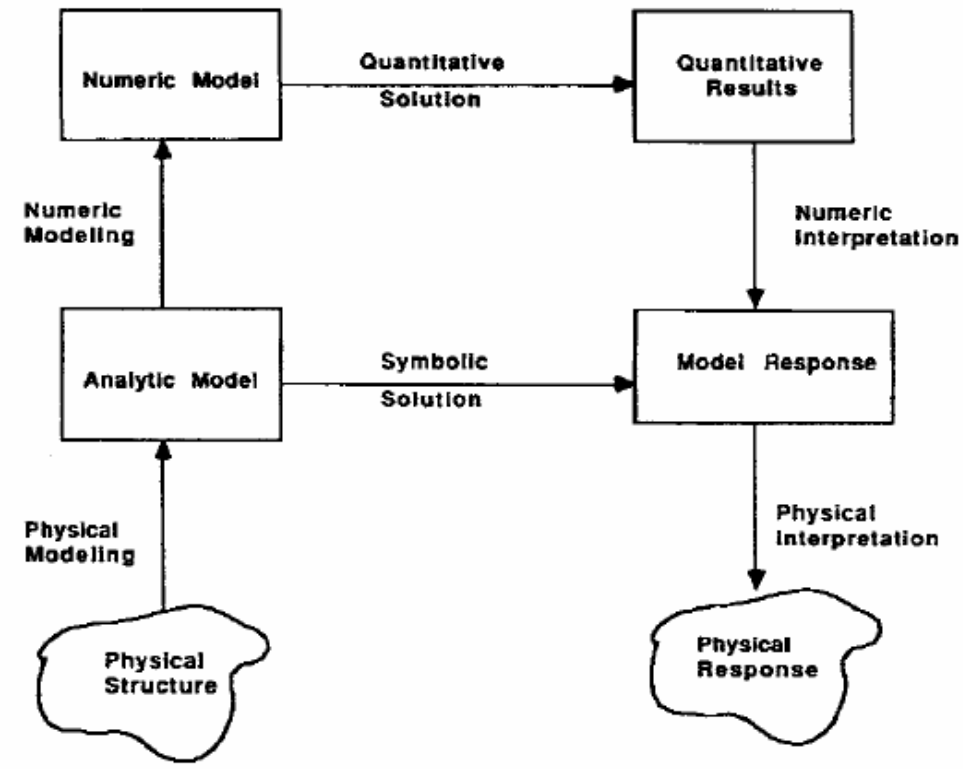

Figure 4.1 Mathematical Modeling Processes [38]

The mathematical modeling activities presented include model generation, interpretation of numerical results, and development and control of numerical algorithms as a series of interrelated activities.

All mechanical models are characterized mathematically by very complex expressions, many of which, until the advent of electronic computation, stood outside the reach of the scientific and engineering communities. Recently, the computer has made it possible to solve many problems of mechanics, dramatically expanding the capabilities for mathematical modeling [33].

We will first consider here a first order shear deformation theory applicable to laminated cylindrical shells of shallow curvature, shown in figure 4.2. The thickness and in-plane dimensions of the shell are denoted by h, a, and b respectively. The displacements in the x, θ, and z are denoted by u, v, and w respectively. The radius, R, is assumed to be much larger than the thickness, h. In addition, transverse shear strains γ_{xz} and $\gamma_{\theta z}$ are no longer negligible, although the thickness strain ϵ_z is neglected.

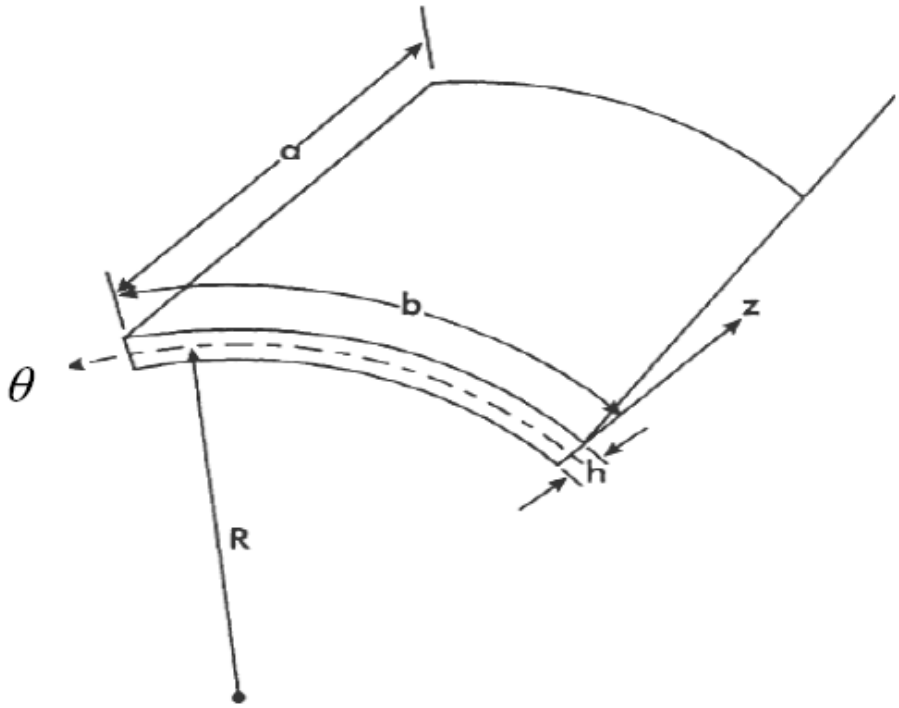

Figure 4.2 Nomenclature for cylindrical shell [33]

The classical theory of elasticity gives the following strain-displacement relations applicable to the geometry shown in figure 4.2 [33].

$$\varepsilon_x = \frac{\partial u}{\partial x}, \varepsilon_\theta = \frac{1}{(1+z/R)}\frac{\partial v}{\partial \theta} + \frac{w}{R}, \varepsilon_z = \frac{\partial w}{\partial z} = 0$$

$$\varepsilon_{\theta z} = \frac{1}{(1+z/R)}\frac{\partial w}{\partial x} + \frac{\partial v}{\partial z} - \frac{v}{(1+z)R^2} \tag{4.1}$$

$$\gamma_{xz} = \frac{\partial u}{\partial z} + \frac{\partial w}{\partial x}, \gamma_{x\theta} = \frac{\partial v}{\partial x} + \frac{1}{(1+z/R)}\frac{\partial u}{\partial \theta}$$

The first order theory assumes the following displacements

$$u = u^o(x,\theta) + z\varphi_x(x,\theta)$$
$$v = v^o(x,\theta) + z\varphi_\theta(x,\theta) \tag{4.2}$$
$$w = w^o(x,\theta)$$

where u^o, v^o, w^o are the axial, tangential, and transverse displacements of the mid-surface respectively, and φ_x and φ_θ are the rotations of the cross-sections originally formed to x and θ axes [33]. Since we assume that the shell is shallow, z/R is small compared to unity. Eqns. (4.1) and (4.2) yield in matrix form:

$$\begin{Bmatrix} \epsilon_x \\ \epsilon_\theta \\ \gamma_{x\theta} \end{Bmatrix} = \begin{Bmatrix} \epsilon_x^0 \\ \epsilon_\theta^0 \\ \gamma_{x\theta}^o \end{Bmatrix} + z \begin{Bmatrix} \kappa_x \\ \kappa_\theta \\ \kappa_{x\theta} \end{Bmatrix} \tag{4.3}$$

Where $[\epsilon_i^0]$ and $[\kappa_i]$ are the mid-surface strains and curvatures, respectively, given by [33]

$$\epsilon_x^0 = \frac{\partial u^o}{\partial x}, \epsilon_\theta^0 = \frac{\partial v^o}{\partial \theta} + \frac{w}{R}, \gamma_{x\theta}^o = \frac{\partial u^o}{\partial \theta} + \frac{\partial v^o}{\partial x}$$

$$\kappa_x = \frac{\partial \varphi_x}{\partial x}, \kappa_\theta = \frac{\partial \varphi_\theta}{\partial \theta}, \kappa_{x\theta} = \frac{\partial \varphi_x}{\partial \theta} + \frac{\partial \varphi_\theta}{\partial x} \tag{4.4}$$

In addition, the interlaminar shear strains are

$$\gamma_{xz} = \varphi_x + \frac{\partial w}{\partial x}, \gamma_{\theta z} = \varphi_\theta + \frac{\partial w}{\partial x} - \frac{v}{R} \tag{4.5}$$

It is noted that these results are of exactly the same form as for flat, laminated plates of rectangular cross-section with the exception of the w/R term appearing in the mid-surface tangential strains ϵ_θ^0 and $-v/R$ term appearing in the interlaminar shear strains $\gamma_{\theta z}$. Since the analysis assumes that displacements u, v, and w are small compared to the plate thickness h and the radius of the plate R is much larger than h, the additional terms w/R and $-v/R$ in eqns. (4.1) and (4.5) drop out.

According to classical theory of shells, the membrane stress resultants $N_x, N_\theta, N_{x\theta}$ and the stress couples $M_x, M_\theta, M_{x\theta}$ for the shell are [33]

$$(N_x, N_\theta, N_{x\theta}) = \int_{-h/2}^{h/2} \left(\sigma_x^{(k)}, \sigma_\theta^{(k)}, \tau_{x\theta}^{(k)}\right) dz \tag{4.6a}$$

$$(M_x, M_\theta, M_{x\theta}) = \int_{-h/2}^{h/2} \left(\sigma_x^{(k)}, \sigma_\theta^{(k)}, \tau_{x\theta}^{(k)}\right) z dz \tag{4.6b}$$

where $\sigma_x^{(k)}, \sigma_\theta^{(k)}$, and $\tau_{x\theta}^{(k)}$ are the in-plane stresses in the k^{th} layer. Integration of the stresses yields the constitutive equations for extension and bending of cylindrical shell [33]

$$\begin{bmatrix} N \\ M \end{bmatrix} = \begin{bmatrix} A & B \\ B & D \end{bmatrix} \begin{Bmatrix} \epsilon^o \\ \kappa \end{Bmatrix} \tag{4.7}$$

where $[A], [B]$, and $[D]$ are the extensional, coupling and bending stiffness matrices, respectively, defined in reference [33].

$[\epsilon^o] = \left[\epsilon_x^0,\ \epsilon_\theta^0,\ \gamma_{x\theta}^0\right]$, and $[\kappa] = [\kappa_x,\ \kappa_\theta,\ \kappa_{x\theta}]$ are as defined in eqn. (4.4)

4.2 Anisotropic Stress Functions

The Airy stress function is limited to isotropic problems. For an extension to more complex problems, including anisotropic problems, the stress function $\Phi(x, y)$ can be written as

$$\Phi(x, y) = 2Re[\Phi_1(z_1) + \Phi_2(z_2) \tag{4.8}$$

where $\Phi_1(z_1)$ and $\Phi_2(z_2)$ are arbitrary functions of $z_1 = x + s_1 y$ and $z_2 = x + s_2 y$, respectively which are similar to eqn.(3.65). Combining the definition of stress components from the Airy stress function and satisfying the compatibility equation, the following relation is obtained for anisotropic solids in the absence of body forces:

$$C_{22}\frac{\partial^4\Phi}{\partial x^4} - 2C_{26}\frac{\partial^4\Phi}{\partial x^3\partial y} + (2C_{12} + C_{66})\frac{\partial^4\Phi}{\partial x^2\partial x^2} - 2C_{16}\frac{\partial^4\Phi}{\partial x\partial y^3} + C_{22}\frac{\partial^4\Phi}{\partial y^4} = 0 \tag{4.9}$$

which reduces to the following simplified equation for isotropic problems,

$$\frac{\partial^4\Phi}{\partial x^4} - 2\frac{\partial^4\Phi}{\partial x^2\partial x^2} + \frac{\partial^4\Phi}{\partial y^4} = \nabla^2(\nabla^2\Phi) = 0 \tag{4.10}$$

The characteristic equation of the homogenous partial differential eqn. (4.9) is

$$C_{11}s^4 - 2C_{16}s^3 + (2C_{12} + C_{66})s^2 - 2C_{26}s + C_{22} = 0 \tag{4.11}$$

For an orthotropic material with axes of orthotropy $(1,2)$ coinciding with Cartesian (x, y) axes, $C_{16} = C_{26} = 0$, the characteristic eqn. (4.11) is reduced to [39]:

$$s^4 + \left(\frac{E_1}{\mu} - 2v_1\right)S^2 + \frac{E_1}{E_2} = 0 \tag{4.12}$$

Finally, the stress components are defined from the second derivatives of the complex stress function Φ_i''

$$\begin{aligned}\sigma_{xx} &= 2Re[\mathrm{s}_1^2\Phi_1''(\mathrm{z}_1) + \mathrm{s}_2^2\Phi_2''(\mathrm{z}_2)]\\ \sigma_{yy} &= 2Re[\Phi_1''(\mathrm{z}_1) + \Phi_2''(\mathrm{z}_2)]\\ \sigma_{xy} &= 2Re[s_1\Phi_1''(\mathrm{z}_1) + s_2\Phi_2''(\mathrm{z}_2)]\end{aligned} \tag{4.13}$$

and the displacements are obtained from the first derivatives of the complex stress function, Φ_i':

$$u_x = 2Re[p_1\Phi_1'(\mathrm{z}_1) + p_2\Phi_2'(\mathrm{z}_2)] \tag{4.14a}$$

$$u_y = 2Re[q_1\Phi_1'(z_1) + q_2\Phi_2'(z_2)] \tag{4.14b}$$

where

$$p_i = C_{11}s_i^2 + C_{12} - C_{16}s_i, \quad q_i = C_{12}s_i + \frac{C_{12}}{s_i} - C_{26}, \quad i = 1,2 \tag{4.15}$$

4.3 Analytical Solutions for Near Crack Tip

Several analytical solutions for near crack tip fields in orthotropic materials have been proposed. Some of them can only be applied to specific applications, while others can be applied to general orthotropic media [39]. The line-spring model discussed in section 3.3.3.2 is applicable to determine the stress intensity factors for surface crack problems in an orthotropic medium for both material types 1 and 2 (eqn. (3.65)).

4.3.1 Unified Near Crack Tip Stress and Displacement Field (Both Types)

This formulation is based on the work by Sih *et al*. [40] who used the stress function eqn. (4.8) for an infinite anisotropic plate with a central crack and solved the final displacement fields.

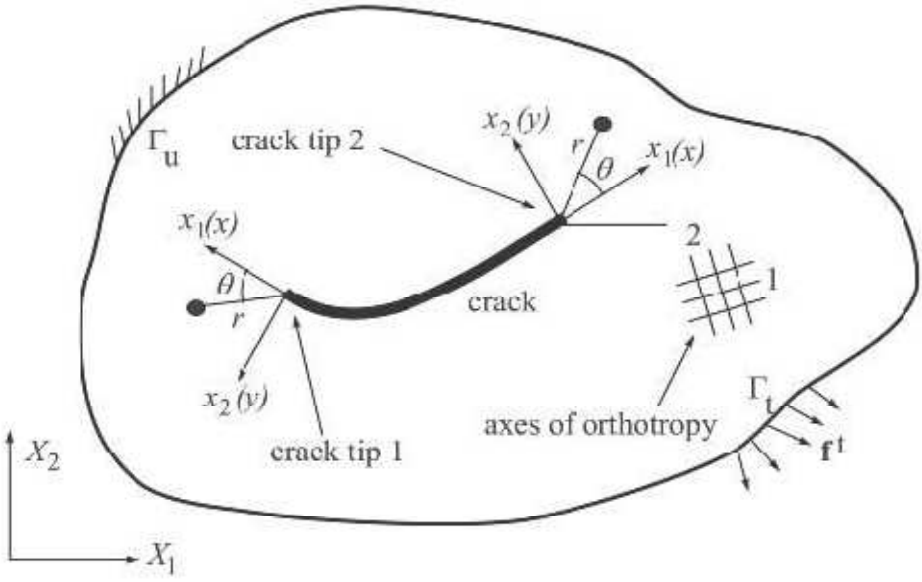

Figure 4.3 Local coordinates at both crack tips [39]

Assume an anisotropic body containing a crack is subjected to arbitrary forces with general displacement and traction boundary conditions. Global Cartesian coordinates are (X_1, X_2) and local Cartesian coordinate $(x_1 = x,\ y_1 = y)$ and local polar coordinate (r, θ) are defined on the crack tip as illustrated in figure 4.3. Recalling the characteristic eqn. (4.11) of the governing fourth-order partial differential equation are always complex or

purely imaginary ($s_k = s_{kx} + is_{ky}$, *k= 1, 2*) and occur in conjugate pairs as $s_1, \bar{s}_1$ and $s_2, \bar{s}_2$.

Sih *et al*. derived the two-dimensional displacement and stress fields in the vicinity of the crack tip by means of analytical functions and complex variables ($s_k = s_{kx} + is_{ky}$, k= 1, 2). The stress components for pure Mode I are defined as,

$$\sigma_{11}^I = \frac{K_I}{\sqrt{2\pi r}} Re\left[\frac{s_1 s_2}{s_1 - s_2}\left(\frac{s_2}{(cos\theta + s_2 sin\theta)^{1/2}} - \frac{s_1}{(cos\theta + s_1 sin\theta)^{1/2}}\right)\right]$$

$$\sigma_{22}^I = \frac{K_I}{\sqrt{2\pi r}} Re\left[\frac{1}{s_1 - s_2}\left(\frac{s_1}{(cos\theta + s_2 sin\theta)^{1/2}} - \frac{s_2}{(cos\theta + s_1 sin\theta)^{1/2}}\right)\right] \quad (4.16)$$

$$\sigma_{12}^I = \frac{K_I}{\sqrt{2\pi r}} Re\left[\frac{s_1 s_2}{s_1 - s_2}\left(\frac{1}{(cos\theta + s_1 sin\theta)^{1/2}} - \frac{1}{(cos\theta + s_2 sin\theta)^{1/2}}\right)\right]$$

and the displacements are

$$u_1^I = K_I \sqrt{\frac{2r}{\pi}} Re\left\{\frac{1}{s_1 - s_2}\left[s_1 p_2 (cos\theta + s_2 sin\theta)^{1/2} - s_2 p_1 (cos\theta + s_1 sin\theta)^{1/2}\right]\right\}$$

$$u_2^I = K_I \sqrt{\frac{2r}{\pi}} Re\left\{\frac{1}{s_1 - s_2}\left[s_1 q_2 (cos\theta + s_2 sin\theta)^{1/2} - s_2 q_1 (cos\theta + s_1 sin\theta)^{1/2}\right]\right\} \quad (4.17)$$

$$u_3^I = 0$$

4.4 Finite Element Modeling

The finite element method (FEM) has undoubtedly become the most popular and powerful analytical tool for studying the behavior of a wide range of engineering and physical problems. Several general purpose finite element software have been developed, verified and calibrated over the years and are now available to almost anyone. One of the important applications of FEM is the analysis of crack propagation problems [39].

The ANSYS software is one of the finite element method packages available to analyze crack problems which have different layered elements for discretization and modeling composite materials. Among them SOLID46 (3-D layered structural solid shell, figure 4.4) is used for simulating shell structures. The element possesses the continuum solid element topology and features eight-node connectivity with three degrees of freedom at each node: translations in the nodal $x, y,$ and z directions. The element allows to model up to 250 different material layers. Accuracy in modeling composite shells is governed by the first order shear deformation theory.

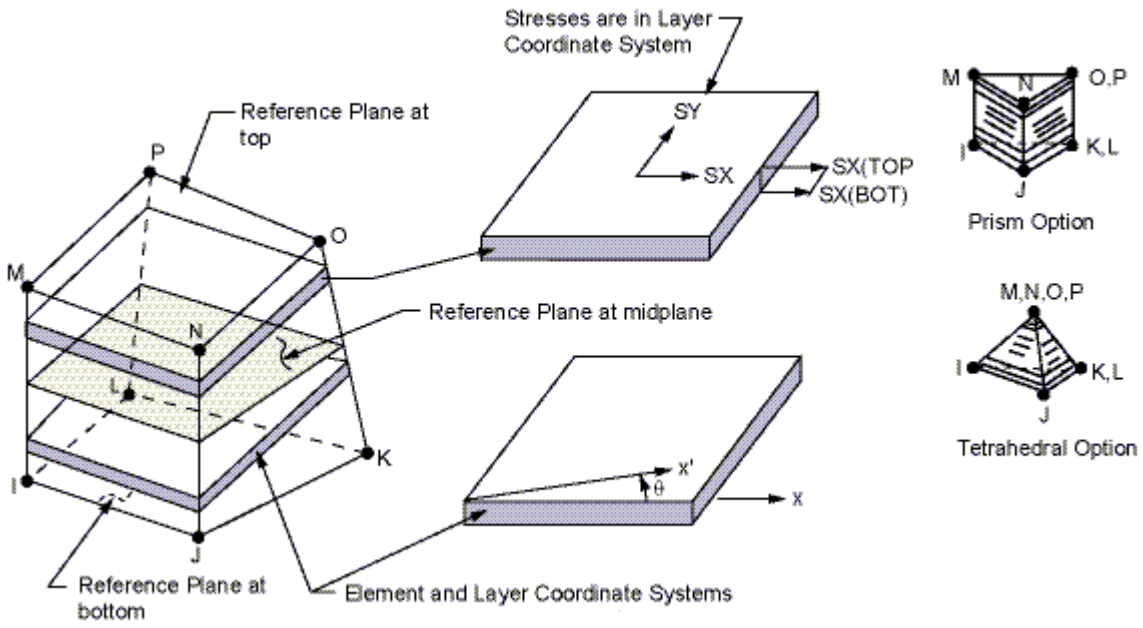

Figure 4.4 SOLID46 Geometry [ANSYS library]

4.5 Surface Cracked Composite Shell Modeling in ANSYS

The composite shell is modeled using ANSYS, which is used for pre and post-processing of the model with FEA as the solver. The model is created in the preprocessing stage of the model generation and the results are viewed in the post-processing stage. The composite shell is created using SOLID46 (3-D layered structural solid shell) element. The properties of the lamina are given as inputs using ANSYS material library and the real constant command is used for defining layers of the composite material shell structure.

The surface cracks in a shell are generated by cutting out an elliptical or circular cylindrical volume with negligible width on the outer or inner surfaces of the shell structure having circular or elliptical cross section and oriented in any direction on the surface of the cylinder which may be tangentially, axially or at an angle with respect to the cylinder axis as cracks in mechanical structure are very random in orientation and shape. It is in most cases propagating from one surface or side to the other. However, in order to simplify the analysis to the scope the FEA package such simple cracks are created to have circumferential or axial orientation.

The crack is described schematically as seen in figure 4.5., which is modeled by removing semi-elliptic volume or semi-circular cylindrical volume from the cylindrical shell at the mid-section. All the crack parameters are described in the figure.

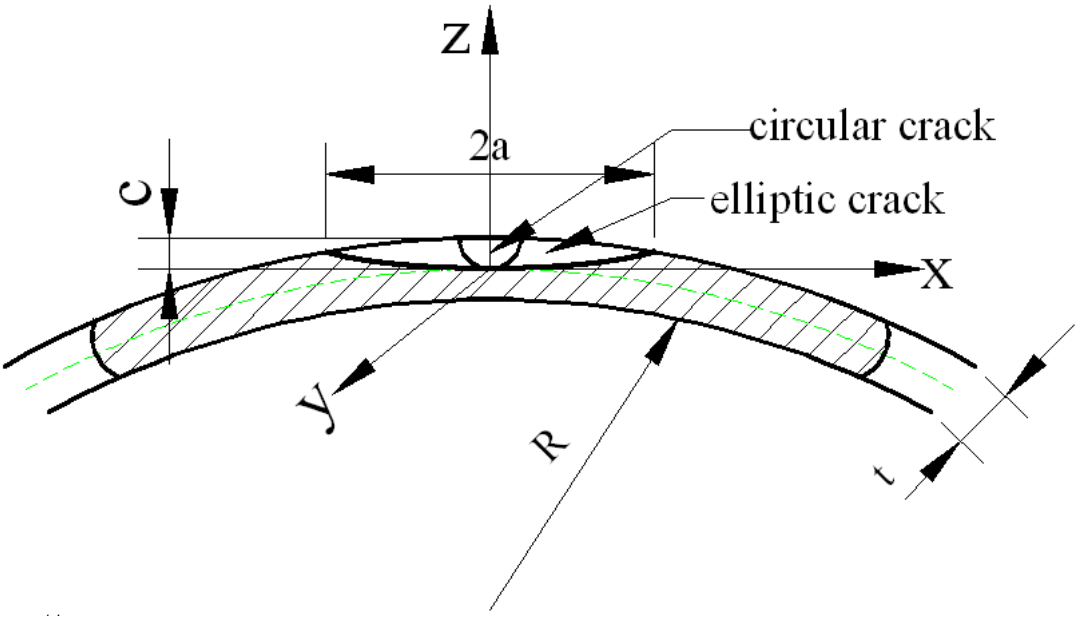

Figure 4.5 Surface crack parameters on a cylindrical shell

The surface crack parameters to be considered in the modeling are:

$^{c}/_{t} = 0.4, \qquad ^{a}/_{t} = 3,$

where a is the crack length, and c is the crack depth.

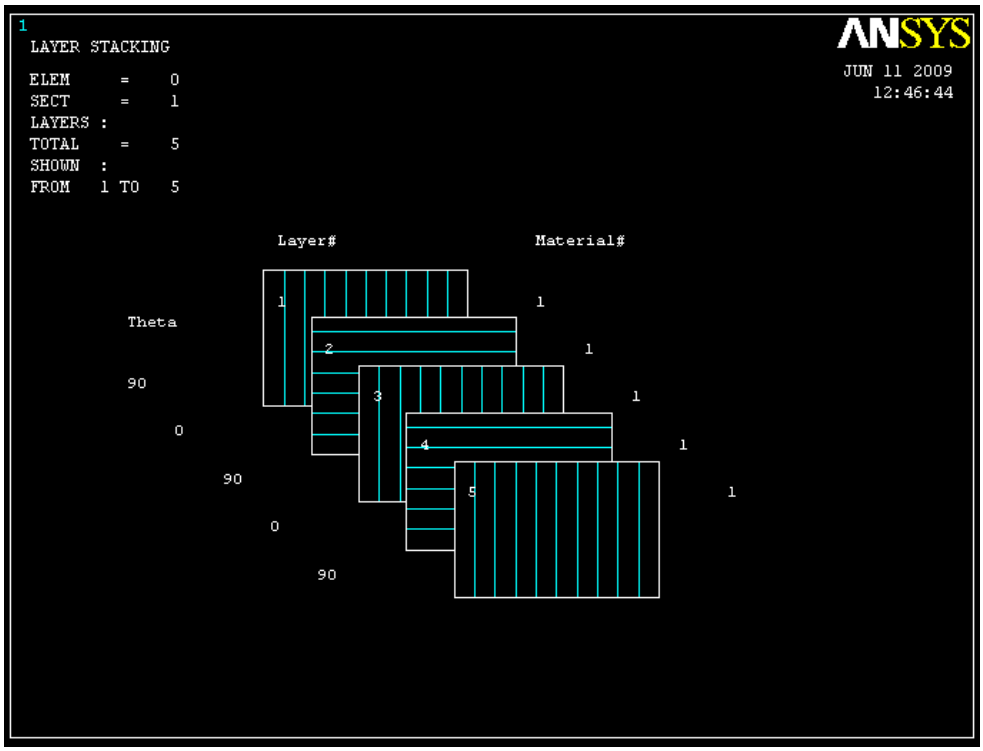

Figure 4.6 The staking sequence of the layers within the laminated shell structure

As a practical matter, we consider the material Hercules AS4/3501-6. This material is made of thin carbon fibres (approximately 10μm or 0.001 cm in diameter) which are

placed in an epoxy prepreg and pressed into thin sheets, with all the fibers running in one direction. The sheets are then stacked so that in each layer the fibres run perpendicularly to the fibres of the previous layer. The sheets are then heated and pressed together, so that the epoxy forms a continuous matrix that holds the fibers together. The resulting laminate is of the form ... 0°/90°/0°/90° ... (figure 4.6).

Moreover, each layer is quite thin (approximately 500μm), and a shell of this material, which has 2.5mm thickness contains 5 layers.

Let us consider, therefore, modeling of such a composite shell that is made of alternating layers, with layer 1 having fibres which run along the axial-direction, and with layer 2 having fibres which run along the tangential-direction stacked along the z axis.

4.5.1 Description of the Parameters of the Model

Crack description:

As seen in figure 4.5 a semi-elliptic crack is generated by removing out an elliptical volume having a crack length $a = 7.5 \times 10^{-3} m$, a depth of $c = 1.0 \times 10^{-3} m$, and a narrow width of $0.2 \times 10^{-3} m$. The surface crack in this case is oriented tangentially and axially on the outer and inner surface of the shell structure as shown in figure 4.7.

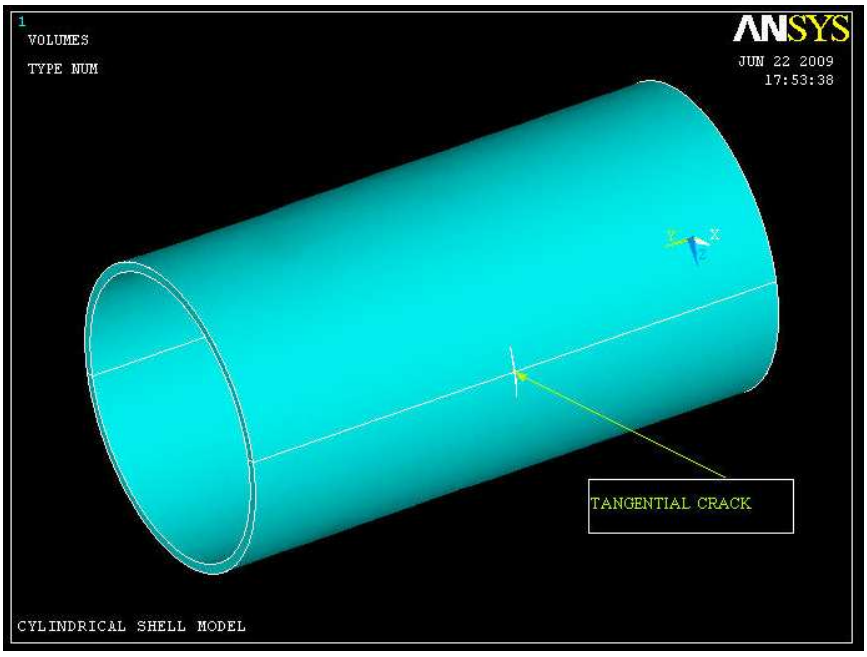

Figure 4.7 Model of composite shell having tangential elliptic surface crack.

Meshing the Model

The model is meshed with automatic mesh generation command “Auto Mesh Generation”. As can be seen from figure 4.8, the model is meshed with more refined elements in the

vicinity of the crack and coarsely meshed in areas away from the crack to economize the computation time.

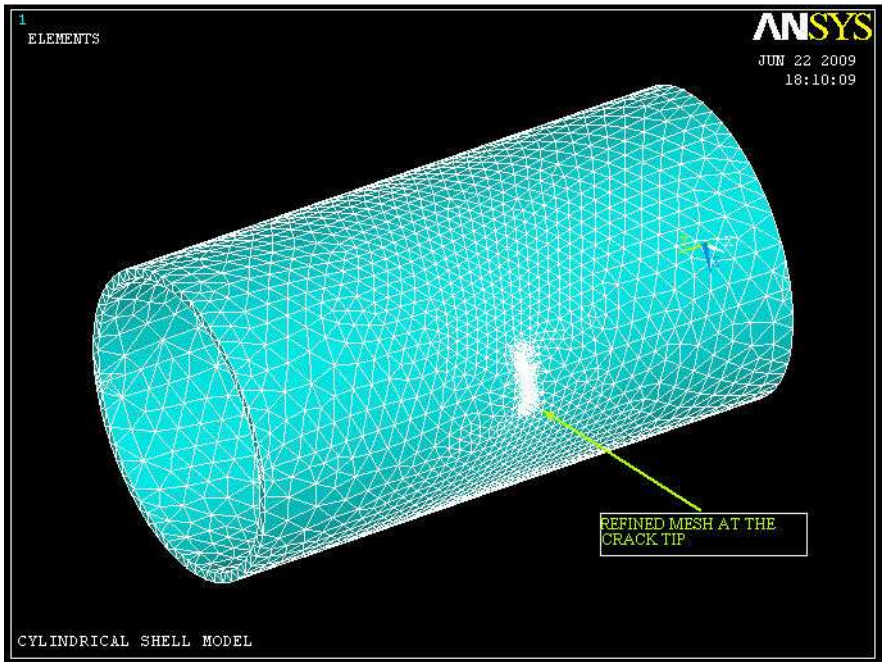

Figure 4.8 Model of meshed composite shell having tangential elliptic surface crack for analysis

Geometric parameters of the model

Outer diameter = 80mm

Layer thickness = 0.5mm

Inner diameter = 75mm

Length of the cylinder =150mm

Total thickness = 2.5mm

Material of the laminate

The material of the laminate is made of linear elastic orthotropic material with the following properties:

Material= Carbon/Epoxy with:

$\sigma_1^F = 2000\text{Mpa}, \quad \sigma_2^F = 52\text{Mpa}, \quad \text{and } \tau_{12} = 70\text{Mpa}$

Density $= 1550\, kg/m^3$

$E_x = 161\text{GPa}, E_y = 9\text{GPa}, E_z = 9\text{GPa}$

$PR_{xy} = 0.26\ , PR_{yz} = 0.01\ , PR_{xz} = 0.26$

$G_{xy} = 6.1\text{GPa}\ , G_{yz} = 1\text{GPa}\ , G_{xz} = 6.1\text{GPa}$

Staking sequence $= [90/0/90/0/90]°$

4.5.2 Loading and Boundary conditions

The cylindrical shell is constrained as shown in figures 4.9 and 4.10 in two cases as the analysis is going to be done for Mode I loading condition in which the surface cracks are oriented externally and internally on the cylindrical shell. For cracks, which are oriented tangentially both external and internal (figure 4.9) the shell is constrained symmetrically at $Y = 0$ and $Z = 0$ plane, and the pressure load of 100Mpa is applied in the axial direction for simulating purpose. Also for cracks, which are oriented axially both external and internal (figure 4.10) the shell is constrained symmetrically at $Y = 0$ and $Z = 0$ plane, and the pressure load of 200Mpa is applied in the tangential direction for simulating purpose. These two pressure loads are based on the thin cylinder pressure formulas that are subjected to defined internal pressure.

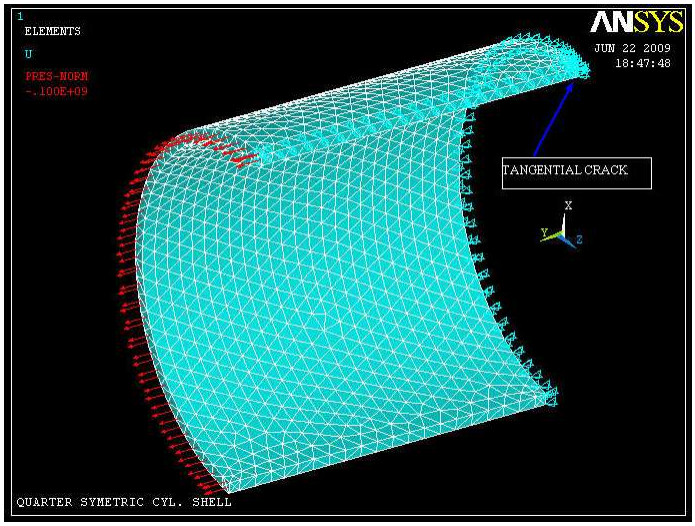

Figure 4.9 Quarter symmetric model with boundary condition and load for tangential crack

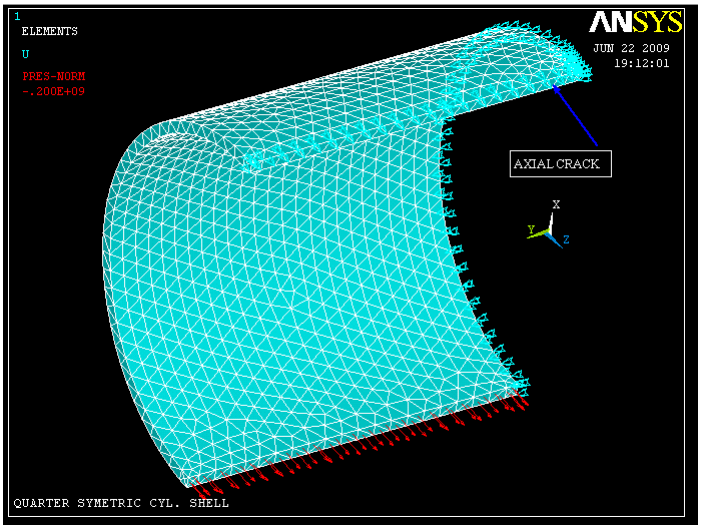

Figure 4.10 Quarter symmetric model with boundary condition and load for axial surface crack

CHAPTER FIVE
RESULTS AND DISCUSSIONS

5.1 Introduction

Many have attempted to apply fracture mechanics to fibre-reinforced composites, and have met with mixed success. Conventional fracture mechanics methodology assumes a single dominant crack that grows in a self-similar fashion, i.e., the crack increases in size (either through stable or unstable growth), but its shape and orientation remain the same. Fracture of a fibre-reinforced composite, however, is often controlled by numerous microcracks distributed throughout the material, rather than a single macroscopic crack. There are situations where fracture mechanics is appropriate for composite, but it is important to recognize the limitations of theories that were intended for homogeneous materials.

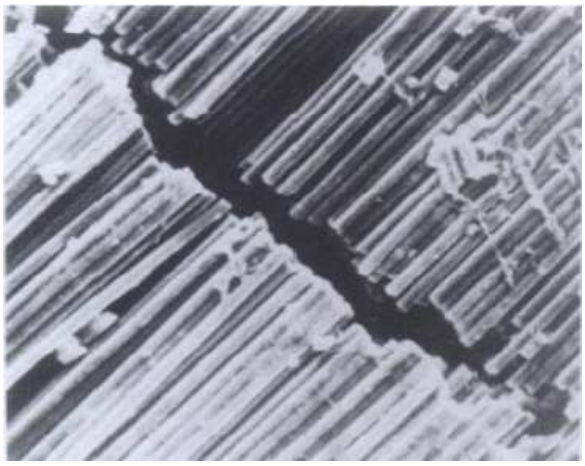

(a) Fibre rupture

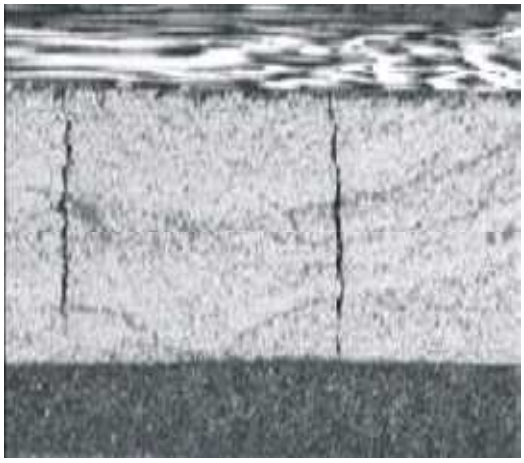

(b) Matrix transverse crack

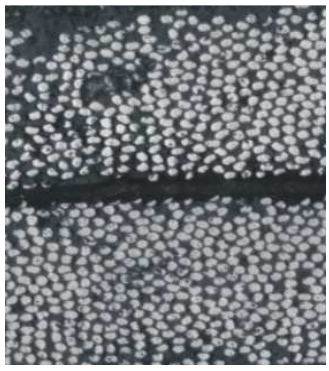

(c) Delamination

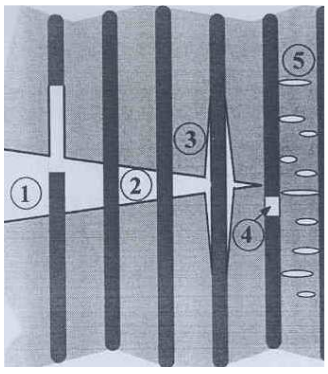

1. Fibre pull-out
2. Fibre bridging
3. Fibre-matrix debonding
4. Fibre failure
5. Matrix cracking

(d) In plane damage

Figure 5.1 Fracture mechanisms of composite materials

Unlike isotropic materials, one advantage of composite materials is that fracture seldom occurs catastrophically without warning, but tends to be progressive with subcritical damage widely dispersed through the material as shown in (figure 5.1). Tensile loading can produce matrix cracking, fibre bridging, fibre rupture, fibre pullout, and fibre matrix debonding. Ultimate tensile failure of a fibre-reinforced composite often involves several of these mechanisms. Out-of-plane stress can lead to delamination because the fibres do not contribute significantly to the strength in this direction

The finite element analysis done in ANSYS by simulating the composite cylindrical shell structure having surface crack is to determine the stress and strain distributions around the crack tip. The loading conditions applied are all for the Mode I loading (opening mode) for which the cracks are oriented tangentially and axially on both surfaces of the cylindrical shell i.e., external and internal.

Theoretically, the numerical computation of the stress intensity factors, or of the energy release rate, can be performed using different techniques as it was highlighted in chapter three like J-integral, the virtual crack closure technique (VCCT), and the line-spring model. Stability of crack growth can be easily assessed by computing the values of the energy release rate (G) at different crack lengths (a) and calculating the derivative of the energy release rate with respect to the crack length, i.e. if $\partial G/\partial a < 0$, there is stable crack growth.

5.2 Model with Tangential Crack

The tangential surface crack is oriented in to two positions on the cylindrical shell structure, externally and internally

5.2.1 Model with External Tangential Crack

The main motive in this work is to investigate the distribution of stresses or strains around the surface crack in a fibre-reinforced composite shell structure. For the external tangential surface crack induced in to the shell structure by removing out an elliptical volume having a depth of 1mm contains both layers of the laminate with 0 and 90 degrees of orientation with respect to the X-axis. On the outer layer, 90 degree ply, the crack will cut the fibres perpendicularly and on the next lower layer, 0 degree ply, the crack will not cut the fibre rather passes parallel to it. In this case, the remotely applied stress induces the stress

distribution around the crack tip which opens the crack in Mode I loading condition that the stress distribution provides an indication as to where the fracture could initiate.

At the maximum penetration point of the crack tip, the opening action (Mode I crack) of the far field applied stress faces resistance from the fibre. If the stresses induced in the vicinity of the crack are larger than the fibre ultimate longitudinal strength, the fibres will break and the crack will propagate. If it is not the case, the maximum stress induced in the vicinity of the crack tip will find a way to be deflected towards the lower strength matrix material of the structure. This deflection of the maximum induced stress in the vicinity of the crack tip to a lower strength matrix material will produce a shielding effect of the stresses in the structure. This shielding effect of stresses in the fibre-reinforced composite material produces a scattered distribution of stresses in the farthest portion of the structure away from the crack tip. The shielding effect is visible in all the stress plots as shown in the following figures (5.2-5.10). The induced stresses in the vicinity of the crack will produce failures in the shell structure, i.e., fibre breaking and matrix material cracking.

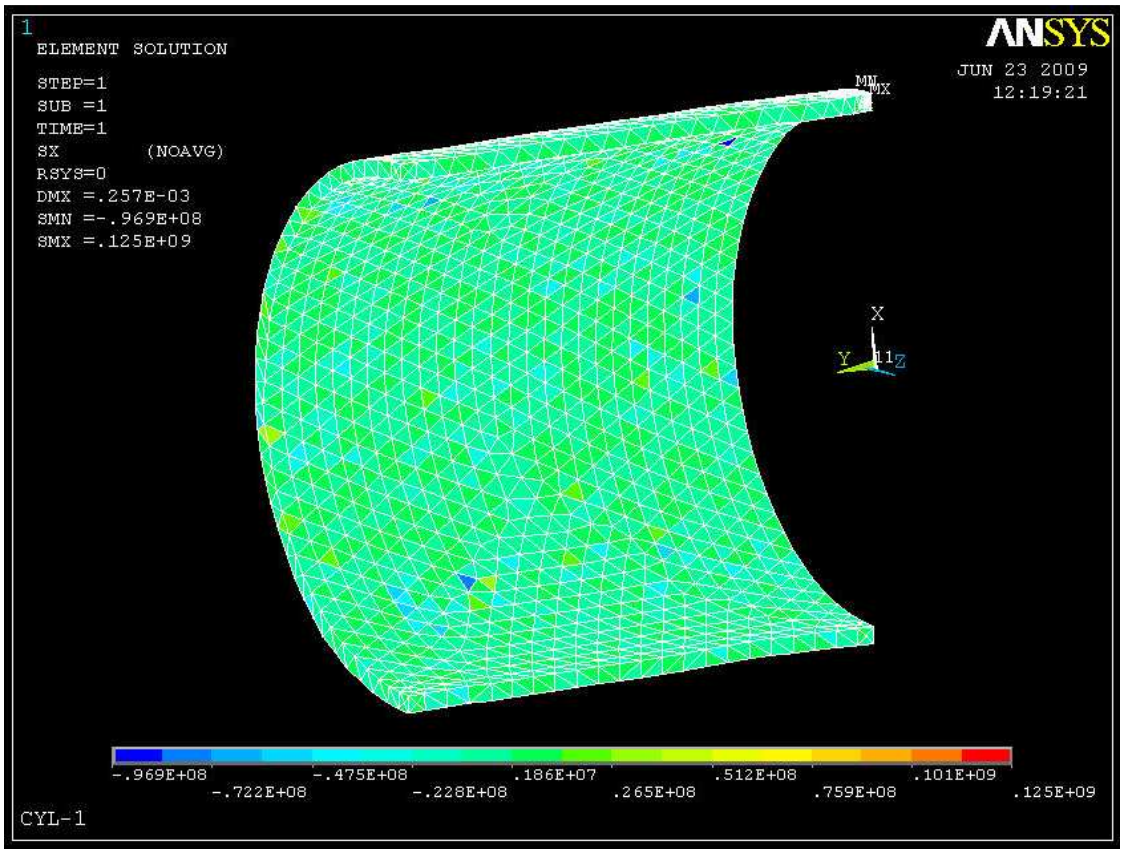

Figure 5.2(a) Distribution of X-component stress plot for external tangential crack

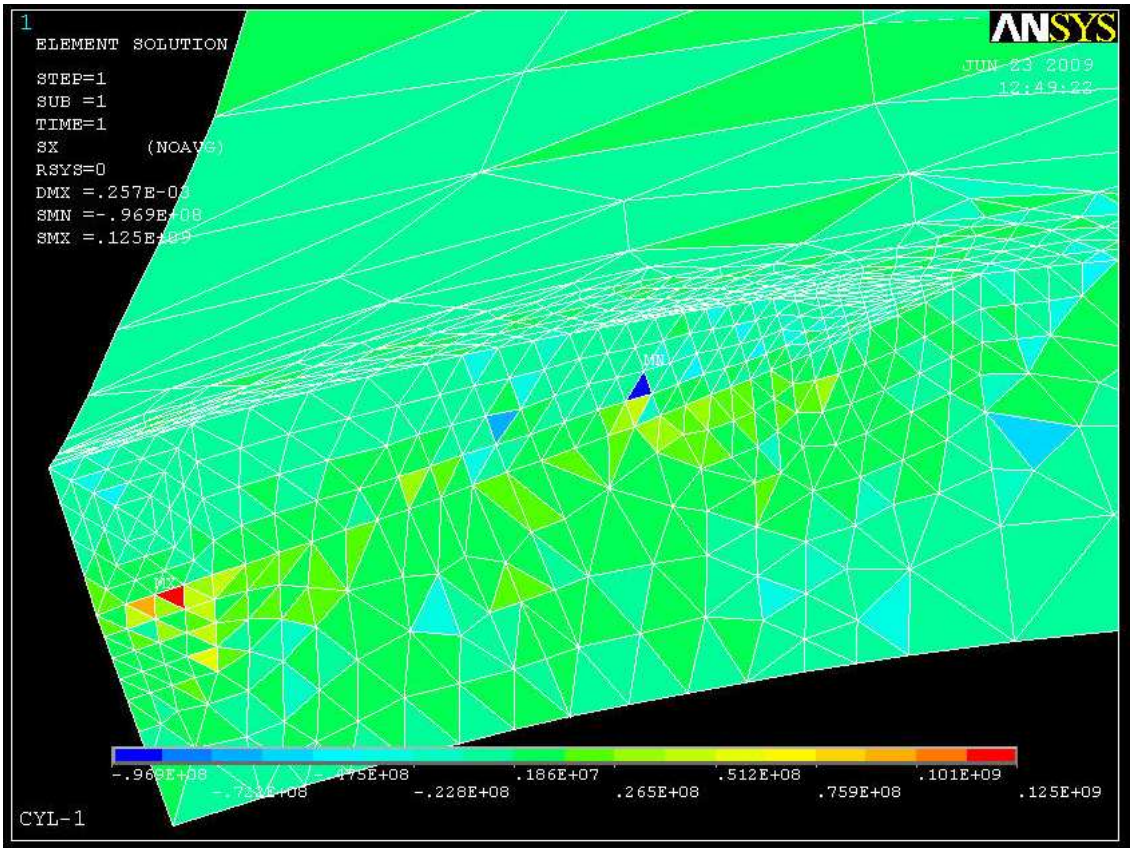

Figure 5.2(b) Magnified X-component stress plot for external tangential crack

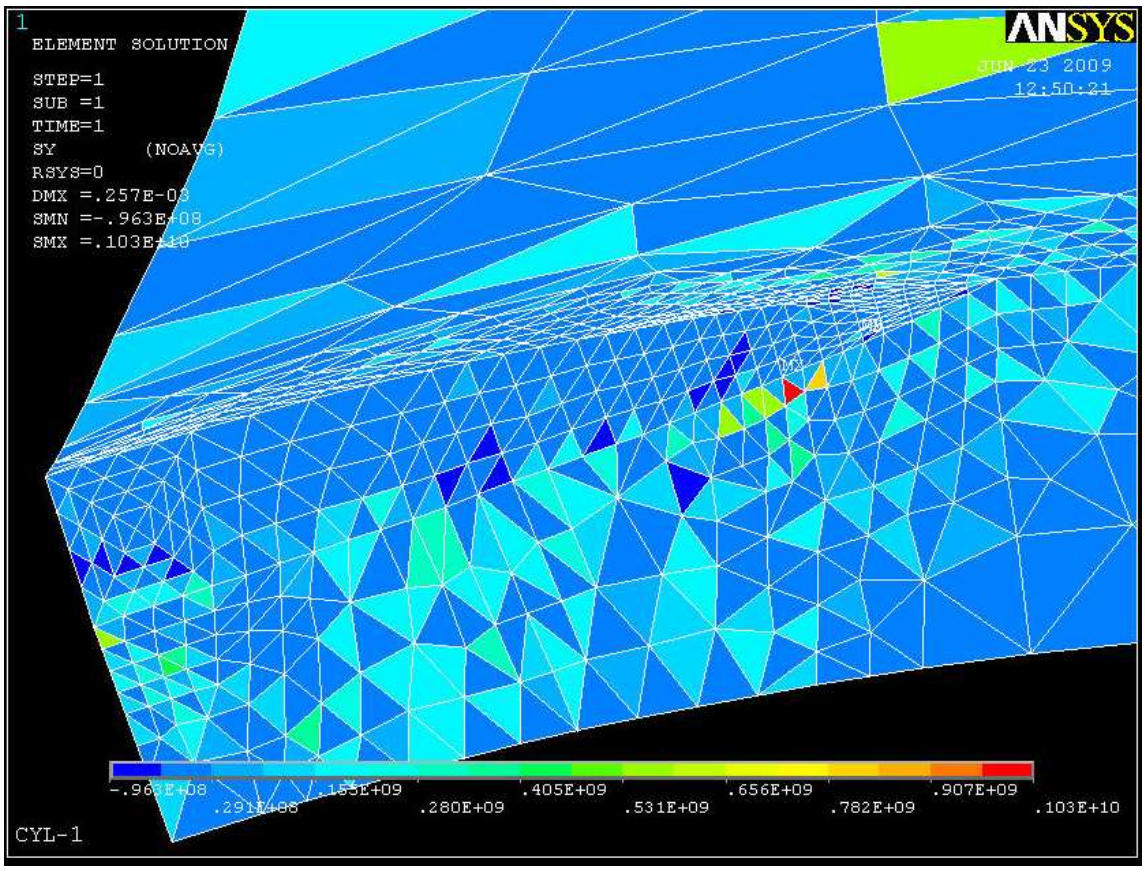

Figure 5.3 Magnified Y-component stress plot for external tangential crack

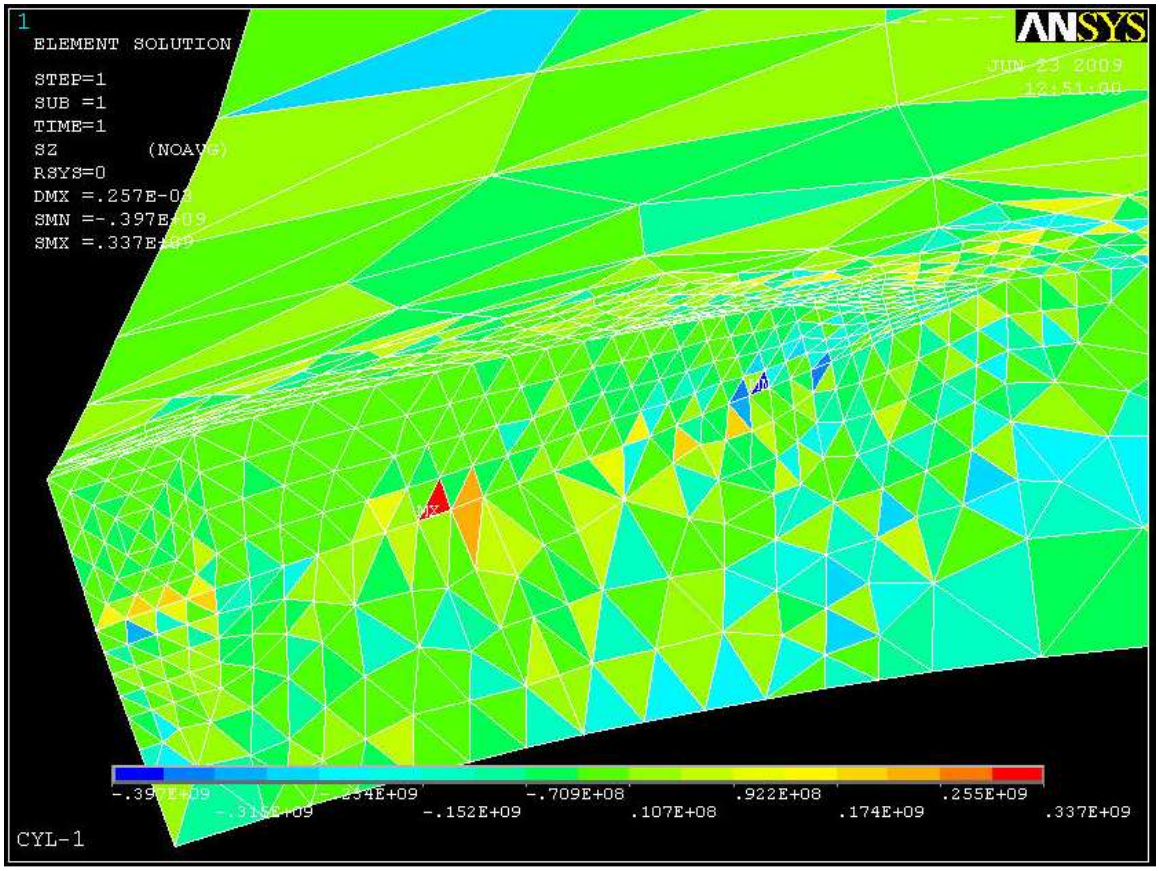

Figure 5.4 Magnified Z-component stress plot for external tangential crack

As seen clearly in the figures (5.2-5.4), the unidirectional stresses in the X, Y, and Z directions, the maximum stresses shown are distributed in the vicinity of the crack tip but are not uniform around the crack front rather localized somewhere near the crack face. But the shear stress distribution (figures 5.5-5.7), show somewhat different orientation a slight farthest away the crack faces. Due to the reinforcement by the fibres in the matrix and differences in the orientations of the layers in the laminate of the fibre-reinforced composites, different locations in the shell structure have got different stress and strain intensity levels that show spots of different stress distributions throughout the structure. This condition is clearly seen in figures 5.6 and 5.7 as the shear stress is maximum away from the crack tip somewhere in the shell structure. It is difficult to predict the positions as to where the maximum crack tip stresses will lie in the laminated shell structure in the absence of any experimental data on fibre fracture initiation and propagation during loading. Fibre failure is assumed to occur due to the maximum principal stress exceeding the ultimate tensile strength of the fibre in each lamina, but crack propagation is a cumulative effect of all the laminate in the structure that makes the prediction of maximum stress position more difficult.

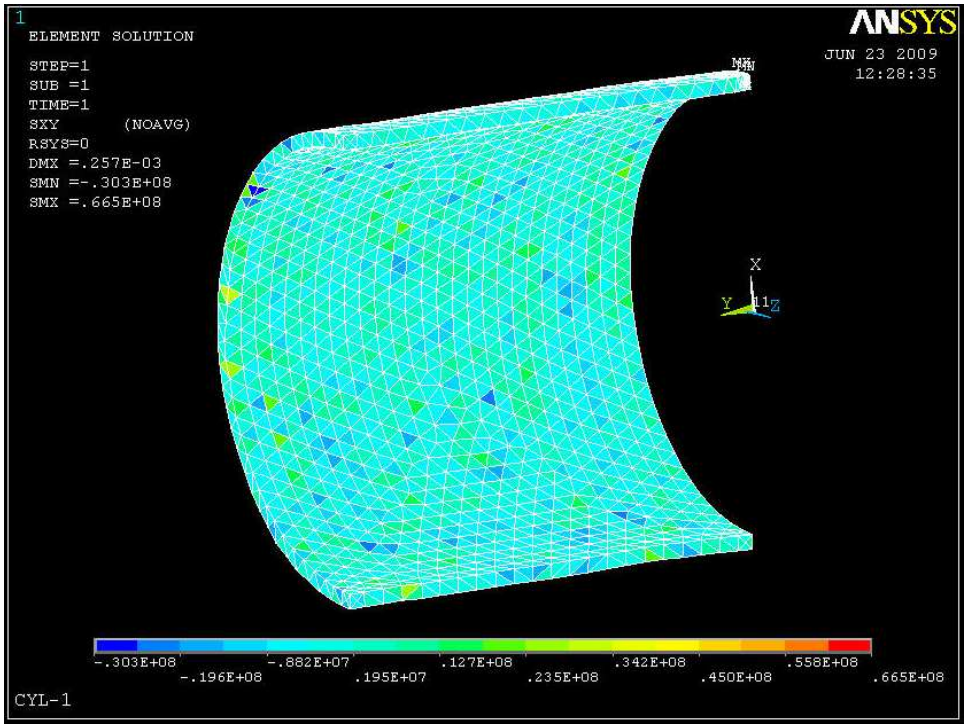

Figure 5.5(a) Distribution of XY-shear stress plot for external tangential crack

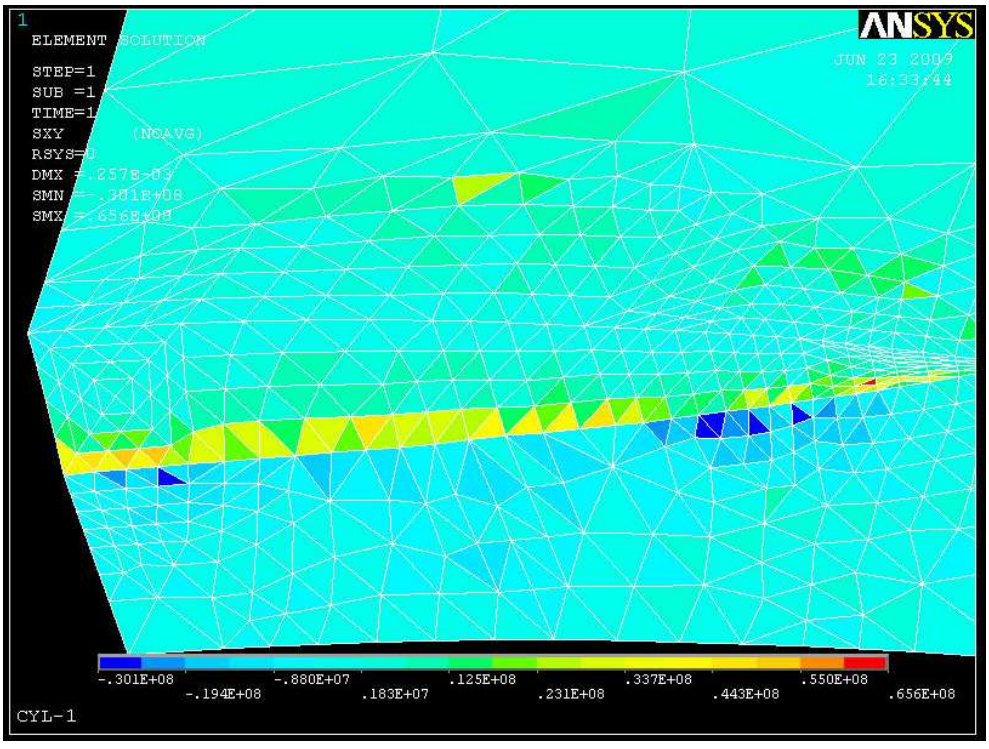

Figure 5.5(b) Magnified XY-shear stress plot for external tangential crack

The stress coupling effect in composite materials or the inter laminar adhesion transfers the load applied in the axial direction to the whole body of the shell in radial directions as seen in the shear stress plots. In addition the shear stress induced within the shell is also

showing some form of scattering and localized patterns that will have its own contribution for the advance of crack. Naturally, fracture of the weakest or damaged fiber should not result in material failure. Instead, the matrix should evenly redistribute the load from the broken fiber to the adjacent ones and then load the broken fiber at a distance from the cross-section at which it failed.

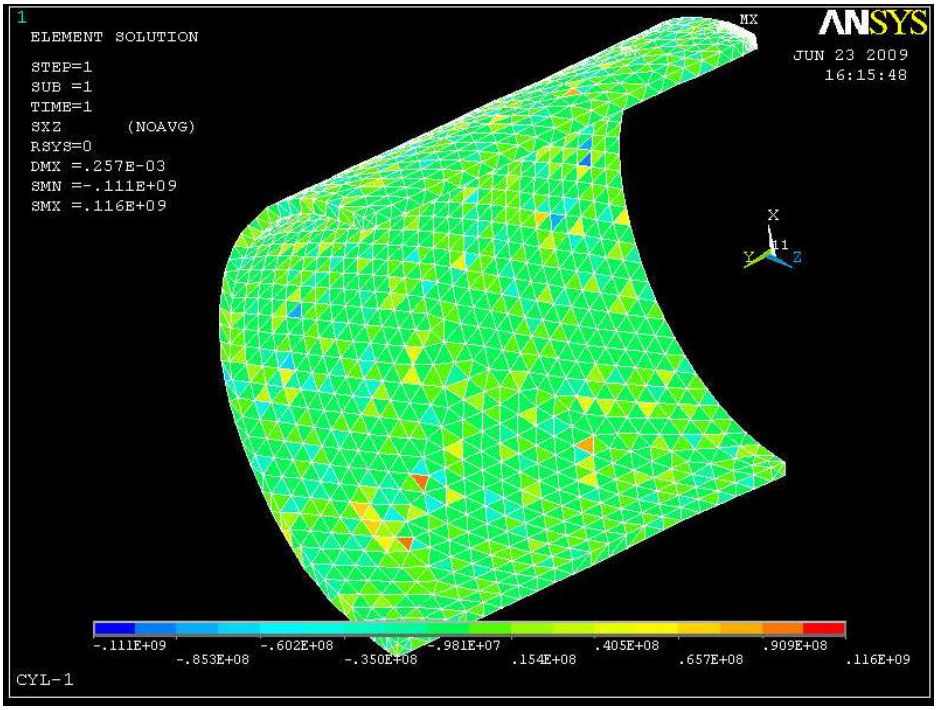

Figure 5.6(a) Distribution of XZ-shear stress plot for external tangential crack

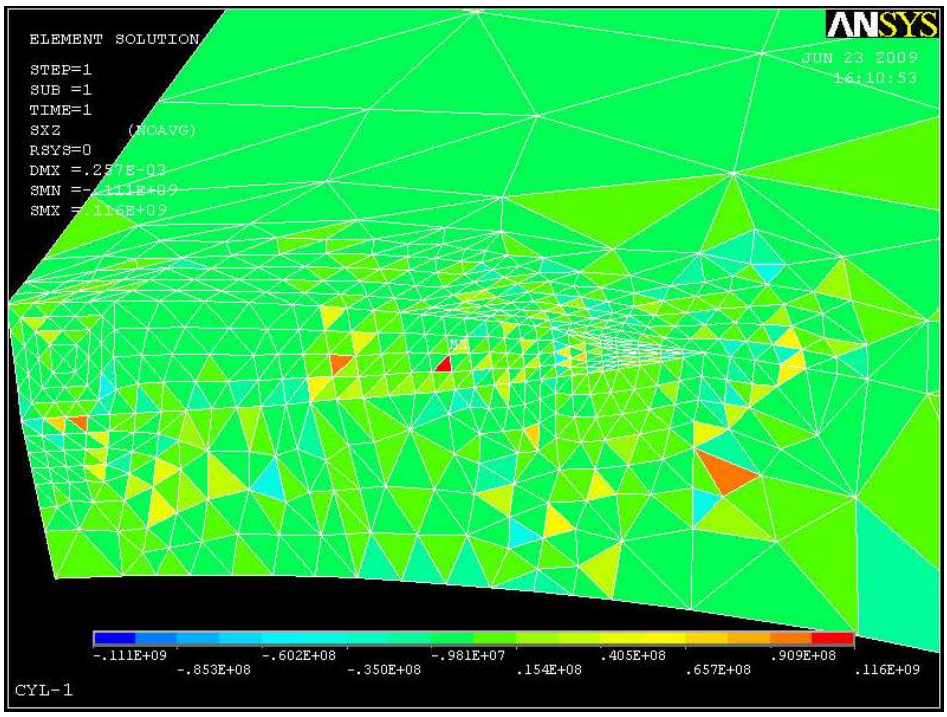

Figure 5.6(b) Magnified XZ-shear stress plot for external tangential crack

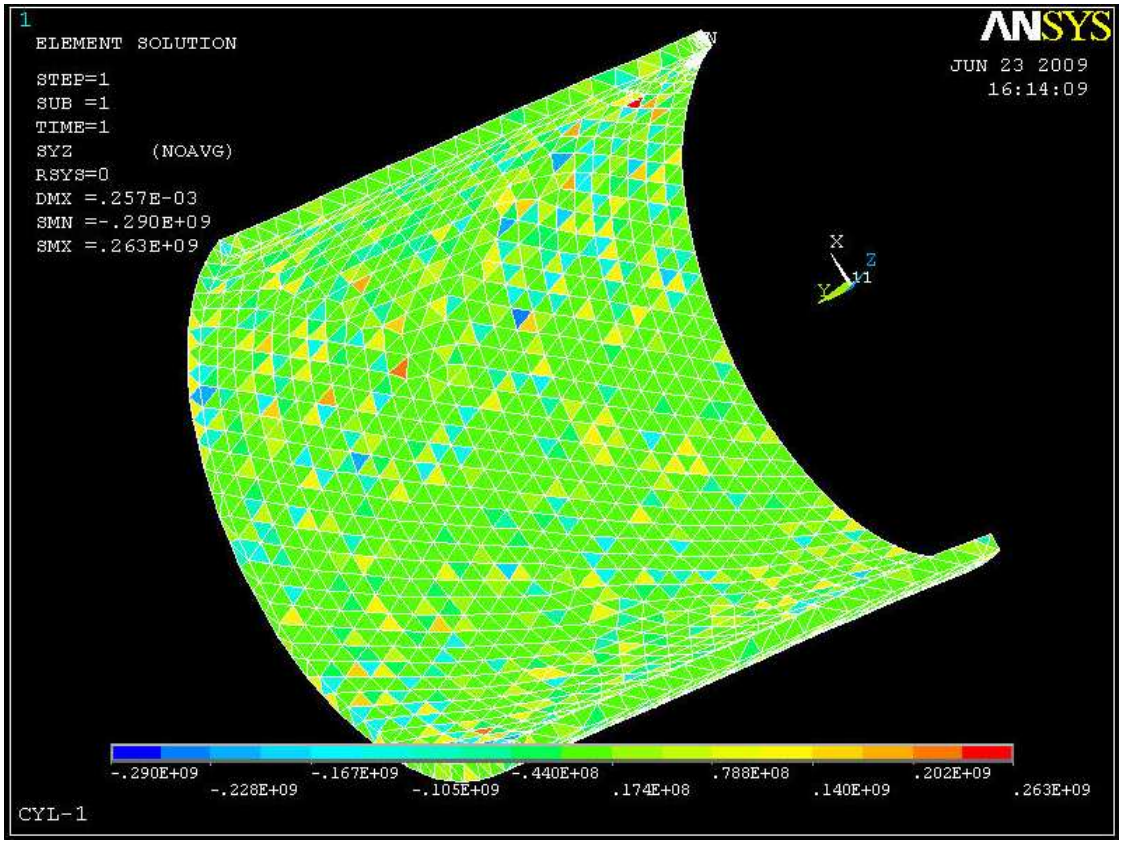

Figure 5.7(a) Distribution of YZ-shear stress plot for external tangential crack

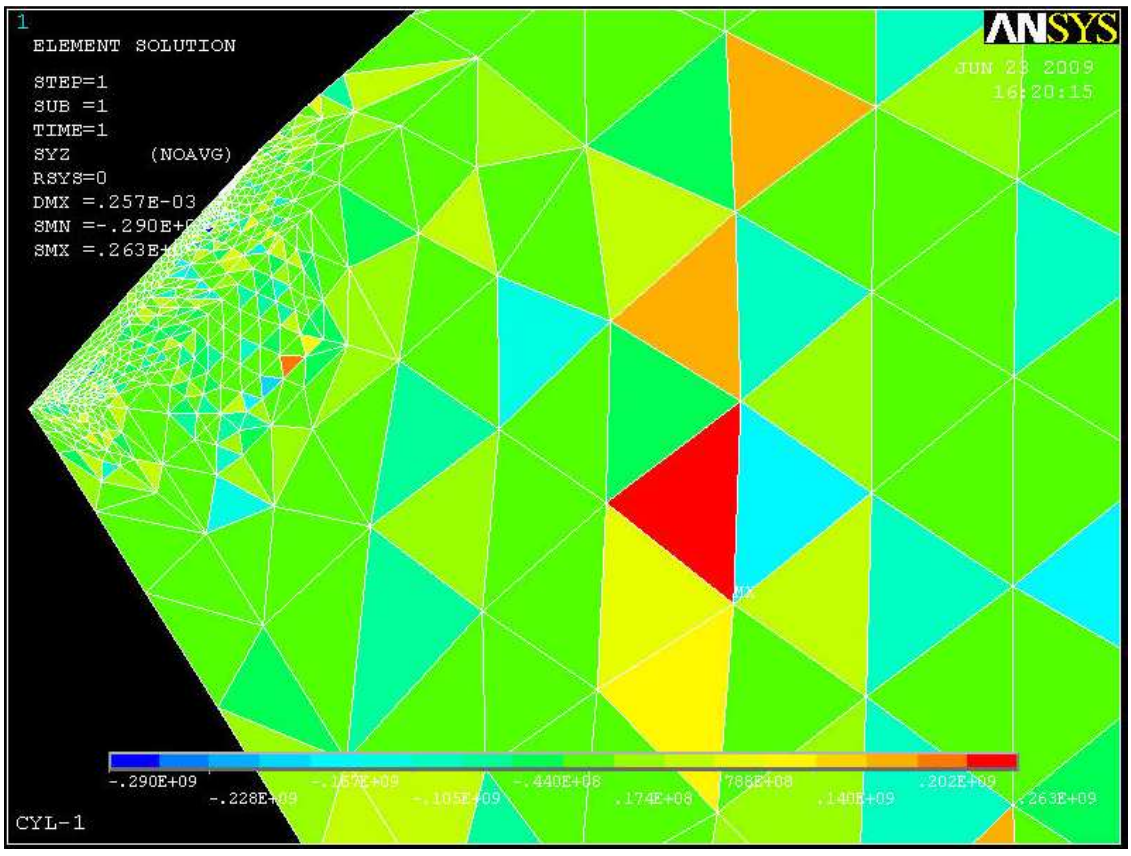

Figure 5.7(b) Magnified YZ-shear stress plot for external tangential crack

The localized stress intensity, von Misses stress and the von Misses total strain plots (figures 5.8-5.10) reveal that their maximum values are shielded in front of the maximum penetration point of the crack. This is happened due to the greater resistance of the propagation of the localized stress in the structure is faced at the narrowest part of the elliptic surface crack in the composite material shell structure. At this position the fibres in front of the crack advance are not directly cut by the crack creation phase and so that the fibres and matrix interaction hinders the crack propagation that comes from the opening mode by the far field stress. That is to say, there is a 90 degree ply for which the fibres are oriented perpendicular to the crack advance that will act to hinder the crack propagation.

Near the outer surface of the shell, the last lamina is oriented parallel to the axis of the shell so that the local stress propagation is perpendicular to the fibres which makes the fibres to bend in front of the local stress. This bending action of the fibres will be supported by the compression of the matrix material in the laminate that makes the local stresses to be hindered and accumulated at this location making local maximum stress. If the local stress tries to advance to the lower part of the lamina, it will also face the other 90 degree lamina which also hiders it so that it will be accumulated at this location creating local maxima.

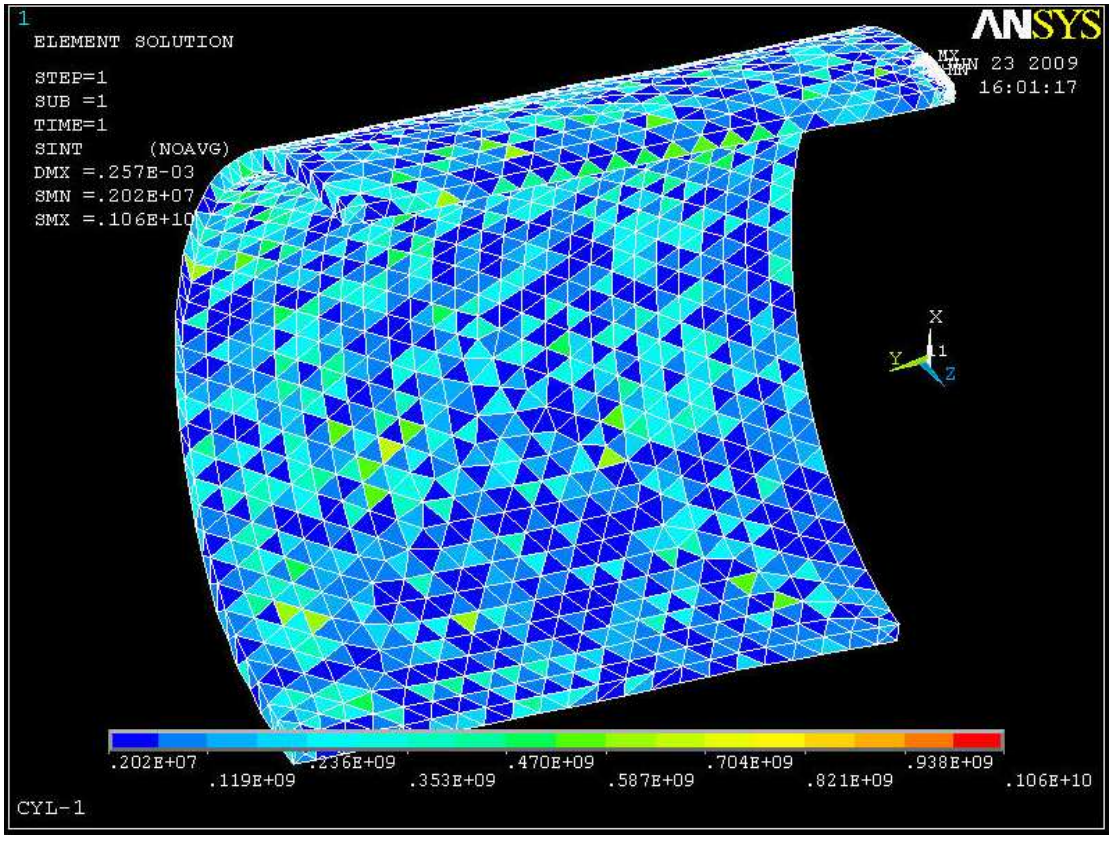

Figure 5.8(a) Distribution of stress intensity plot for external tangential crack

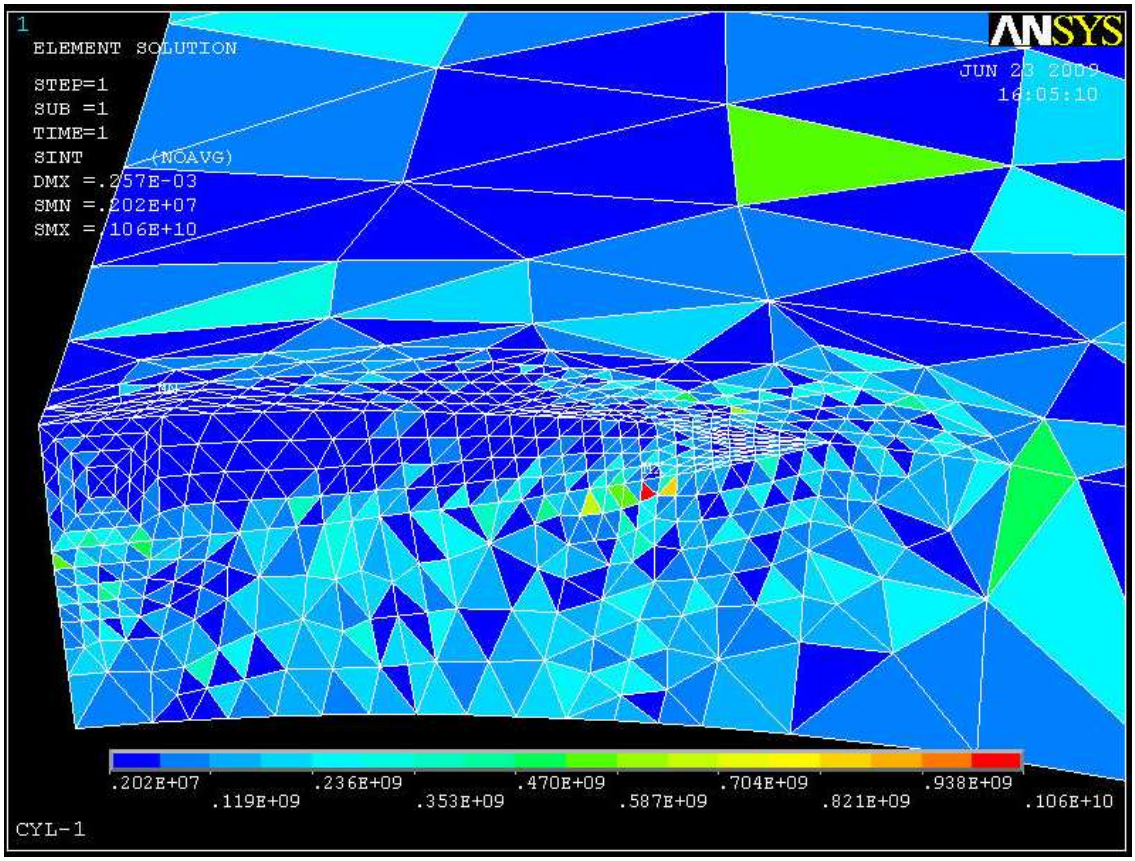

Figure 5.8(b) Magnified stress intensity plot for external tangential crack

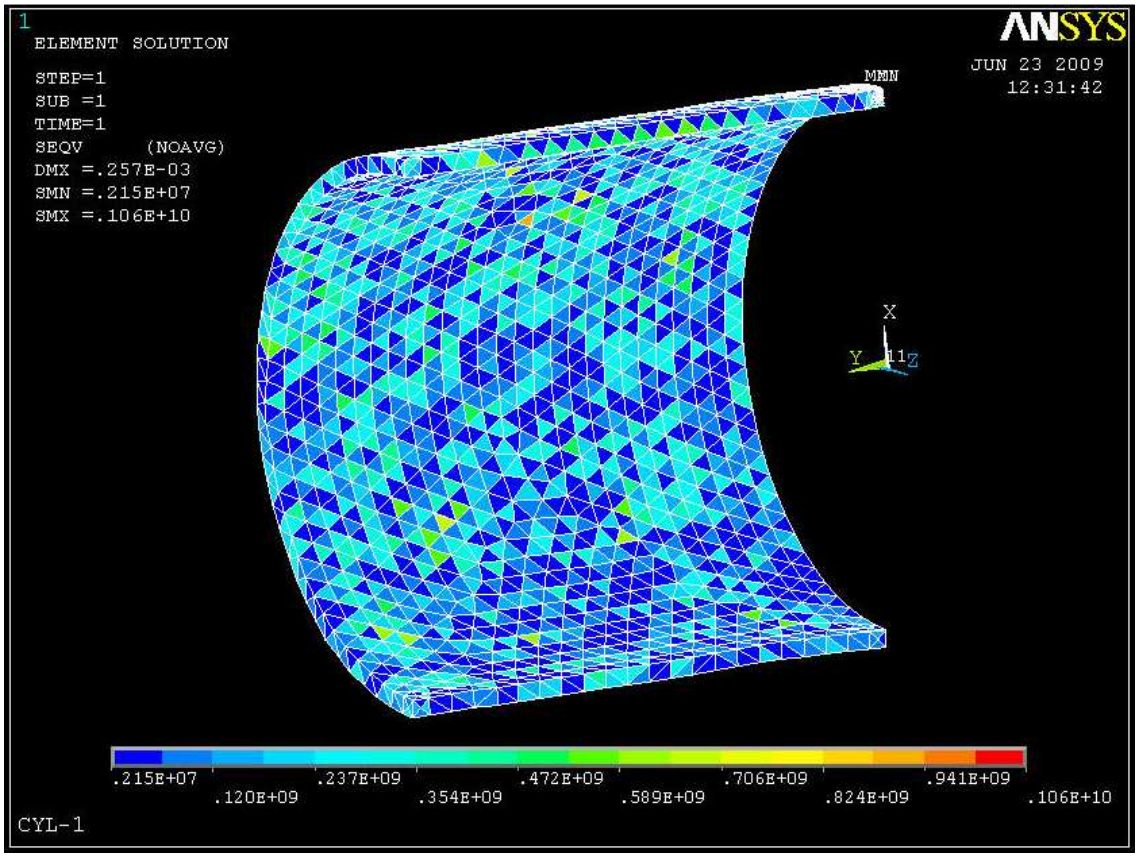

Figure 5.9(a) Distribution of von Misses stress plot for external tangential crack

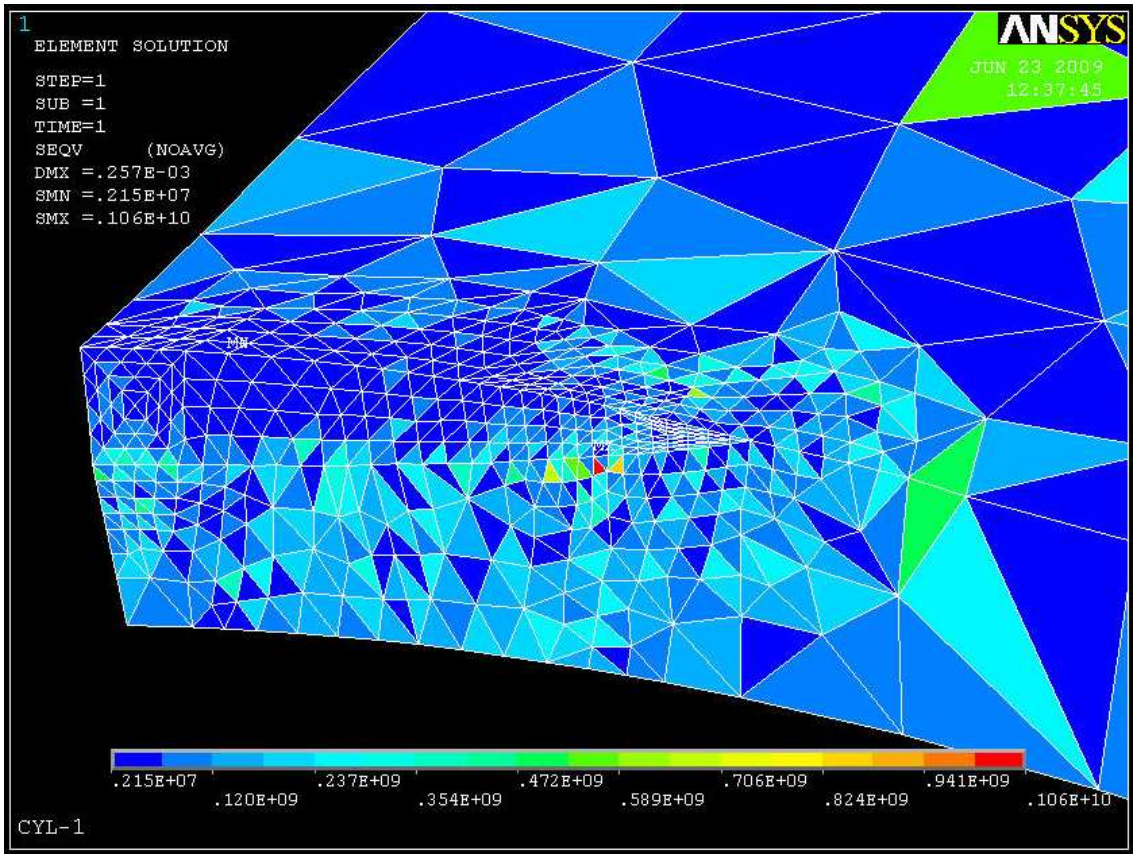

Figure 5.9(b) Magnified von Misses stress plot for external tangential crack

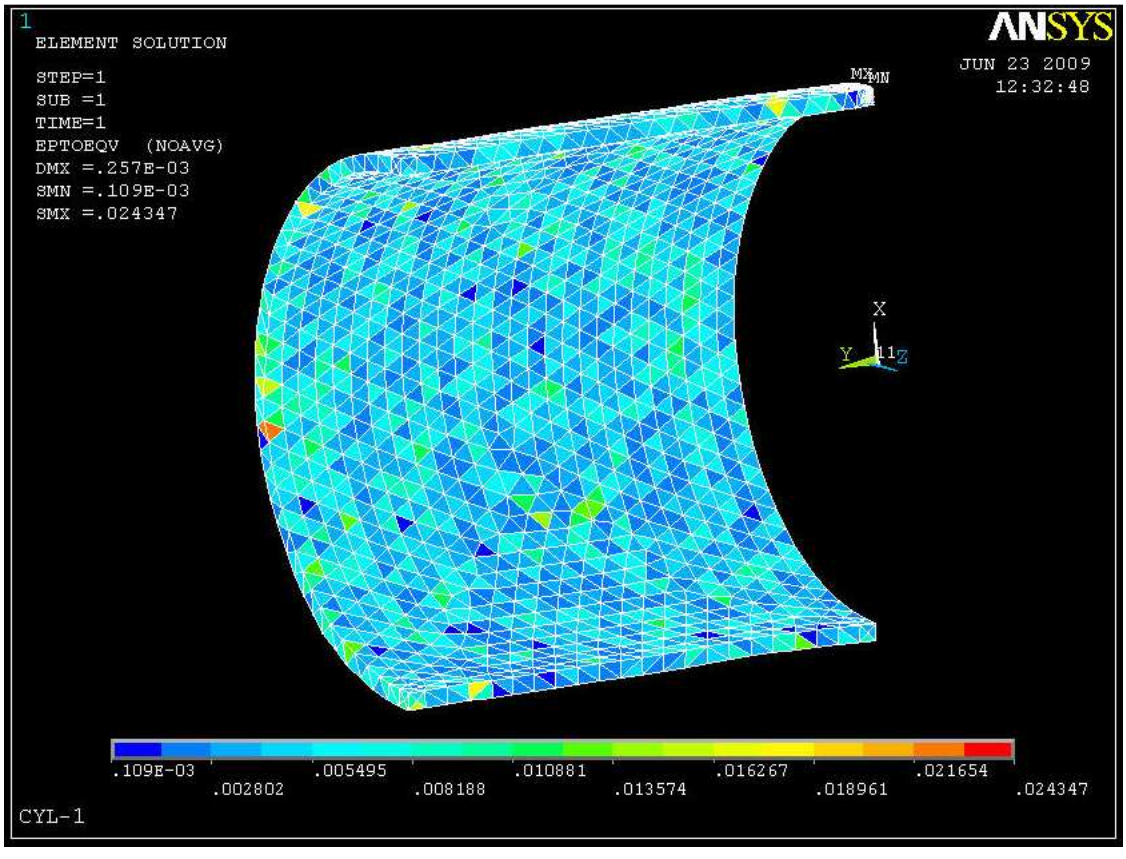

Figure 5.10(a) Distribution of von Misses total strain plot for external tangential crack

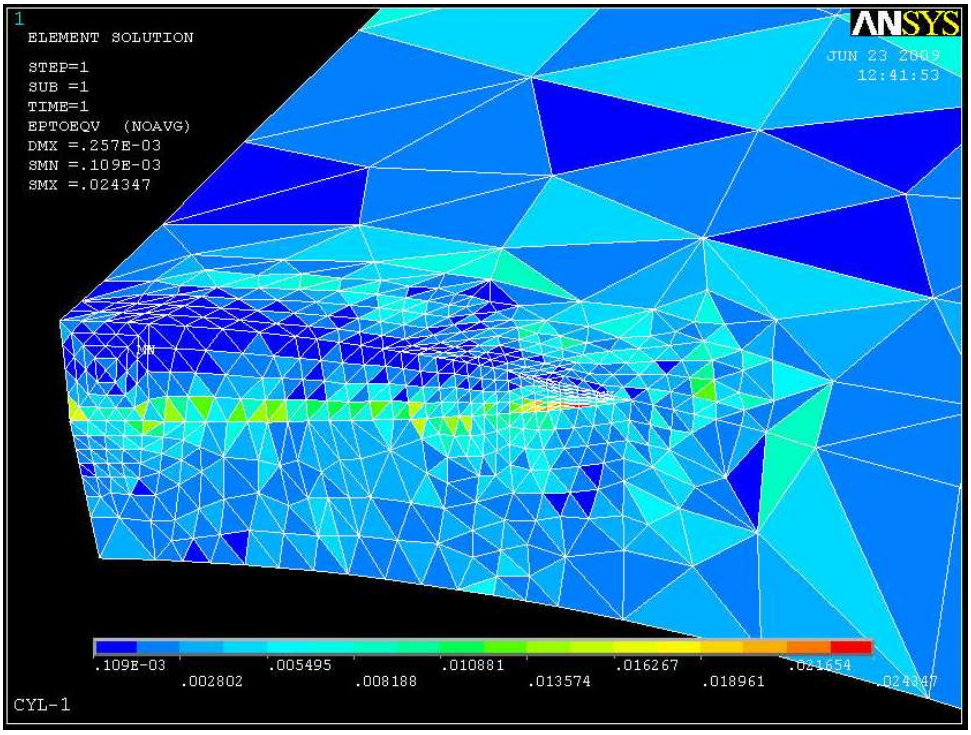

Figure 5.10(b) Magnified von Misses total strain plot for external tangential crack

5.2.2 Model with Internal Tangential Crack

The distribution of stresses and strains around the crack for the tangential surface crack oriented in the interior of the shell (figures 5.11-5.13) reveals that their maximum value for the stress is observed at the maximum penetration point of the crack and for the strain it is observed some how far away the maximum penetration point of the crack but it is on the elliptic contour.

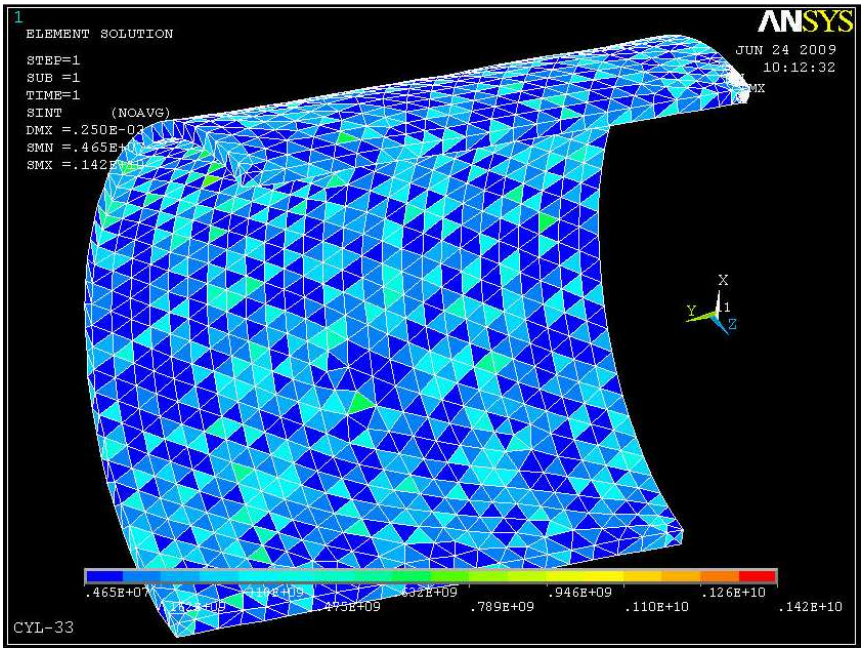

Figure 5.11(a) Distribution of stress intensity plot for internal tangential crack

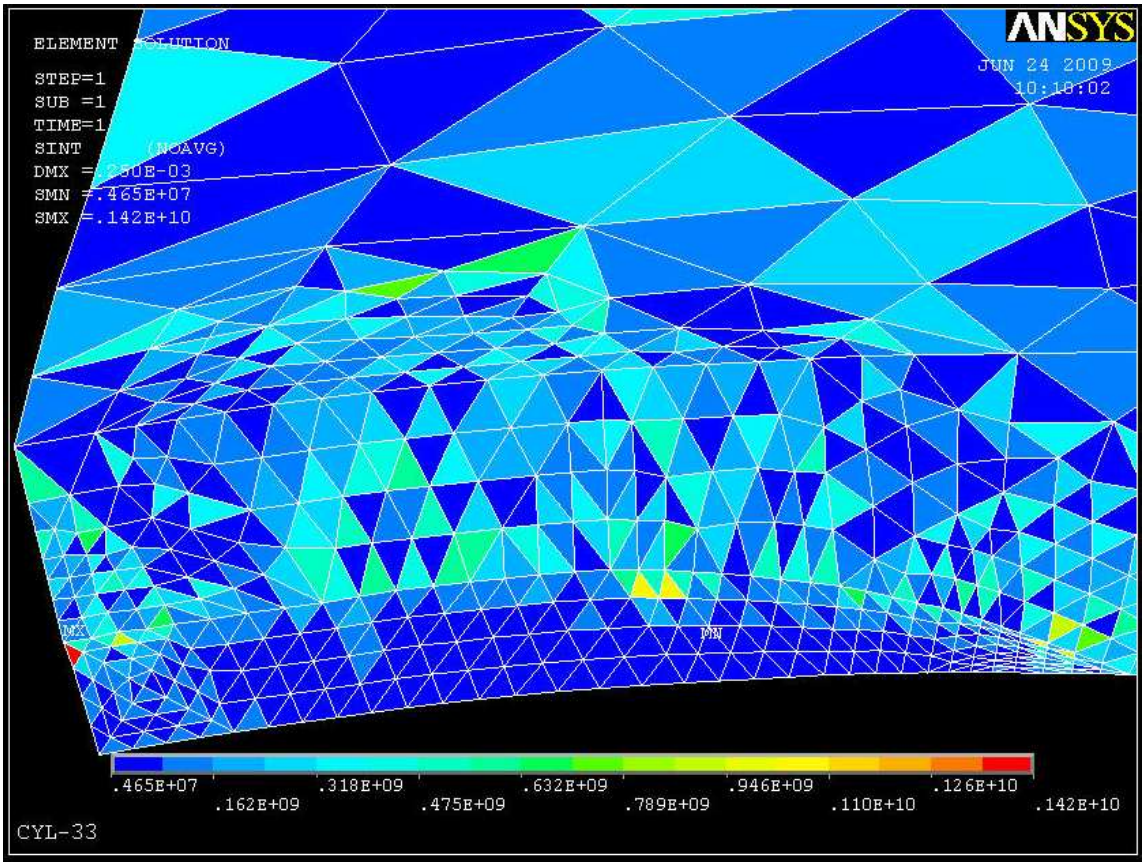

Figure 5.11(b) Magnified stress intensity plot for internal tangential crack

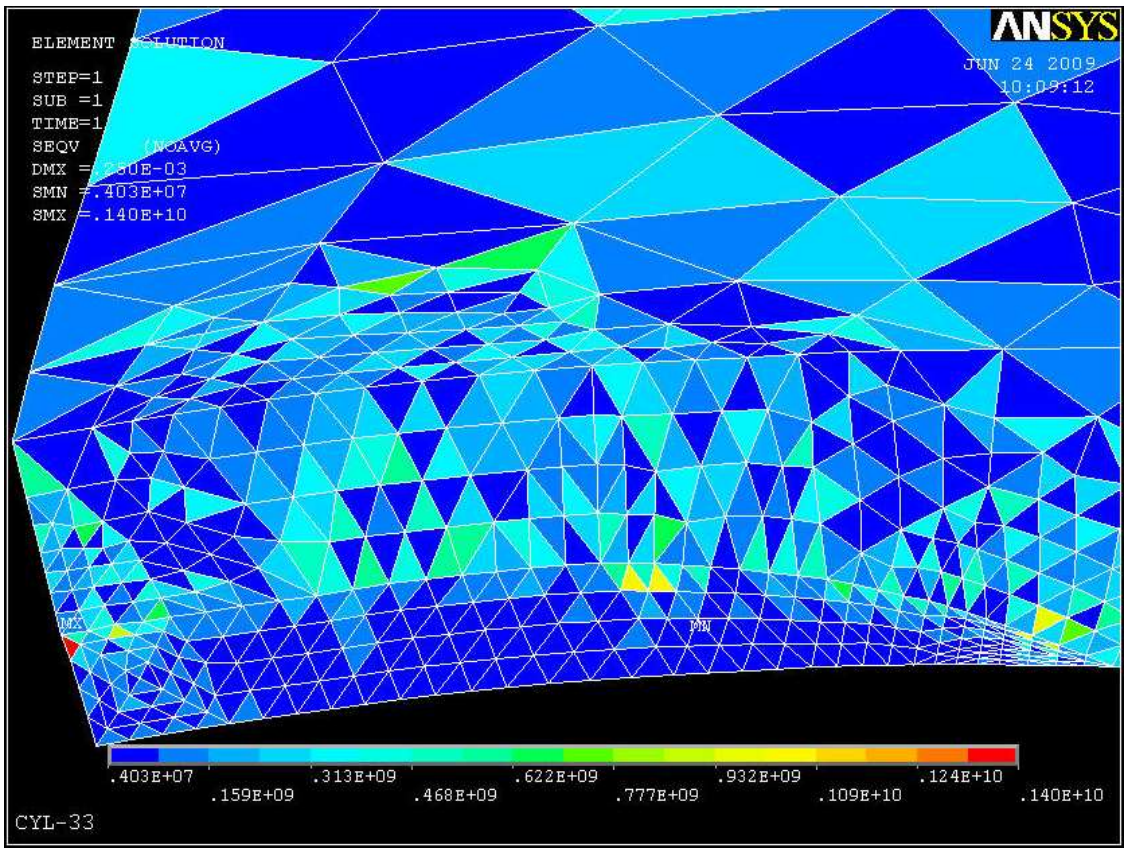

Figure 5.12 Magnified von Misses stress plot for internal tangential crack

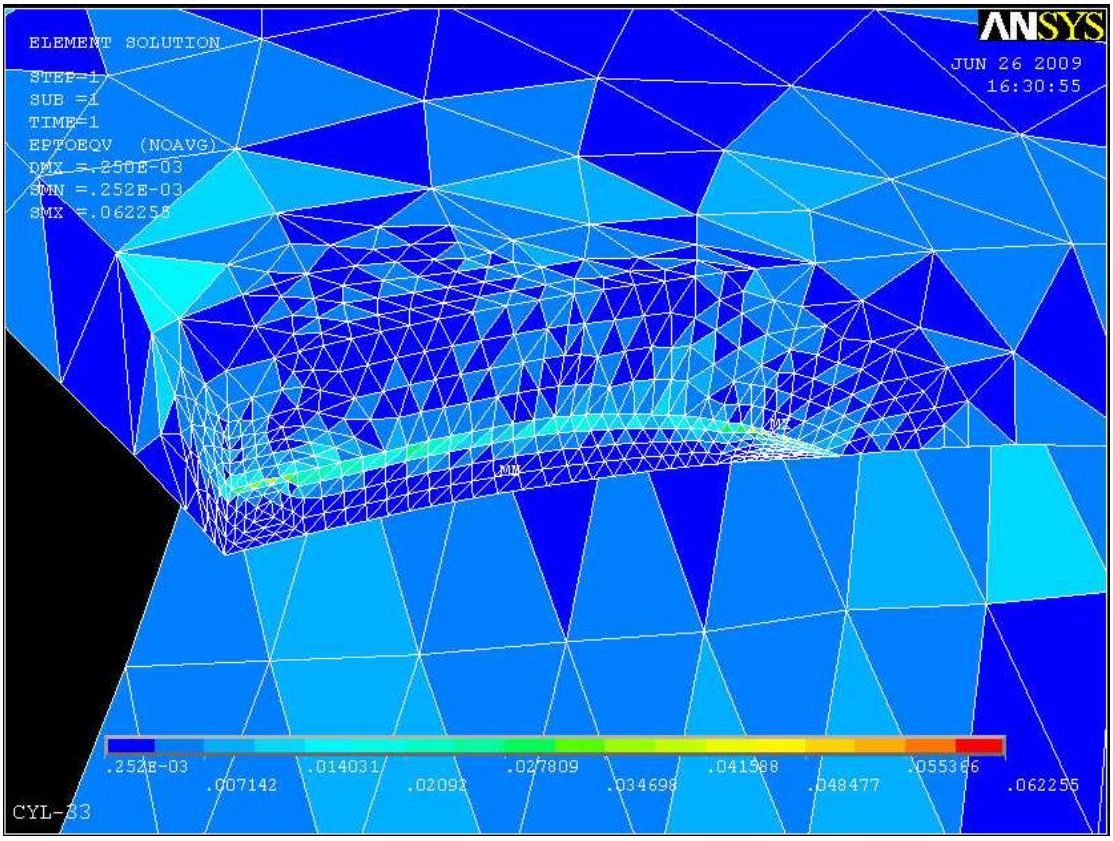

Figure 5.13 Magnified von Misses total strain plot for internal tangential crack

5.3 Model with Axial Crack

Considering again a model with an axial crack, made of the same material as the previous one and with same geometrical parameter but of different boundary condition loaded tangentially figure 4.10. It will let us deduce on how stress propagates in the body of the shell structure subjected to remote loading for the Mode I loading condition in a similar manner to that of the axial loading. In order to make the analysis so reasonable, the meshed shell model presented is generated by the ANSYS automatic mesh generation command with very fine elements near the surface crack contour.

The axial surface crack is also oriented in to two positions on the cylindrical shell structure, externally and internally

5.3.1 Model with External Axial Crack

With similar arguments discussed in the previous portions it is also observed that the crack front stresses are shielded away. The stress intensity and von Misses stress distribution depicted in figures 5.14 -5.15 show that their maximum values are observed on the inside parts of the shell structure for the surface crack located at the outer surface.

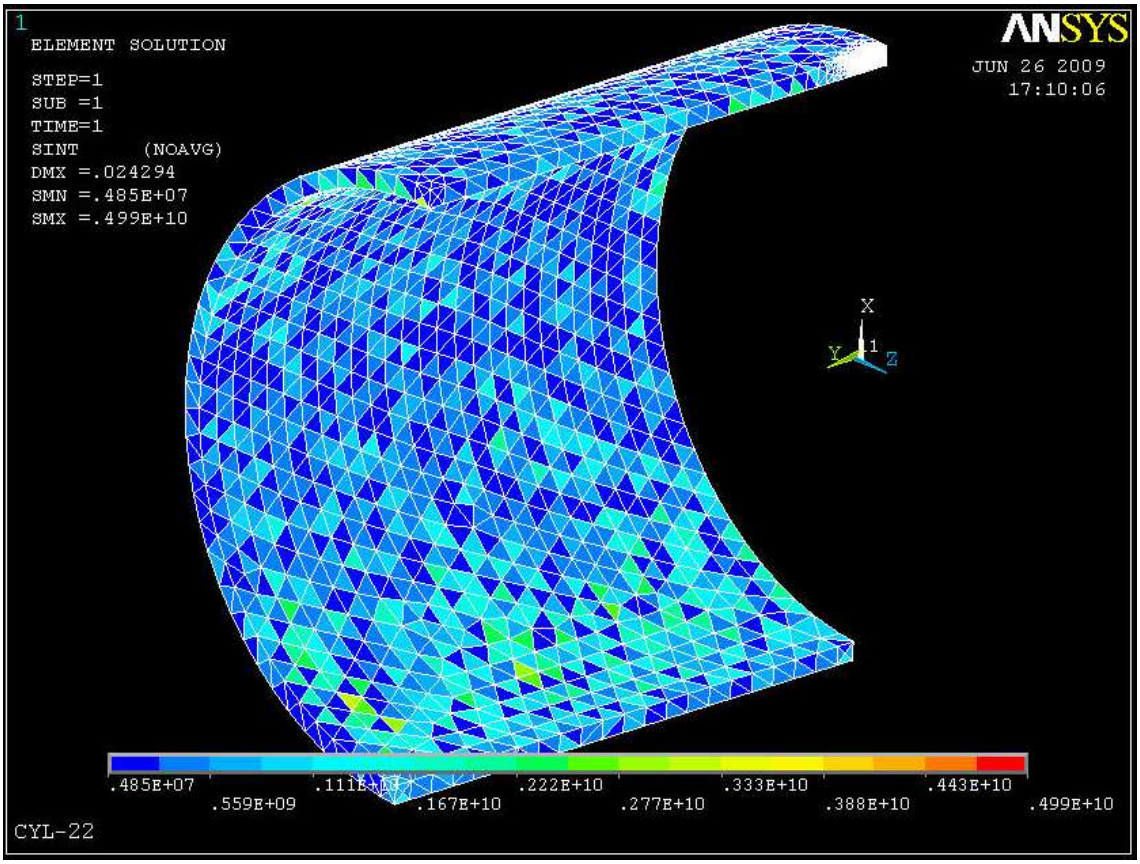

Figure 5.14(a) Distribution of stress intensity plot for external axial crack

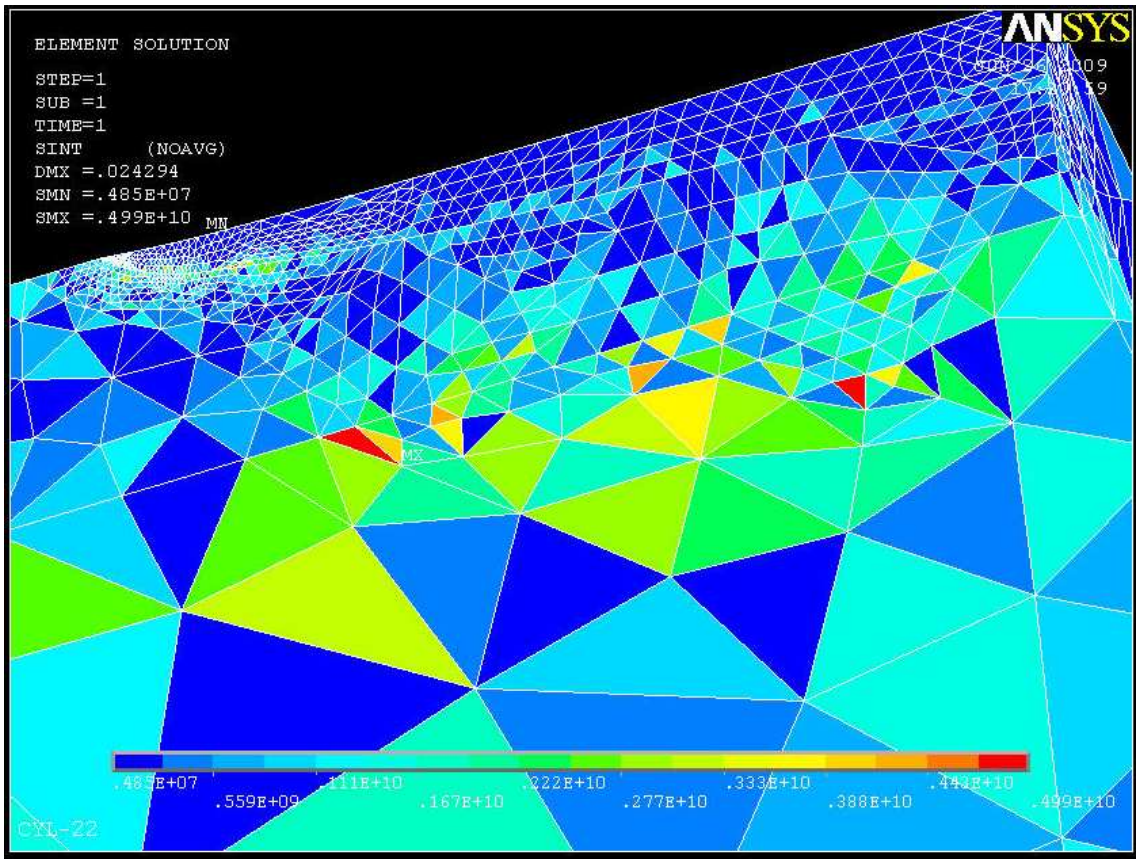

Figure 5.14(b) Magnified stress intensity plot for external axial crack

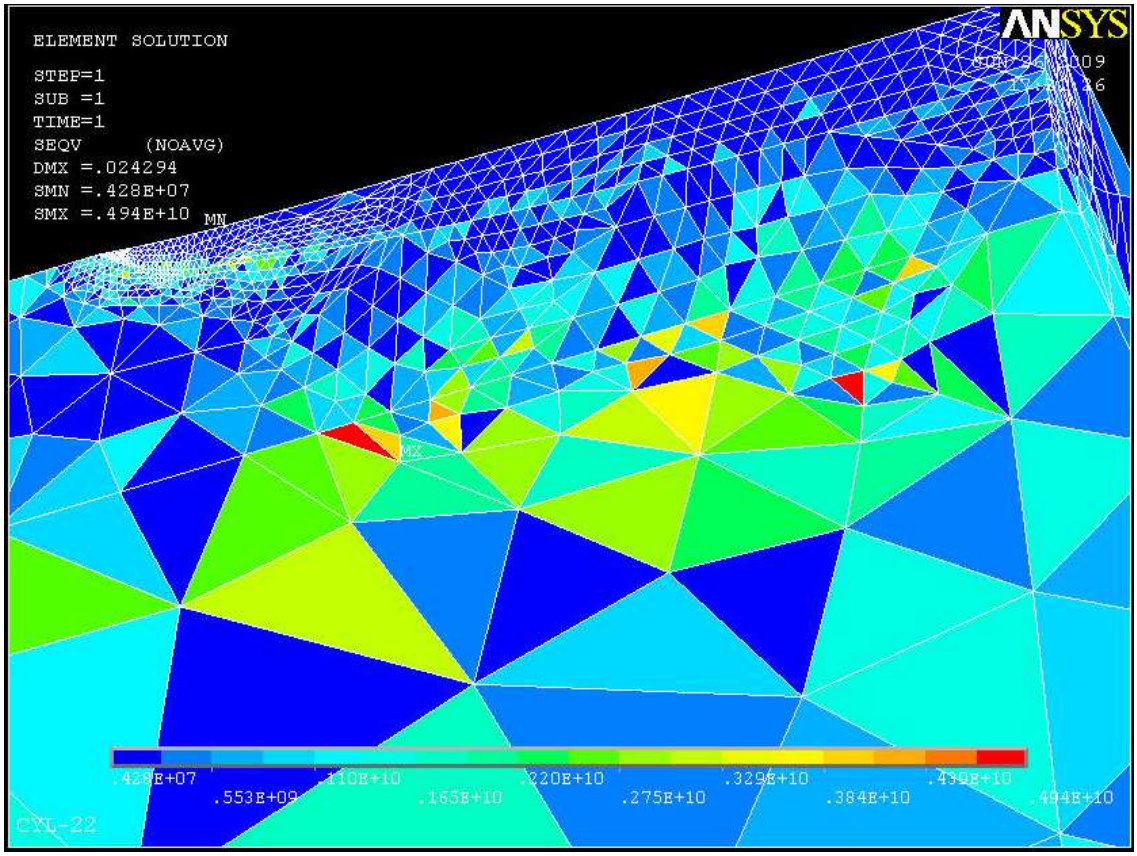

Figure 5.15 Magnified von Misses stress plot for external axial crack

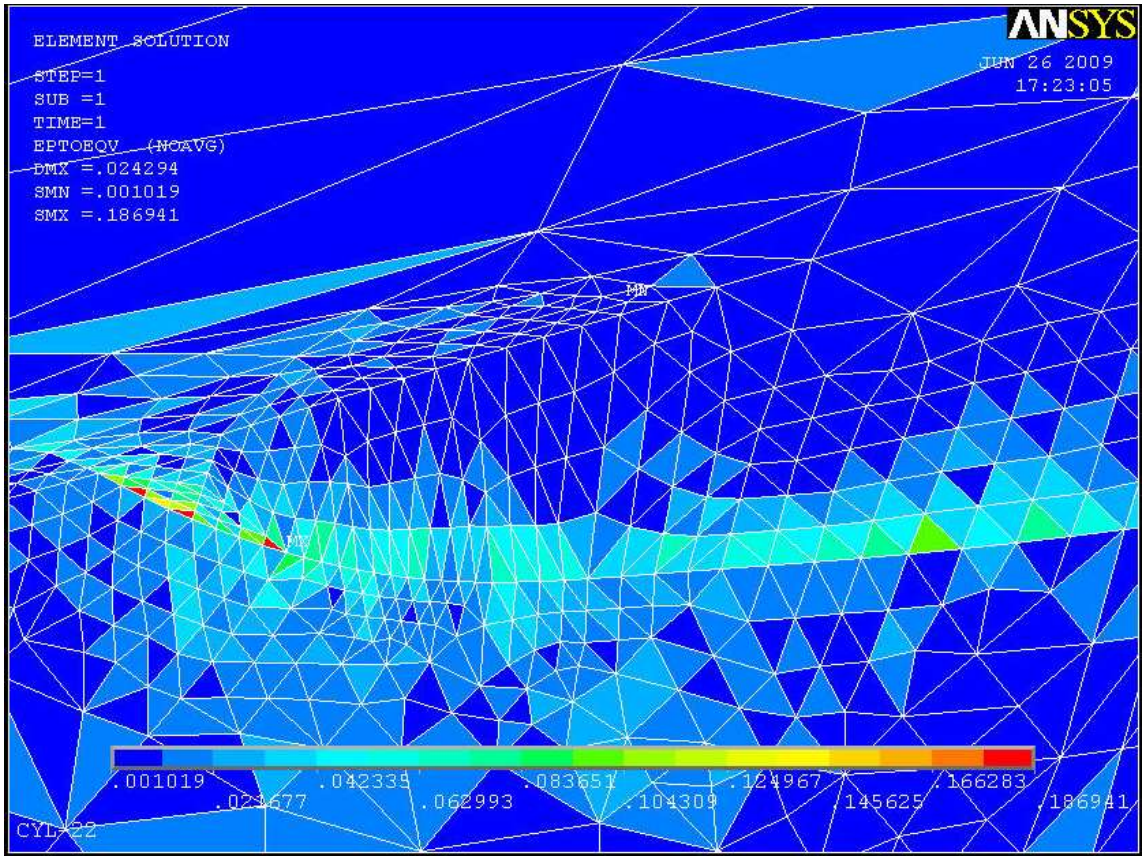

Figure 5.16 Magnified von Misses total strain plot for external axial crack

5.3.2 Model with internal Axial Crack

According to figures 5.17-5.19, the stress and strain distribution also highlights the case of somehow shielding of critically damaged zone that may be on the plane of the surface crack advancement away from the maximum penetration point.

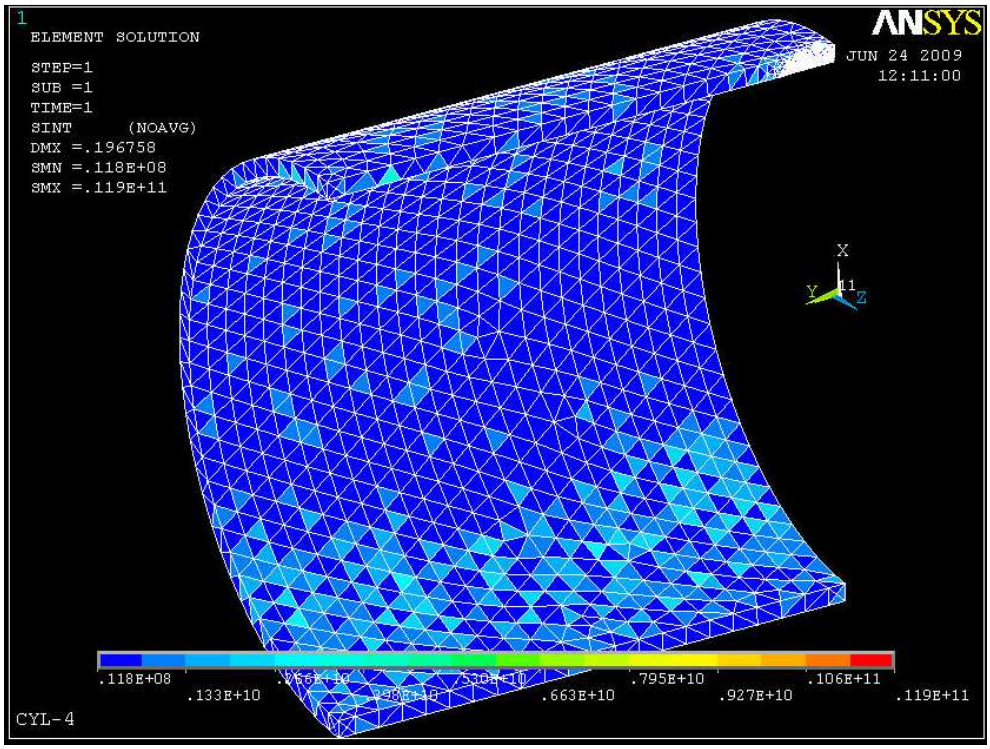

Figure 5.17(a) Distribution of stress intensity plot for internal axial crack

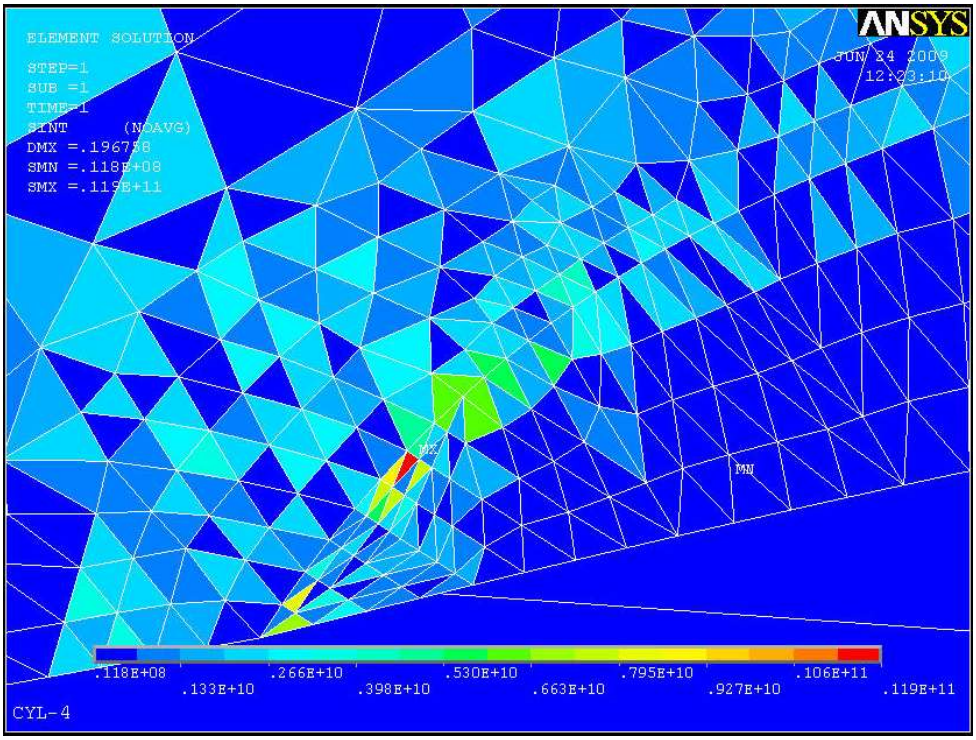

Figure 5.17(b) Magnified stress intensity plot for internal axial crack

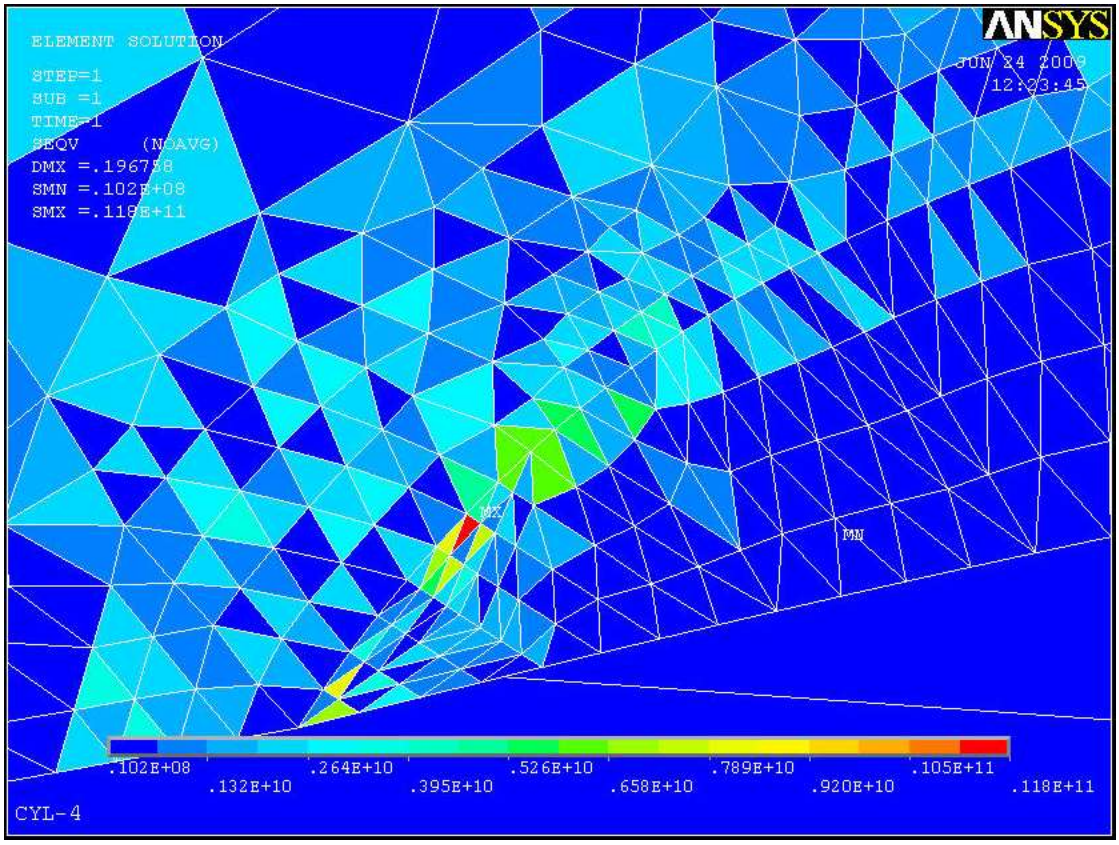

Figure 5.18 Magnified von Misses stress plot for internal axial crack

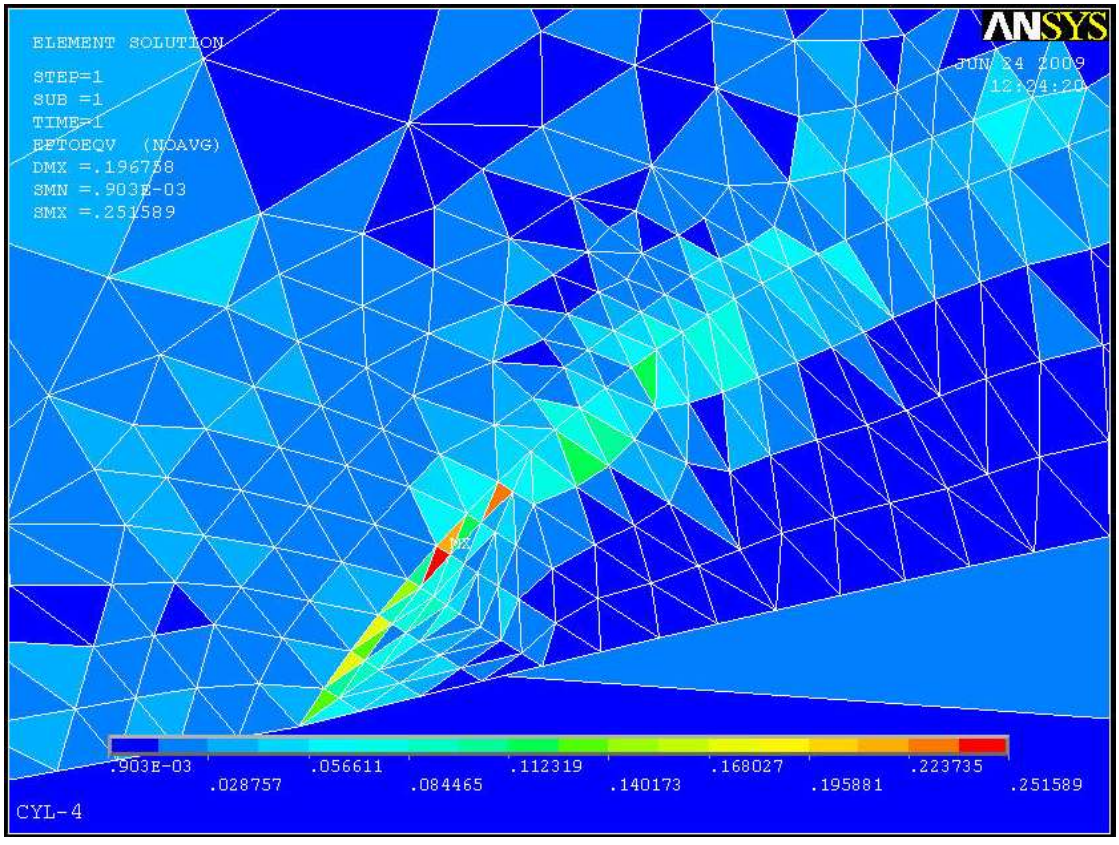

Figure 5.19 Magnified von Misses total strain plot for internal axial crack

To utilize high strength and stiffness of fibers in a composite material suitable for engineering applications, fibers are bound with a matrix material whose strength and stiffness are, naturally, much lower than those of fibers (otherwise, no fibers would be necessary). Matrix materials provide the final shape of the composite structure and govern the parameters of the manufacturing process. Optimal combination of fiber and matrix properties should satisfy a set of operational and manufacturing requirements. The stiffness of the matrix should correspond to the stiffness of the fibers and be sufficient to provide uniform loading of fibers.

In order to conclude the numerical simulation of surface crack problems, the presented localized and shielded stress and strain distribution reveals how stress and strain varies in the composite cylindrical shell. Similar to that found in[6], the stress analysis around the crack tip in a surface cracked composite cylindrical shell structure reveals the mode of variation that is caused by the combined effects of fiber-matrix debonding, fiber rupture, matrix cracking and delamination between the adjacent layers are in a good agreement. Even though the mechanical characterization taking into account these different modes of failure is complex, the finite element analysis performed has given an insight of variation of stress and resistance to crack propagation of composite materials. Though, it doesn’t mean that the elliptical surface crack introduced in the tangential direction both external and internal is the actual shape as it is difficult to model exact elliptical shape on the circular curvature of the cylindrical shell; rather it is an approximation of an elliptical crack for the tangential orientation.

CHAPTER SIX
CONCLUSION AND RECOMMENDATIONS

6.1 Conclusion

Methods and corresponding computer simulation for probabilistically assessing fracture behavior of surface cracked composite shell structure have been discussed. The fracture in composite structures was simulated via a finite element package (ANSYS), independent of stress intensity factors and fracture toughness parameters. The approach described herein is inclusive in that it integrates composite mechanics (for composite behavior) with finite element analysis (for global structural response) and incorporates the assessment of stress analysis around the crack tip during composite structural fracture. Compared to Isotropic materials, (traditional materials like aluminum for which composites are substitutive in the air craft industry for being light in weight), composites have higher resistance to fracture and have unpredicted stress distribution pattern as shown somewhere in the previous sections. As compared to the plots of stress and strain distribution around the surface crack in isotropic material (figures 6.1-6.8) to that of composite materials, the stress and strain distribution of isotropic material shows a uniform distribution which can be predicted to be at the maximum penetration points of the surface crack. The difference in the stress distribution contour in the two mentioned material shows that the composite materials are capable of transferring the critical stresses and strains from the critical damage zones to the undamaged zones that is why composite materials show stress and strain shielding of critically damage zones and this also show that their load carrying capacity than isotropic materials.

Furthermore, the crack tip contouring mode difference comes for both materials due to the difference in microstructural composition and the sharp corners in isotropic material becomes the critical area for stress initiation and propagation , that is to say, there is no shielding effect in case of isotropic materials. As stresses and strains at around the crack in isotropic materials are maximum and critically distributed at the critical portions of the surface crack i.e., maximum penetration point of the surface crack, the material exposure to these critical stresses and strains at this location becomes higher. The higher exposure of the critical damaged portions will not have enough resistance and the material will fail easily in a different manner to that of composite materials since they have a shielding capacity of critically damage zones.

6.1.1 Isotropic Material Model with Surface Crack

a) External tangential surface crack in isotropic material shell

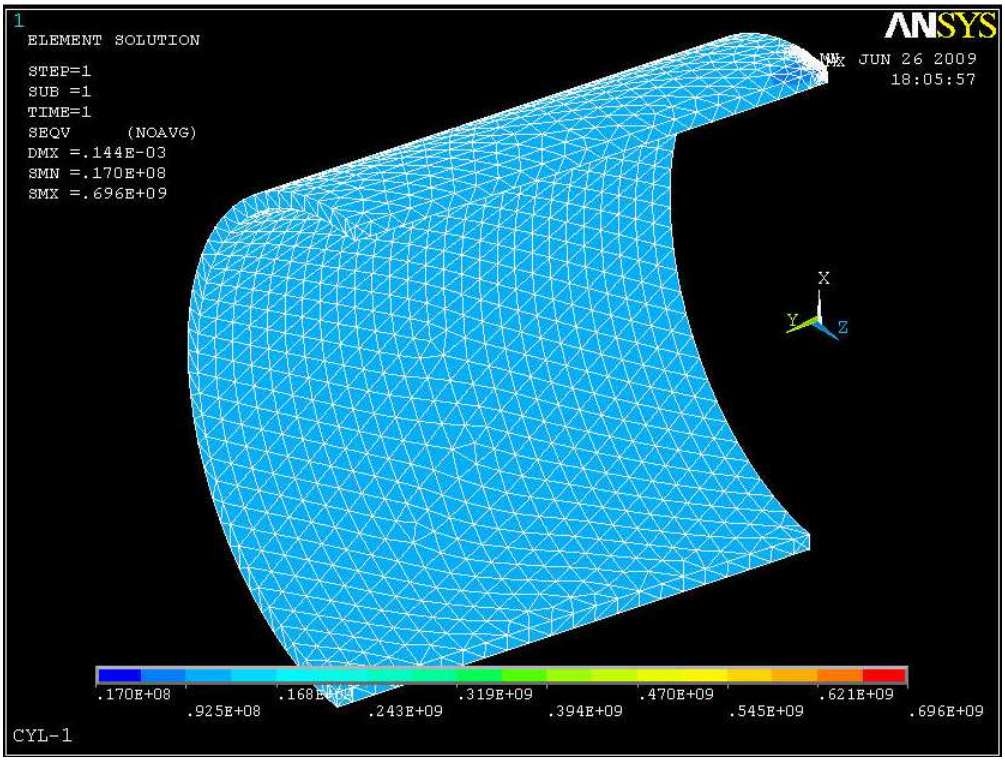

Figure 6.1(a) Distribution of von Misses stress plot for external tangential crack in isotropic shell

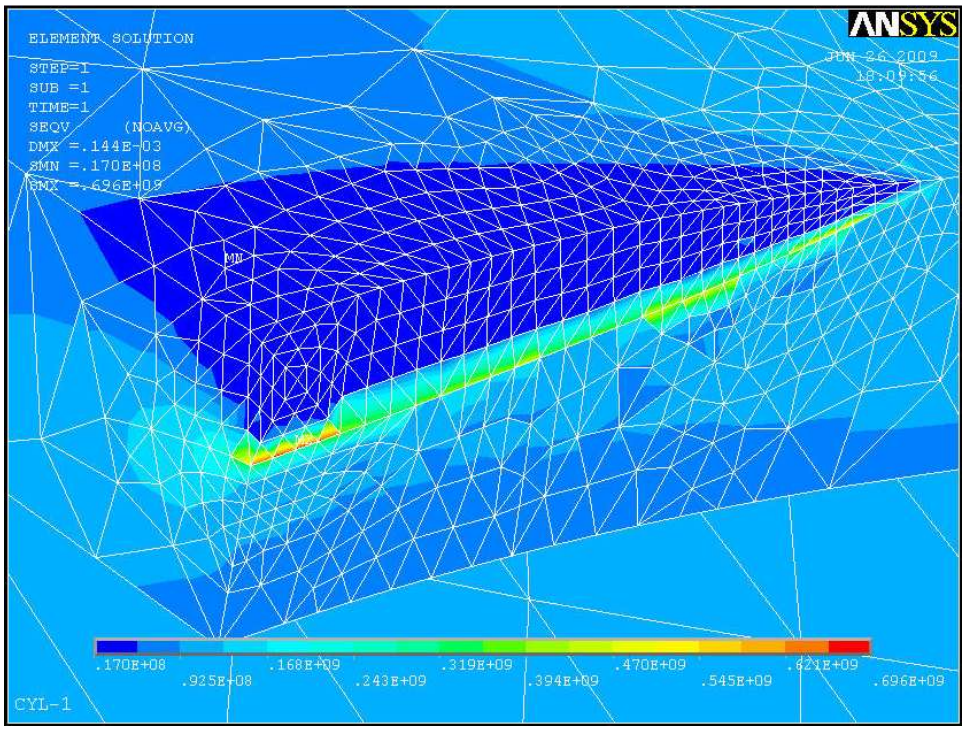

Figure 6.1(b) Magnified von Misses stress plot for external tangential crack in isotropic shell

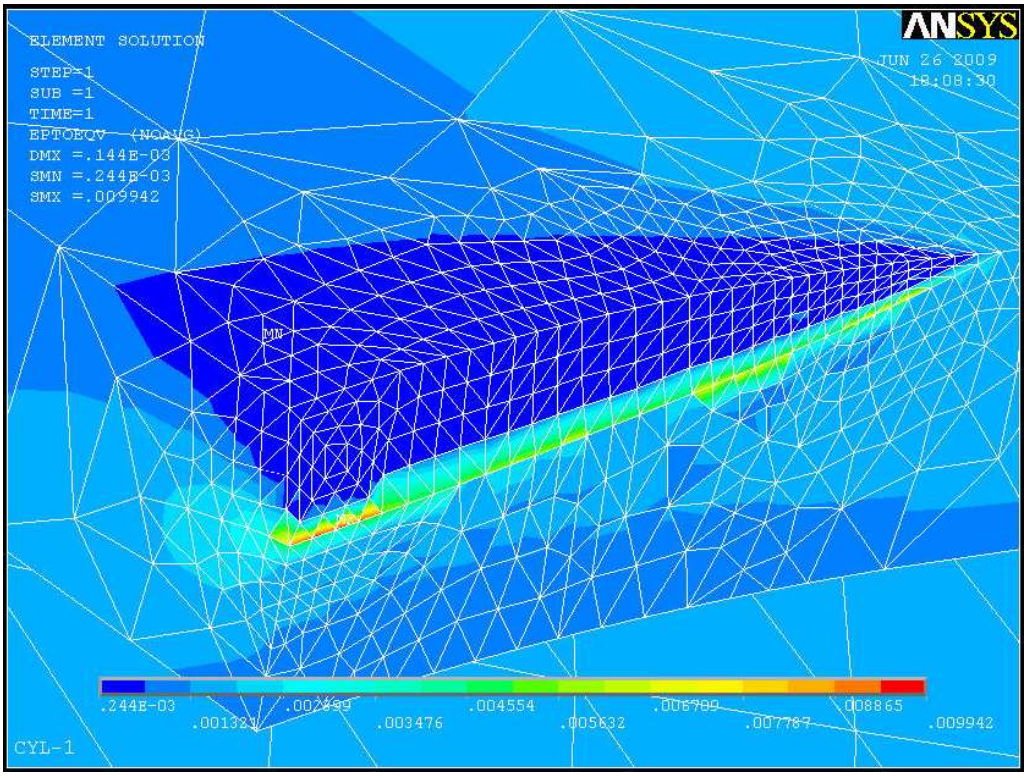

Figure 6.2 Magnified von Misses total strain plot for external tangential crack in isotropic shell

b) Internal tangential surface crack in isotropic material shell

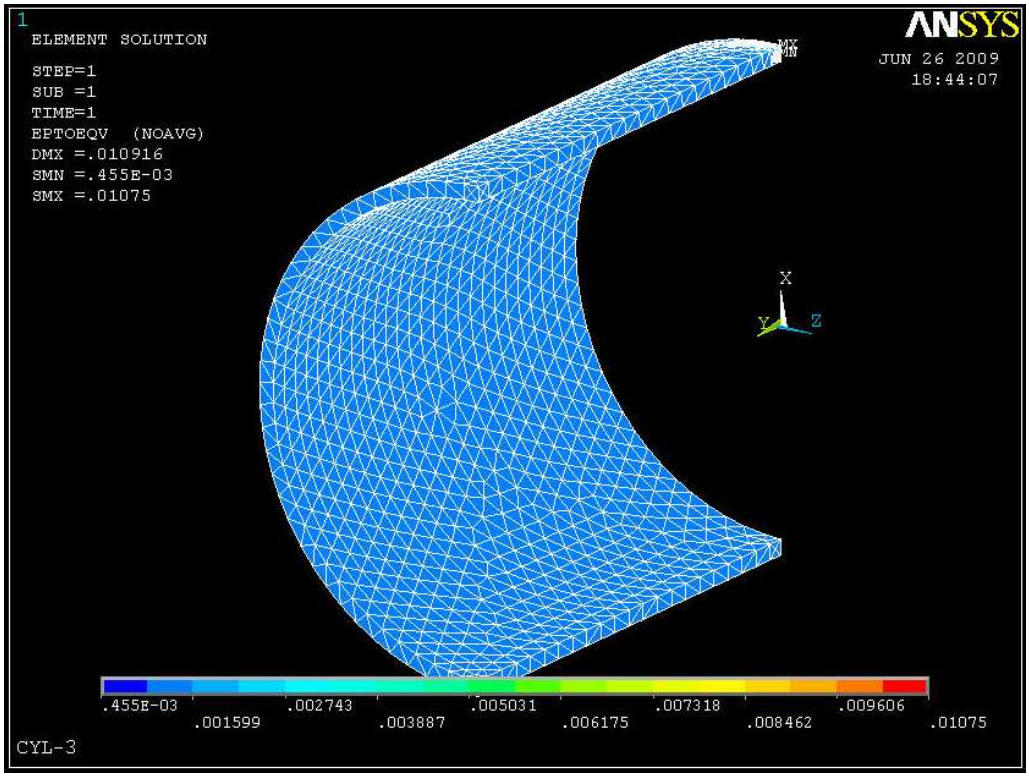

Figure 6.3(a) Distribution of von Misses stress plot for internal tangential crack in isotropic shell

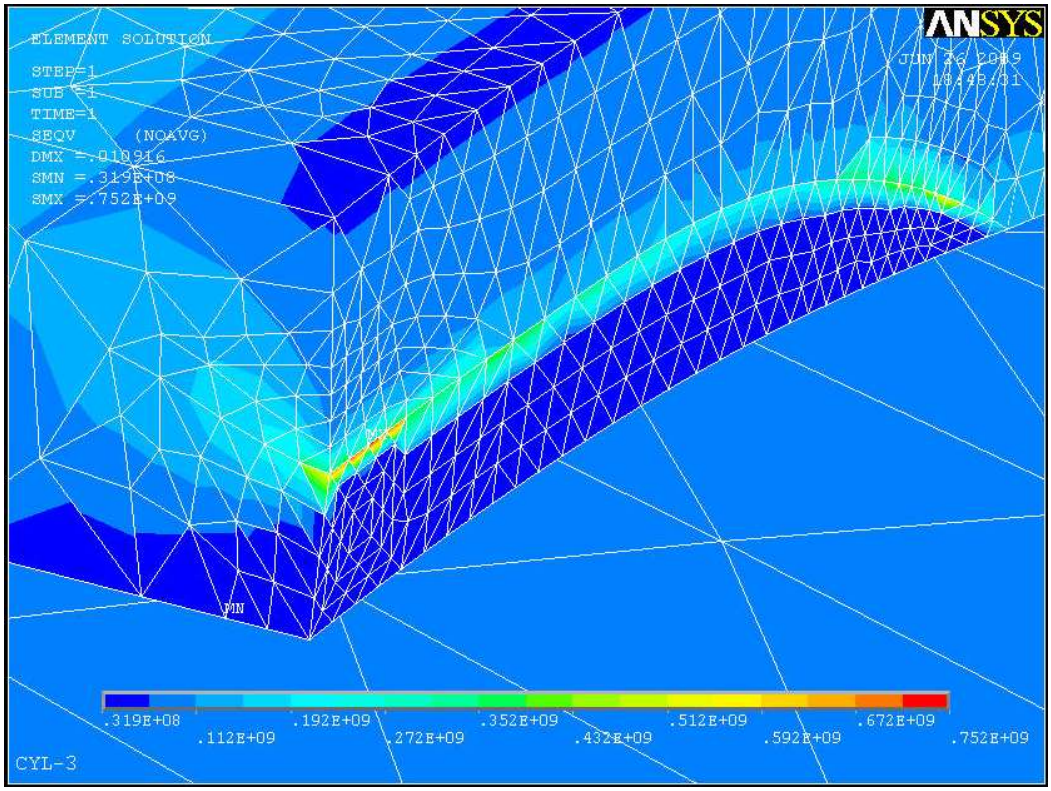

Figure 6.3(b) Magnified von Misses stress plot for internal tangential crack in isotropic shell

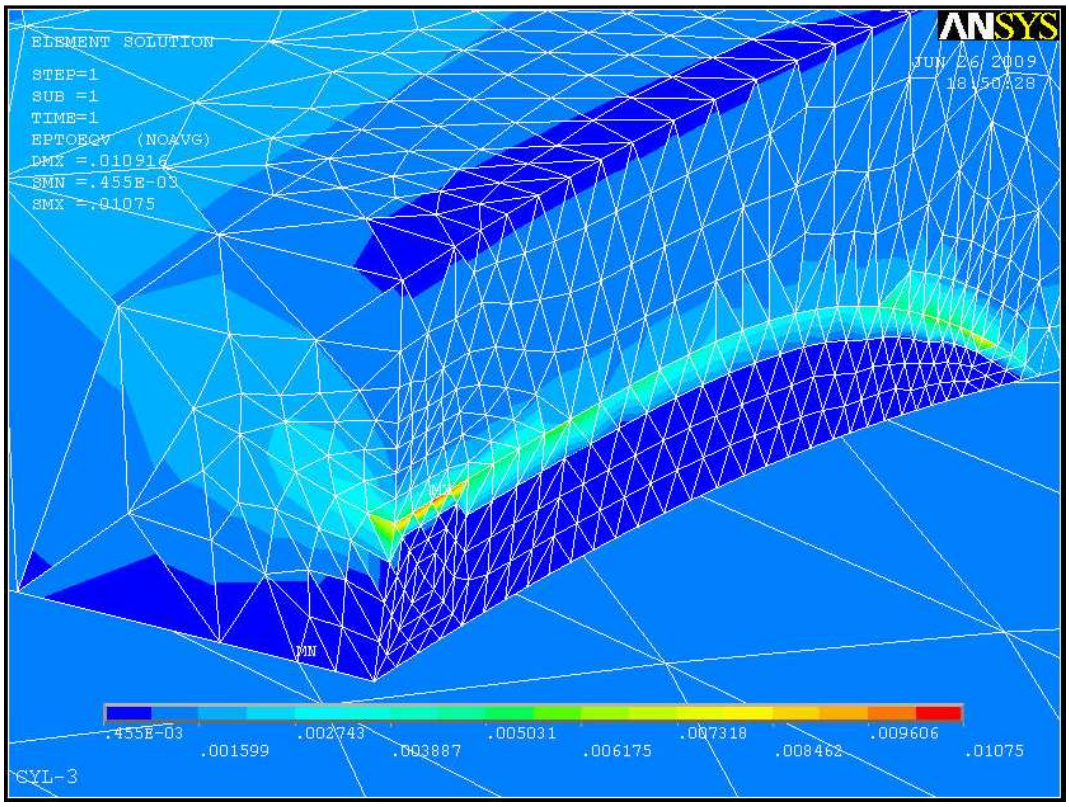

Figure 6.4 Magnified von Misses total strain plot for internal tangential crack in isotropic shell

c) External axial surface crack in isotropic material shell

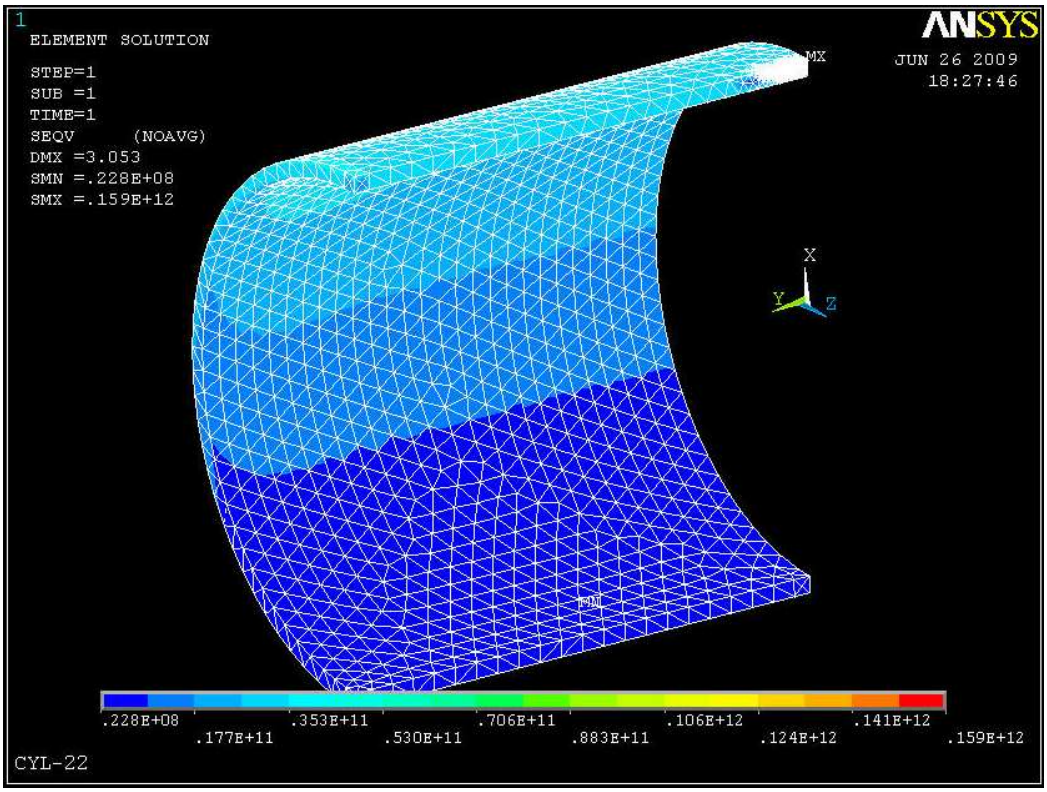

Figure 6.5(a) Distribution of von Misses stress plot for external axial crack in isotropic shell

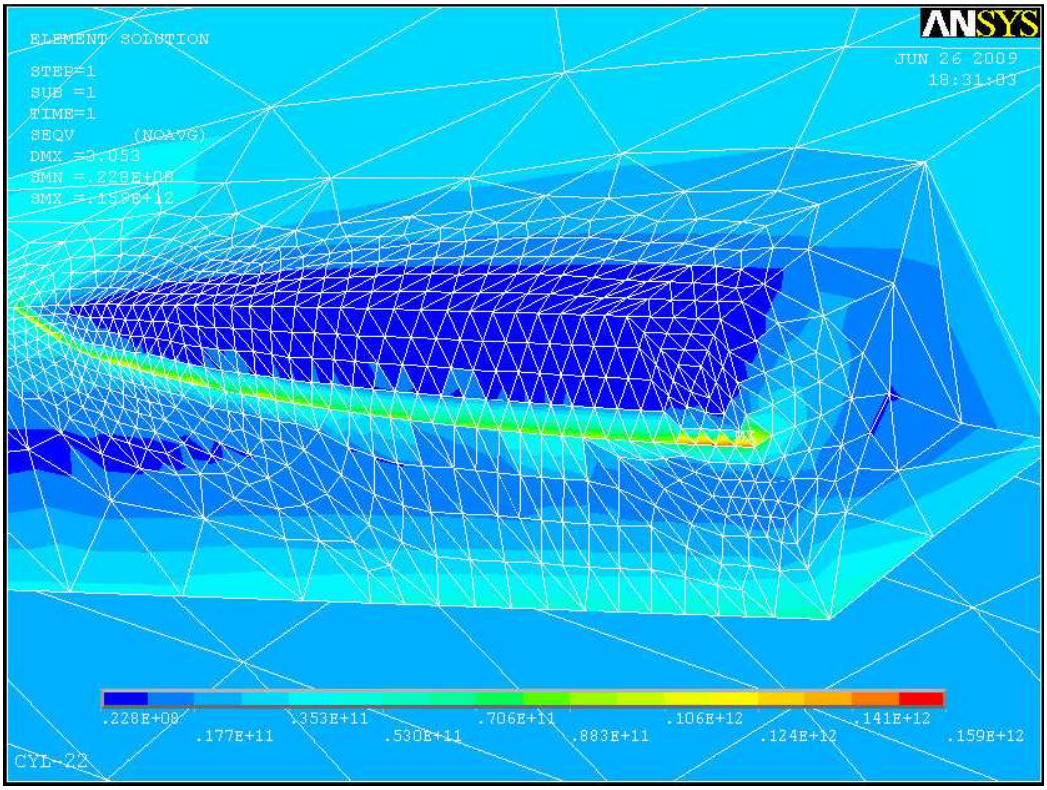

Figure 6.5(b) Magnified von Misses stress plot for external axial crack in isotropic shell

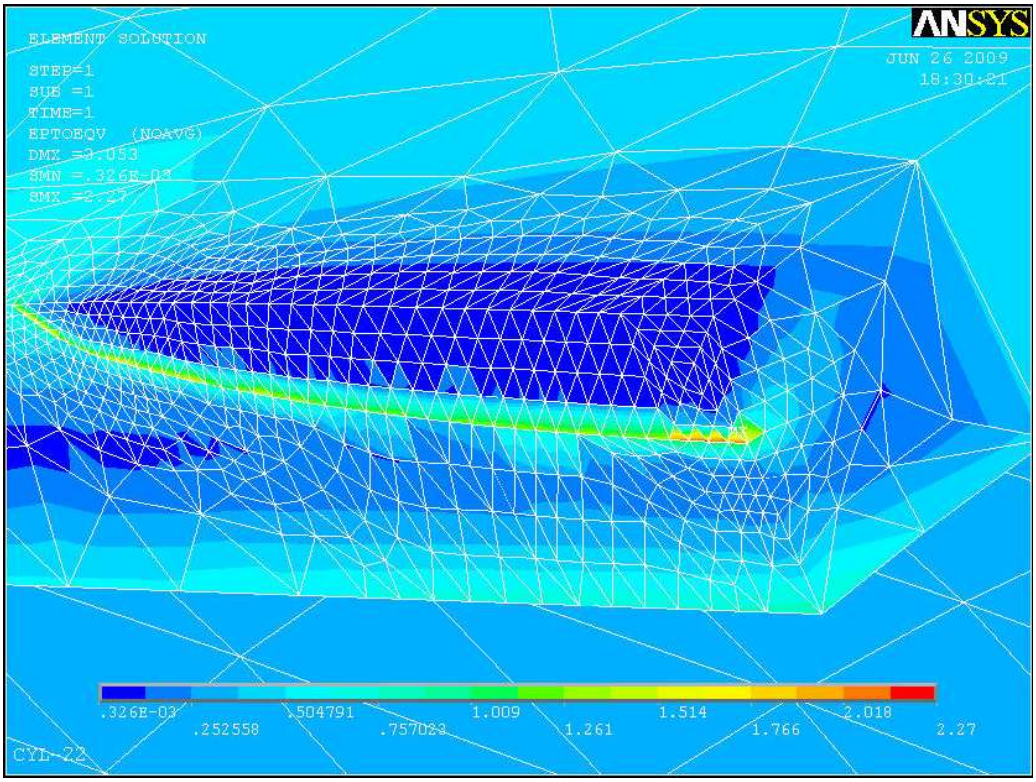

Figure 6.6 Magnified von Misses total strain plot for external axial crack in isotropic shell

d) Internal axial surface crack in isotropic material shell

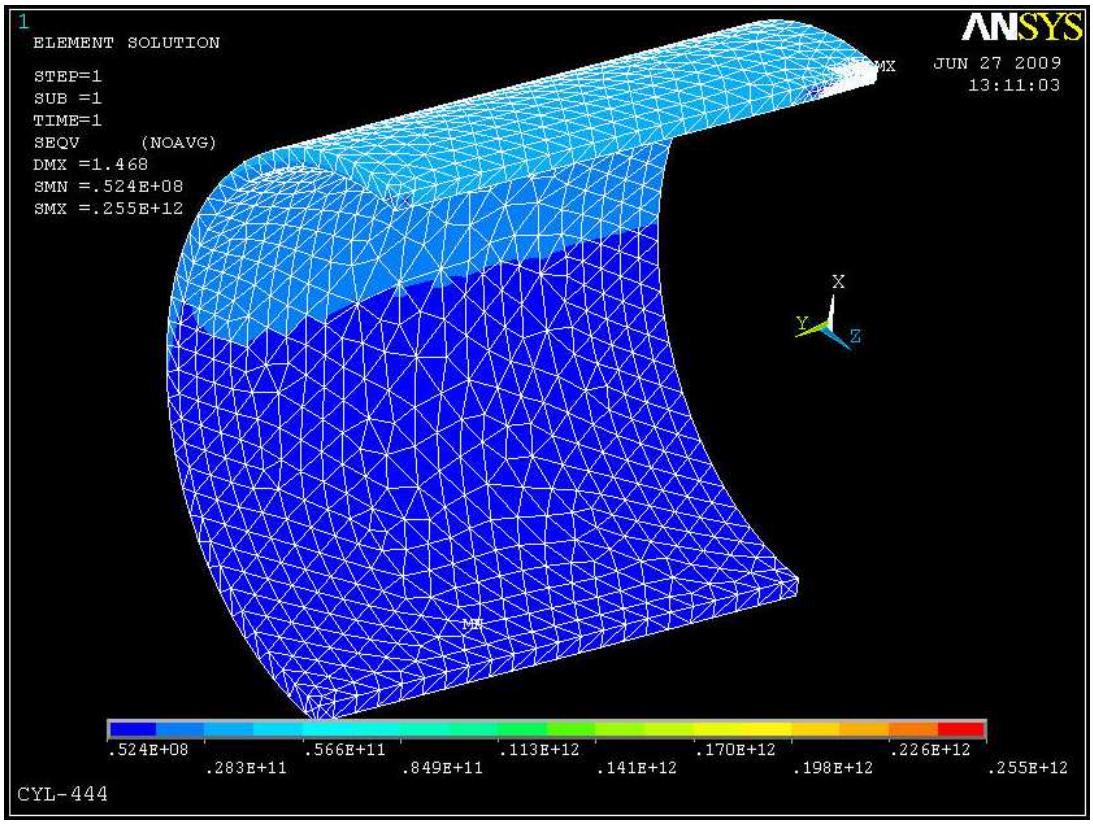

Figure 6.7(a) Distribution of von Misses stress plot for internal axial crack in isotropic shell

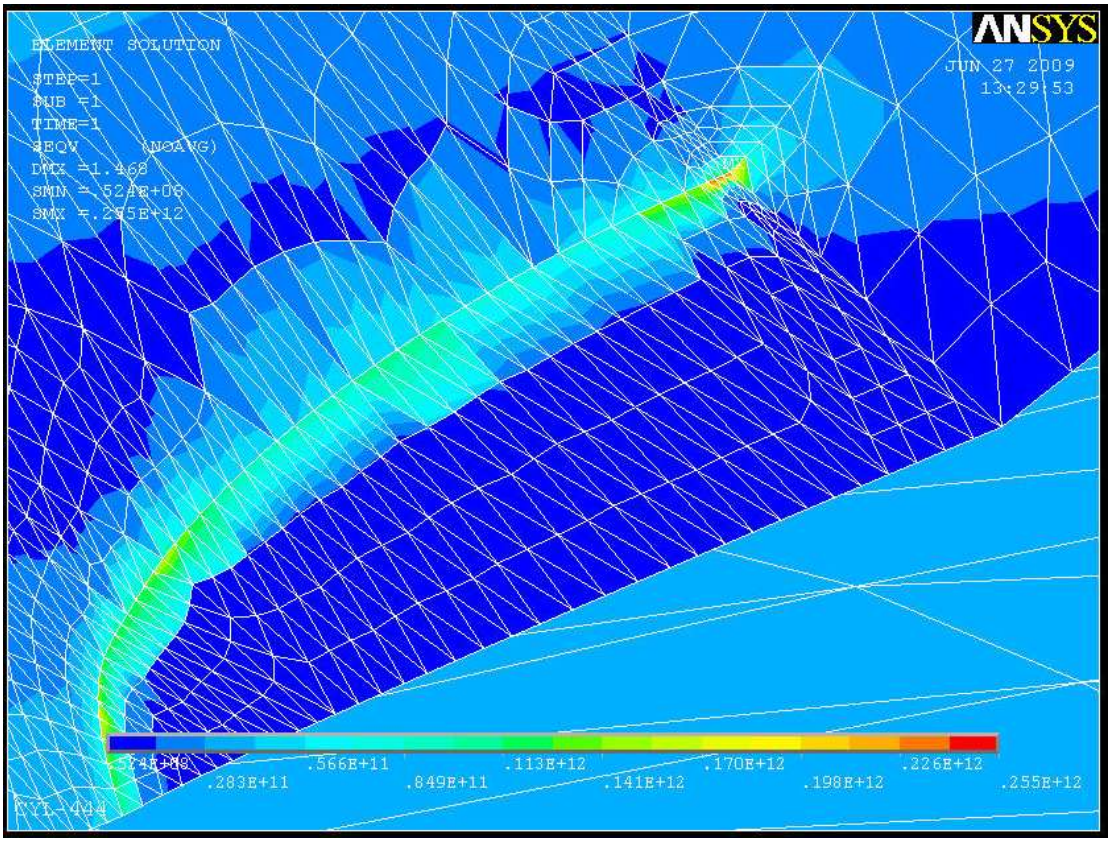

Figure 6.7(b) Magnified von Misses stress plot for internal axial crack in isotropic shell

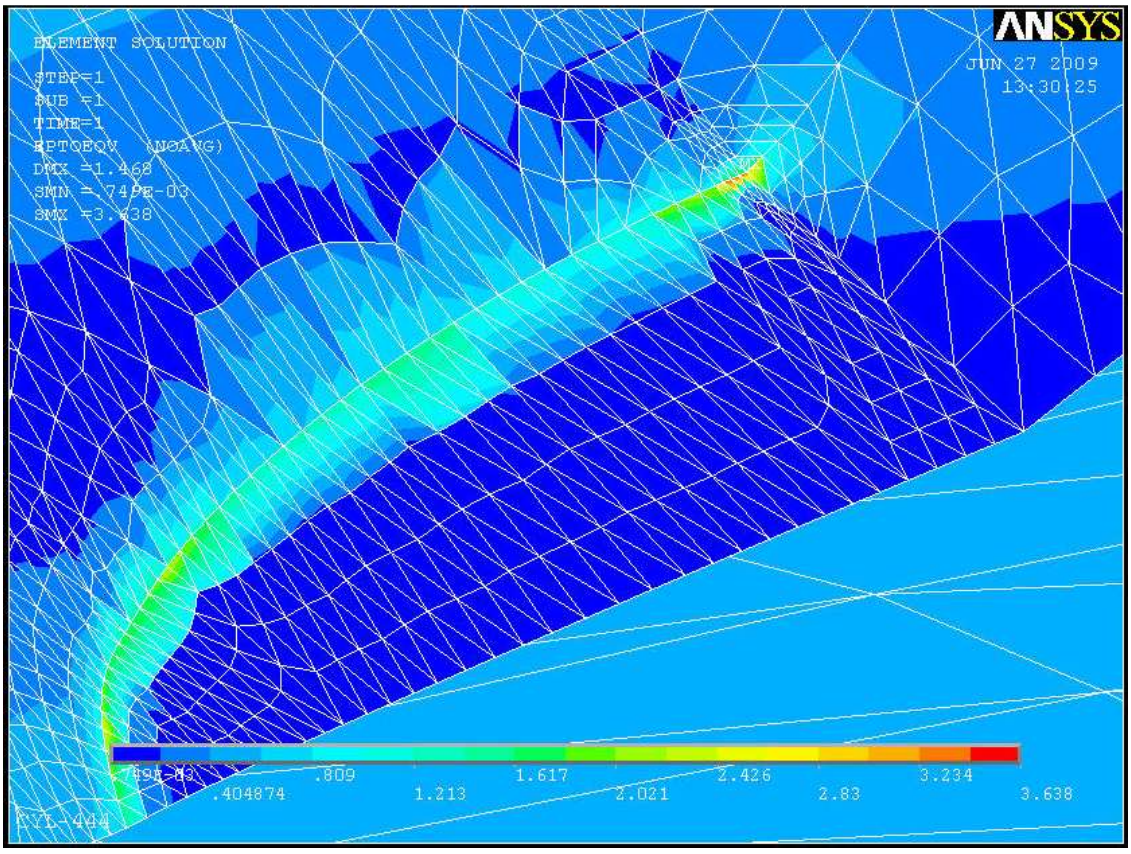

Figure 6.8 Magnified von Misses total strain plot for internal axial crack in isotropic shell

As described in the discussion of this paper elsewhere, the composite shell structure revealed the advantage of higher specific strength and specific stiffness as compared to conventional materials as presented before.

From the results obtained, the following conclusions may be drawn:

1. The composite shell structure has shown strong resistance to crack propagation due to matrix compression and fibre bending in the Mode I fracture mechanism.
2. The maximum shielding effect of the damaged zone is observed for the axial surface crack oriented on the external surface of the cylindrical shell structure while the maximum critical stress is for the internal axial crack. This is due to the maximum critical stress at the crack surface is propagating freely into the next un cracked ligament without any fibre bridging through the matrix material as the fibre in the next lamina is oriented axially. The stress propagation continues until it gets resistance from the fibres bending and matrix compression and produces a failure mechanism of fibre-matrix debonding and matrix cracking at the crack advancement.
3. The internal axial crack orientation has shown the maximum critical von Misses stress distribution around the surface crack because of the nature of curved geometry of the shell structure and the far field tangentially applied stress tries to open the surface crack.
4. For the axial pressure in Mode I loading condition the crack oriented internally in the tangential position of the cylindrical shell structure have also shown a maximum critical von Misses stress distribution as compared to the outer tangential surface crack orientation.
5. The von Misses stress and strain distribution is observed at the crack tip with some shielding effect at the surface crack front.
6. The cumulative distribution for strains and stresses is most sensitive to the crack region and still composites show much more resistance to crack than isotropic materials due to the fibre blocking of the crack advance.
7. Composite materials have shown complex and unpredicted fracture behaviour characterization as seen clearly from the stress and strain distributions as compared to conventional isotropic materials which usually shows specific crack tip plastic zones.

In general, this study has showed the stress and strain distributions in a composite material shell structure subjected to surface cracks in Mode I loading condition and the possible location of failure in the fibres, damage initiation and evolution in matrix materials, interfacial debonding between the fibre and matrix, and fibre bridging. The internal surface crack orientation in the composite material as well as conventional isotropic materials shell structures, which is usually the problem in pressure vessel application due to eroding and fatigue, has shown the maximum critical crack opening stress distribution around the surface crack that makes cylindrical shell structure fail the first subjected to these cracks. Moreover, in comparison to the conventional isotropic materials, a composite material shell structure has shown very strong resistance to crack initiation and propagation. Hence, they are very suitable and recommended for structures that need very high curiosity of catastrophic failure.

6.2 Recommendation and Future Works

The use of composites, advanced composites, in modern structural building is becoming predominantly important to assure the reliability of such structures which involve high risk and cost of fabrication. In this paper the stress analysis of composite shell structures with surface crack is presented by considering a cylindrical shell structure. However, in addition to material non linearity, there could be geometrical nonlinearity, which makes the analysis more difficult. Thus, one of the feature continuations of this work could be extending it to geometrically non linear shell structures.

In the current paper the stress analysis is curried out using the finite element method package ANSYS due its availability, but it lacks choice of solid elements which can be used for discretizing into finite elements of the thin solid shell structure. In this case one of the future directions is to develop the solid model and its finite element discretization (meshing) in a more versatile software package having these solid elements to have very good results.

In the present work, the numerical simulation of surface crack problems in a composite material cylindrical shell structure is presented in the finite element method package ANSYS. In order to compare the numerical results obtained with that of the experimental outcomes, one of the future continuations of this work could be conducting an experiment for the same structure, surface crack geometry, and loading conditions under a well established laboratory

REFERENCES

1. Anderson, T.L, *Fracture Mechanics Fundamentals and Application,* CRC Press, 2005
2. *Engineering Materials Hand book, volume 1: Composites*. ASM International, Metals Park, OH, 1987
3. Kaw, A., *Mechanics of Composite Materials*, CRC Press, 1997.
4. Marcel Dekker, *Practical Fracture Mechanics in Design*, A series of textbooks and Reference books in the Ohio state university of Mechanical Engineering, Columbus, Ohio, 2005.
5. Sohn, S.W., Kwon, D.A., Hong, S.H., "A Study on Mode I Inter laminar Fracture Toughness of Foam Core Sandwich Structures", *International Journal of the Korean Society of Precision Engineering*, pp. 2:47-53, 201.
6. Jiregna Hirko, "Stress Analysis of a Composite Material Shell Having a Crack", *M.S Thesis, Addis Ababa University,* Addis Ababa, Ethiopia, 2008
7. Young-Shin Lee, Je-Jun Lee, Youn-Ki Kang, and Sun-Young Song, "A Study on the Structural Stress Analysis of the Steel and the GFRP Laminated Composite Cylindrical Shell with a Stiffened Circular Cutout", *Key Engineering Material*, Vol. 326-328, 2006, pp.1837-1840
8. Raju, I.S., Newman, J.C., "Stress Intensity factors for Internal and External Surface Cracks in Cylindrical Vessels" *Trans. of the ASME., J. of Pressure Vessel Technology*, Vol. 104, 1982, pp. 293-298.
9. Nishoka T., Atluri, S.N., "Analysis of Surface Flaw in Pressure vessels by a New 3-Dimensional Alternating Method", *Trans. of the ASME., J. of Pressure Vessel Technology*, Vol. 104, 1982, pp. 299-306.
10. Ezzat, H., Erdogan, F., "Elastic-Plastic fracture of Cylindrical Shells Containing a Part-Through Circumferential Crack", *Trans. of the ASME., J. of Pressure Vessel Technology*, Vol. 104, 1982, pp. 324-330.
11. Newman, J.C., Raju, I.S., "Stress Intensity factors for Internal Surface Cracks in Cylindrical Vessels", *Trans. of the ASME., J. of Pressure Vessel Technology*, Vol. 102, 1980, pp. 342-346.
12. Lee, Y. S., Ryu, C. H., Choi, M. H. and Kim, Y. W., "A Study on Stress Analysis of Orthotropic Composite Cylindrical Shells with a Circular or an Elliptical Cutout", *KSME International Journal*, Vol. 18, 2004, No. 5, pp. 808-813

13. Ronald Krueger, *Computational Fracture Mechanics for Composites State of the Art and Challenges*, National Institute of Aerospace, Hampton, Virginia, USA
14. Haftchenari, H., Darvizeh, M., Darvizeh, A., Ansari, R., Sharma, C.B., "Dynamic Analysis of Composite Cylindrical Shells Using Differential Quadrature Method (DQM)", *Science Direct, Composite Structures* Vol. 78, 2007 pp. 292-298
15. Roberto C. Pavan, Guillermo J. Creus, "Anisotropic Damage in Composite Shell Structures"**,** *Av. Osvaldo Aranha,* 99, 90035-190, Porto Alegre-RS-Brasil
16. Khdier, A. A., "Analysis of the Dynamic Response of Cross-Ply Laminated Shallow Shells with Various Boundary Conditions", *J. King Saud univ.*, Vol. 12, Eng.Sci. (1), pp. 85-116 (A.H. 1420/200)
17. Yves Ousset, "Numerical Simulation of Delamination Growth in Layered Composite Plates", *Eur. J. Me &. A/Solids*, Vol. 18, 1999, pp. 291-312
18. Sung, W., Go, C., Shih, M., "Finite Element Modeling for Analysis of Cracked Cylindrical Pipes", *Journal of Zhehiang University of Science A*, Vol. 8, 2007 pp. 1373-1379.
19. Charoenphan, S., Plesha, M. E., Bank, L. C., "Simulation of Crack Growth in Composite Material Shell Structures", *Int. J. Numer. Meth. & Engng*, Vol. 60, 2004, pp. 2399-2417
20. Hui-Shen Shen, Xiang,Y., "Buckling and Postbuckling of Anisotropic Laminated Cylindrical Shells under Combined Axial Compression and Torsion", *Science Direct, Composite Structures*, Vol. 84, 2008, pp. 375-386
21. Yu-Fu Liu, Yoshihisa Tanaka, Chitoshi Masuda, "Analysis of the Fibre-Matrix Cylindrical Model with a Circumferential Crack", *International Journal of Fracture*, Vol. 88, 1997, pp. 87-105,
22. George, Z. Voyiadjis and Peter I. Kattan, *Mechanics of Composite Materials with MATLAB*, Springer-Verlag Berlin Heidelberg, 2005
23. Stegmann, J., "Analysis and Optimization of Laminated Composite Shell Structures", *Ph.D. Thesis, Institute of Mechanical Engineering Aalborg University*, Denmark, May 2005.
24. Reddy, J.N., *Mechanics of Laminated Composite Plates, Theory and Analysis*, CRC Press, 1997
25. Storakers, B., Larson, P. L., Rohart, C., "On Delamination Growth in Shallow Shells", *Journal of Applied Mechanics*, Vol. 71, pp. 247-254.

26. Zheng-Ming Huang, “Ultimate Response of Composite Cylinder Under Flexural Load”, *Journal of Applied Mechanics*, Vol. 72, pp. 313-321.
27. Jack R. Vinson, Tsu-Wei Chou, *Composite Materials and Their use in Structures,* Applied Science Publishers, London, 1975
28. Bing-Hua Wu and Erdogan, F., “The Surface Crack Problem in An Orthotropic Plate Under Bending and Tension”, *The National Aeronautics and Space Administration Grant No. NGR-39-007-011*, 1986
29. Erdogan, F. and Binghua Wu, “The Surface and Through Crack Problem in Layered Orthotropic Plates”, *Final Technical Report National Aeronautics and Space Administration Grant No. NAG-I-713*, 1991
30. Reuter, Walter G., Underwood, John H., Newman J. C., *Surface-Crack Growth: Models, Experiments, and Structures,* ASTM, STP 1060
31. Rice, J.R. and Levy, N., “The Part-Through Surface Crack in an Elastic Plate”, *ASME Journal of Applied Mechanics,* Vol. 39, 1972, pp.185-194.
32. Tada, H., Paris, P.C., and Irwin, G.R., *The Stress Analysis of Cracks Handbook, Fracture Proof Design*, Saint Luis, MO, 1985.
33. Ozdil, F., Carlsson, L. A., Liv, X., “Characterization of Mode II Delamination Growth in Glass/Epoxy Composite Cylinders”, *Journal of Composite Materials,* Vol.34, pp. 274-298, 2000.
34. Reissner, E., “The effect of Transverse Shear Deformation on the Bending of Elastic Plate”, *Trans. ASME J. Appl. Mech,* Vol. 12, 1945, pp. A69-A77.
35. Medwadowski, S. J., “A Refined Theory of Elastic, Orthotropic Plate”, *Trans. ASME J. Appl. Mech*, Vol. 80, 1958, pp. 437-443.
36. Erdogan, F., “The Line-Spring Model”, *Interim Report, Lehigh University.*
37. Kaya, A. C. and Erdogan, F., “Stress Intensity Factors and COD in an Orthotropic Strip”, *Int. J. of Fracture*, Vol. 16, 1980, p. 171.
38. Sadd H. M., *Elasticity: Theory, applications, and Numerics,* USA, Elsvier Inc., 2005.
39. Mohammadi S., *Extended Finite Element Method for Fracture Analysis of Structures,* Blackwell, UK, 2008.
40. Sih, G.C., Paris, P. and Irwin, G., “On Cracks in Rectilinearly Anisotropic Bodies”, *International Journal of Fracture Mechanics,* Vol. 1, 1965, pp. 189-203.